Use Authorization

In presenting this dissertation in partial fulfillment of the requirements for an advanced degree at Idaho State University, I agree that the Library shall make it freely available for inspection. I further state that permission to download and/or print my dissertation for scholarly purposes may be granted by the Dean of the Graduate School, Dean of my academic division, or by the University Librarian. It is understood that any copying or publication of this dissertation for financial gain shall not be allowed without my written permission.

Signature_____

Date _____

Advanced Tracking Strategies for Linear and Nonlinear Control Systems: Theory and Applications

by

Ahmed Mohamed Abdelhady Khamis

A dissertation

submitted in partial fulfillment of the requirements

for the degree of

Doctor of Philosophy in Engineering and Applied Science

College of Science and Engineering, Idaho State University

Spring 2014

To the Graduate Faculty:

The members of the committee appointed to examine the dissertation of AHMED KHAMIS find it satisfactory and recommend that it be accepted.

_____ Major Advisor

Dr. D. Subbaram Naidu (Professor of Electrical Engineering)

_____ Committee Member

Dr. Hossein Mousasvinezhad (Professor of Electrical Engineering)

_____ Committee Member

Dr. Dawid Zydek (Assistant Professor of Electrical Engineering)

_____ Committee Member

Dr. Bennett Palmer (Professor of Mathematics)

_____ Graduate Faculty Representative (GFR)

Dr. Alexander Urfer (Professor of Physical and Occupational Therapy)

Acknowledgments

I would like to express my great indebtedness to my supervisor, **Dr. Subbaram Naidu**, who was abundantly helpful and offered invaluable assistance, support and guidance. **Dr. Naidu** inspired me greatly to work on this dissertation. His willingness to motivate me contributed tremendously to this work. To him, I am sincerely grateful for offering much of his precious time revising and correcting many of the shortcomings of this work. Really, I was honored to work under his supervision. Also, I was very pleased to attend his graduate courses. His professional teaching is amazing and makes the scientific material interesting and easy for understanding.

I would like to extend my appreciation to **Dr. Dawid Zydek**, **Dr. Hossein Mousavinezhad**, **Dr. Bennett Palmer**, and **Dr. Alexander Urfer** for carefully reading and providing useful comments and suggestions on this dissertation.

Deepest gratitude to **Dr. Yehia Elhlwagy** and **Dr. Ahmed Mohsen Kamel**. Your advice on both research as well as on my career have been priceless.

I would like to convey my thanks to **The Egyptian Government** for providing me with financial support during my doctoral at **Idaho State University**.

Words cannot express how grateful I am to **my father, mother, my father-in-law,** and **mother-in law** for all of the sacrifices that they have made on my behalf. Your prayer for me was what sustained me thus far.

I would like to express appreciation to **my wife**, who was always my support in the moments when there was no one to answer my queries.

At the end, I would like to dedicate this dissertation to my small family. Without you, this dissertation could not be completed. May God bless everyone.

Contents

List of Figures

List of Tables

Abstract

The research in the doctoral dissertation addresses the main topic of State-Dependent Riccati Equation (SDRE) arising in regulator and tracking of nonlinear systems. This topic can be thought of as the nonlinear counterpart of linear, quadratic regulator (LQR) based control design. The greatest advantage offered by the SDRE is the design flexibility of tuning the state and input penalty matrices as functions of states. This research develops a new technique used for *infinite-horizon* nonlinear stochastic problems, by integrating the standard Kalman filter with the infinite-horizon SDRE technique.

Next, this research presents a new and computationally efficient online technique for *finite-horizon* nonlinear deterministic problems. This technique is based on change of variables that converts *the nonlinear* differential Riccati equation to *a linear* Lyapunov differential equation. During online implementation, the Lyapunov equation is solved in a closed form at any given time step. Further, an online technique is presented for finite-horizon nonlinear stochastic regulating and tracking problems. The idea of the proposed technique is to integrate the Kalman filter algorithm and the finite-horizon SDRE technique. Unlike the ordinary methods which deal with the linearized system, this technique estimates the unmeasured states of the nonlinear system directly, and this makes the proposed technique effective for a wide range of operating points.

Further, the proposed finite-horizon nonlinear tracking technique is used for angle tracking of the gimbaled system in a missile seeker to demonstrate the effectiveness of the developed technique. Three engagement scenarios, including fixed target, non-maneuvering target, and maneuvering target are presented to demonstrate the effectiveness of the developed technique.

Once the proposed algorithms have been developed and tested by software simulation, the next step is to bridge the gap between software simulation and real world applications. Here, the method of hardware in the loop simulation (HILS) is executed by using an experimental setup based on a microcontroller board manufactured by Zeltom Educational and Industrial Control System Company.

Chapter 1

Introduction

It is well known that the optimal tracking control problem has been the focus of control systems community for several decades since it is usually encountered in real world systems, such as missiles and spacecraft systems [36, 97, 108, 116], robot manipulators [50, 57, 93], mechanical systems [63], etc. Therefore, it is necessary and important to investigate the optimal tracking control for linear and nonlinear systems. In the case of infinite-horizon optimal tracking control, the system is not tracked until the time reaches infinity (on large time), while for the finite case, the system must be tracked to a reference trajectory for a finite duration of time [143]. Since many limitations exist in traditional optimal tracking control approaches, such as plant inversion [144] and linearization [37], it is necessary to design direct optimal tracking control schemes for nonlinear systems. Numerous design methodologies exist for the control design of nonlinear systems. One of the recently developed techniques for the optimal control of nonlinear systems is the State Dependent Riccati Equation (SDRE).

1.1 Background

The *advanced* control theory concerned with multiple inputs and multiple outputs (MIMO) is based on state variable representation in terms of a set of first-order

differential equations. Here, the system (plant) is characterized by state variables in *linear* time-invariant form as

$$\dot{\mathbf{x}}(t) = \mathbf{A}\mathbf{x}(t) + \mathbf{B}\mathbf{u}(t), \tag{1.1.1}$$

$$\mathbf{y}(t) = \mathbf{C}\mathbf{x}(t) + \mathbf{D}\mathbf{u}(t), \tag{1.1.2}$$

where *dot* denotes differentiation with respect to (w.r.t.) t, $\mathbf{x}(t)$, $\mathbf{u}(t)$, and $\mathbf{y}(t)$ are $n-$, $r-$, and $m-$ dimensional *state*, *control*, and *output* vectors respectively, and $\mathbf{A}$ is $n \times n$ state, $\mathbf{B}$ is $n \times r$ input, $\mathbf{C}$ is $m \times n$ output, and $\mathbf{D}$ is $m \times r$ transfer matrices. Similarly, a *nonlinear* dynamical system is characterized by

$$\dot{\mathbf{x}}(t) = \mathbf{f}(\mathbf{x}(t), \mathbf{u}(t), t), \tag{1.1.3}$$

$$\mathbf{y}(t) = \mathbf{g}(\mathbf{x}(t), \mathbf{u}(t), t), \tag{1.1.4}$$

where $\mathbf{f}$ and $\mathbf{g}$ are $n-$ and $m-$ dimensional vectors respectively.

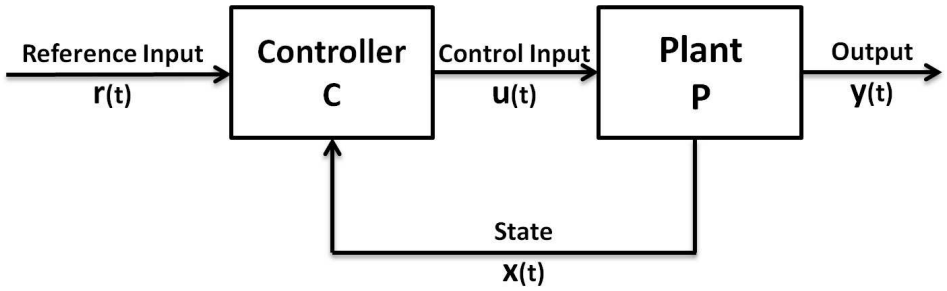

Figure 1.1: Advanced Control Configuration

The advanced theory dictates that all the state variables should be fed back after suitable weighting. We see from Fig.1.1 that in advanced control configuration, the input $\mathbf{u}(t)$ to the plant is determined by the controller driven by system states $\mathbf{x}(t)$ and reference signal $\mathbf{r}(t)$, all or most of the state variables are available for feedback control, and it depends on well-established matrix theory, which is amenable for large scale computer simulation [98].

Optimization is a very desirable feature in day-to-day life. The main objective

of optimal control is to determine control signals that will cause a process (plant) to satisfy some physical constraints and at the same time extremize (maximize and minimize) a chosen performance criterion (performance index or cost function).

The formulation of optimal control problem requires

1. a mathematical description (or model) of the process to be controlled (generally in state variable form),

2. a specification of the performance index, and

3. a statement of boundary conditions and the physical constraints on the states and/or controls.

For the purpose of optimization, we describe a physical plant by a set of linear or nonlinear differential or difference equations. For example, a linear time-invariant system is described by the state and output relations (1.1.1) and (1.1.2) and a nonlinear system described is by (1.1.3) and (1.1.4).

In modern control theory, the optimal control problem is to find a control which causes the dynamical system to reach a target or follow a state variable (or trajectory) and at the same time extremize a performance index. A performance index in general form can be written as

$$J = \mathbf{x}'(t_f)\mathbf{F}\mathbf{x}(t_f) + \int_{t_0}^{t_f} [\mathbf{x}'(t)\mathbf{Q}\mathbf{x}(t) + \mathbf{u}'(t)\mathbf{R}\mathbf{u}(t)]dt, \tag{1.1.5}$$

where, t_0 is *fixed* or given initial time, t_f is *free* (or unspecified in advance) final time, $\mathbf{x}(t_f)$ is a specified final state, $\mathbf{F}$ is a *positive semi-definite matrix*, $\mathbf{x}(t)$ is the error between the desired and the actual values, $\mathbf{Q}$ is a weighting matrix, which is *positive semi-definite* matrix, $\mathbf{R}$ is a *positive definite* matrix and prime ($'$) denotes the transpose [5]. Note that the matrices $\mathbf{Q}$ and $\mathbf{R}$ may be time varying. The particular form of performance index (1.1.5) is called *quadratic* form.

Also, the performance index can be in the general (non-quadratic) form as

$$J = S(\mathbf{x}(t_f), t_f) + \int_{t_0}^{t_f} V(\mathbf{x}(t), \mathbf{u}(t), t)dt, \tag{1.1.6}$$

where, $S(\mathbf{x}(t_f), t_f)$ is called the *terminal* cost function; $S(\mathbf{x}(t), \mathbf{u}(t), t) = \mathbf{x}'(t_f)\mathbf{F}\mathbf{x}(t_f)$ and $V(\mathbf{x}(t), \mathbf{u}(t), t)$ is called the *integral* cost function; $V(\mathbf{x}(t), \mathbf{u}(t), t) = \mathbf{x}'(t)\mathbf{Q}\mathbf{x}(t) + \mathbf{u}'(t)\mathbf{R}\mathbf{u}(t)$. There are many other forms of cost functions depending on our performance specifications. However, the above mentioned performance indices (with quadratic forms) lead to some very elegant results in optimal control systems [98].

1.2 Literature Survey–SDRE

The State Dependent Riccati Equation (SDRE) techniques have emerged as general design methods that provide a systematic and effective means of designing nonlinear controllers, observers and filters [21]. These methods overcome many of the difficulties and limitations of existing techniques, and provide simple algorithms that have been highly effective in a variety of practical and meaningful applications, e.g. missiles, aircraft, unmanned aerial vehicles, satellites and spacecraft, ships, autonomous underwater vehicles, automotive systems, robotics, process control, and biomedical systems [23]. Practical SDRE contributions related to some of these applications can be summarized in the following points

1.2.1 Missiles

The autopilot design of tail-controlled missile using output-feedback nonlinear H2 control was given in [95, 96]. The autopilot design for agile missiles using full-state information nonlinear H1 control was presented in [147]. In [32, 33], the autopilot design for hybrid bank-to-turn and skid-to-turn air-to-air missile using integral servomechanism tracking control was discussed. The autopilot design for a dual-controlled (tail and canard) missiles using state-dependent weightings was given in [94]. In [145],

the development of a novel method of adaptive nonsingular terminal sliding mode control for a class of nonlinear systems subject to disturbances and uncertainties was presented. The development of a standard method for a robust high-performance three-axis nonlinear missile autopilot design was discussed in [22]. The development of guidance law for acceleration-limited and impact-angle constrained trajectories was given in [30, 112]. The fully integrated guidance and control design of agile missiles to improve the mean and standard deviation of the final miss-distance against stressing threats using both algebraic SDRE and differential SDRE schemes was illustrated in [133]. The guidance filter design for a homing ballistic missile intercept problem using passive and active sensor information of azimuth, elevation, and range was given in [42]. In [90], the development of a robust guidance law for a missile undergoing inaccurate prediction of target maneuver was presented. The development of a novel robust second-order sliding mode control law using a back-stepping concept was discussed in [53].

1.2.2 Aircraft

The guidance control of a fighter aircraft during a high angle of attack was presented in [10]. The flutter suppression of aeroelastic wing sections using full-state or partial-state feedback was given in [15, 122, 129]. In [87], the enhancement of the performance of an aircraft flight control system by augmenting it with a SDRE controller implemented in a parallel fashion was discussed. The extension of the analytical multi-objective parameter synthesis method to nonlinear systems via the state-dependent coefficients parameterization method in combination with the receding horizon control technique was given in [45].

1.2.3 Unmanned Aerial Vehicles (UAV)

The trajectory tracking control of a small helicopter and a micro-ducted-fan rotor craft was given in [67]. The attitude and velocity control of a quad rotor UAV for

near-area surveillance and search-and-rescue missions was illustrated in [140]. In [46], the development of an onboard adaptive and robust flight control system that improves control, stability, and survivability of a small unmanned aerial system in off-nominal or out-of-envelope conditions was presented. In [16], the control and real-time flight testing of small autonomous helicopter for autonomous operations through a broad spectrum of maneuvers was given. The Global Positioning System sensor fusion based on SDRE nonlinear filtering for the UAV localization problem was discussed in [103]. The non-linear filter architecture to perform fault detection and isolation on the sensor gyros and accelerometers was given in [139].

1.2.4 Satellites and Spacecraft

The application of a nonlinear control technique for coupled orbital and attitude relative motion of formation flying was discussed in [92]. The position and attitude control of rigid spacecraft [51, 107, 126]. The hyper-sonic guidance of space vehicles during the mid-course phase of flight was given in [34]. In [7, 54], the angular-rate estimation of satellites using either vector measurements obtained from sensors or delayed quaternion measurements obtained from a cluster of star trackers was presented. The formation flying control of multiple satellites and spacecraft was given in [25]. The development of a tracking control algorithm with a nonlinear compensator for the gravity terms acting on the flight equations was discussed in [110].

1.2.5 Ships

The observer design for dynamic positioning of ships to obtain accurate estimates of the low frequency ship motions was discussed in [125]. The autopilot design for real-time way-point guidance of constrained nonlinear oil tanker motion in restricted waterways was presented in [20].

1.2.6 Autonomous Underwater Vehicles

The fault-tolerant and robust steering motion and dive-plane control was given in [100]. The integrated design of a real-time obstacle avoidance system was presented in [131]. In [61], the optimal and robust motion control for homing and docking tasks was discussed.

1.2.7 Automotive Systems

The stabilization of the lateral motion dynamics of a vehicle model was given in [2, 88]. The obstacle-avoiding feed forward and feedback path-tracking steering control for a vehicle using sensitivity-based gain parameterization of controller gains was illustrated in [138]. The analysis of non-linear autonomous systems using eigenstructure-based analysis through the Pseudo-linear (PL) form representation was presented in [49].

1.2.8 Robotics

The manipulator path control of a vertically articulated five-axis robot with experimental validation was presented in [59]. The real-time experimental control of two-link under actuated nonlinear non minimum-phase robot dynamics was discussed in [40]. The experimental control of a planar three link manipulator with two flexible links was given in [35]. In [117], the robust full-state-feedback nonlinear H1 control of the tip position of a single-link flexible manipulator was illustrated. The locomotion control with experimental validation of a three-link snakelike robot based on friction force, under holonomic and nonholonomic constraints was given in [146]. The modeling and controlling the tip position of a one-link flexible manipulator was discussed in [118]. The optimal control law for the optimization of a class of nonlinear singularly perturbed systems was presented in [48]

1.2.9 Process Control

The temperature estimation in rapid thermal processing systems for performing thermal manufacturing operations involved in integrated circuit fabrication was given in [13]. The speed sensor-less observer design for current and voltage source-inverter-fed induction motor drives for separate state and parameter estimations of rotor flux vector and load torque parameters was presented in [14, 106]. The control of the nonlinear non-minimum phase dynamics of a continuously stirred tank reactor was discussed in [31]. In [71], the regulation of the growth of thin films in a high-pressure chemical vapor deposition thin-film reactor for real-time applications in the microelectronic industry was discussed. The control of the tandem cold rolling process of the metal strip with improved tolerance in mill exit thickness was given in [109].

1.2.10 Biological and Biomedical Systems

The control of the artificial human pancreas was presented in [107]. In [9], the human immunodeficiency virus feedback control for combined drug and immune response using full state feedback as well as partial-state measurements was discussed. The optimal administration of chemotherapy in cancer treatment with combined control and state was given [60].

1.2.11 Other Nonlinear Studies

The adaptive SDRE control design was presented in [85, 86, 87]. The design of control systems with parasitic effects of friction and backlash was discussed in [43]. In [105], the robust global delay stabilizations of nonlinear time-delay systems was given. The active structural control of slewing beams was presented in [130]. The synchronization of nonlinear chaotic systems for secure communications by chaotic masking was given in [3, 62]. In [82], the data assimilation based on the global ionospherethermosphere model to predict space weather.

1.3 Dissertation Goal and Contributions

The main goal of this dissertation is to advance the state of the art in nonlinear finite-horizon tracking control based on the SDRE. In the process of achieving that main goal, the following contributions were made:

1. An efficient online technique used for nonlinear stochastic regulator and tracking problems is proposed. The idea of the proposed technique is to integrate the Kalman filter algorithm and the SDRE technique. Kalman filter is used to estimate the unmeasured states which are corrupted with noises in the nonlinear model. Unlike the ordinary methods which deal with the linearized system, this technique estimates the unmeasured states of the nonlinear system directly.

2. A novel online technique used for finite-horizon nonlinear tracking and regulation *deterministic* systems is developed. This technique is based on change of variables that converts the differential Riccati equation to a linear Lyapunov equation. During online implementation, the Lyapunov equation is solved in a closed form at each given time step.

3. A new optimal tracking and regulation technique used for finite-horizon nonlinear *stochastic* systems are developed. This technique based on using the Kalman filter after converting the nonlinear differential Riccati equation to a linear Lyapunov equation. Kalman filter is used to estimate the unmeasured states of the nonlinear model. The optimal control problem of the nonlinear system is solved by using finite-horizon SDRE algorithm, which makes this technique effective for a wide range of operating points.

4. The majority of homing guided missiles use gimbaled seekers. The control technique used for the gimbal system on a tactical missile must provide fast and precise tracking of relative error signals. Poor performance during engagement will result in large miss distances which may lead to low probability of mission success. The dynamical equations describing the gimbal system under consideration are highly nonlinear. In order to accurately calculate the missile-target

line of site (LOS) angle and its rate, accurate nonlinear control of the motion of the gimbaled seeker through the attached DC motors is required. The linear control techniques become inadequate and it becomes necessary to use some other nonlinear control techniques. The new direction of research on finite-horizon nonlinear tracking via SDRE is an appropriate solution.

5. Traditional software-based simulation has the disadvantage of being unable to accurately imitate real-time operational environment. One way to bridge the gap between simulation and real-time conditions is the Hardware in the Loop Simulation (HILS). The HILS is a necessary step towards research and development of engineering systems and in particular in the control systems. The problem of finite-horizon position control of a permanent magnet DC motor based on the nonlinear system dynamics is addressed. The experimental setup consists of a Hilink microcontroller board manufactured by Zeltom Educational and Industrial Control System Company, a corresponding SIMULINK©library for MATLAB©and SIMULINK©, DC motor with encoder, and hall effect current sensor.

1.4 Dissertation Outline

This dissertation is composed of **eight** chapters. **Chapter 1** serves as an introduction. The background, literature survey, dissertation goal, and the contributions of the work are provided in this chapter. **Chapter 2** presents the infinite-horizon nonlinear tracking and regulation using SDRE. **Chapter 3** introduces the infinite-horizon nonlinear tracking and regulating for stochastic systems. The development of the finite-horizon nonlinear tracking and regulating for deterministic systems is presented in **Chapter 4**. The finite-horizon nonlinear tracking and regulating for stochastic systems are discussed in **Chapter 5**. The simulation results for a realistic gimbaled system with three engagement scenarios, including fixed target, non-maneuvering target, and maneuvering target using the finite-horizon nonlinear control via SDRE are shown

in **Chapter 6**. **Chapter 7** focuses on the experimental verification of a practical system, a DC motor position control using HILINK microcontroller board and Matlab/Simulink. Finally, conclusions and future directions of research are detailed in **Chapter 8**.

Portions of the research contributions of this dissertation have so far been published in **one** book chapter [72], **two** international peer-reviewed conference papers [73, 74], and **six** international peer-reviewed conference papers have been accepted for publication [75, 76, 77, 78, 79, 80] as follows:

1. **Khamis, A.**; Zydek, D.; Borowik, G.; Naidu, D. S., "Control System Design Based on Modern Embedded Systems," In Computer Aided Systems Theory , Springer Berlin Heidelberg, 2013 [72].

2. **Khamis, A.**; Naidu, D. S., "Nonlinear Optimal Tracking Using Finite-Horizon State Dependent Riccati Equation (SDRE)", Proceedings of the 4th International Conference on Circuits, Systems, Control, Signals (WSEAS), Valencia, Spain, August 6–8, 2013, pp. 37–42 [74].

3. **Khamis, A.**; Zydek, D.; Borowik, G.; Naidu, D. S., "Control System Design Based on Modern Embedded Systems," 14th International Workshop on Computer Aided Systems Theory - EUROCAST 2013, Las Palmas de Gran Canaria, Spain, p. 346-347, 2013 [73].

4. **Khamis, A.**; Naidu, D. S., "Nonlinear Optimal Tracking With Incomplete State Information Using Finite-Horizon State Dependent Riccati Equation (SDRE)", American Control Conference (2014 ACC), Portland, Oregon, USA, 2014, accepted [78].

5. **Khamis, A.**; Naidu, D. S.; Zydek, D., "Nonlinear Optimal Control With Incomplete State Information Using State Dependent Riccati Equation (SDRE)," 23rd International Conference On Systems Engineering (ICSEng 2014), Las Vegas, NV, USA, accepted [79].

6. **Khamis, A.**; Naidu, D. S.; Zydek, D., "Nonlinear Position Control of DC motor Using Finite-Horizon State Dependent Riccati Equation (SDRE)," 23rd International Conference On Systems Engineering (ICSEng 2014), Las Vegas, NV, USA, accepted [80].

7. **Khamis, A.**; Naidu, D. S., "Nonlinear Optimal Stochastic Regulator Using Finite-Horizon State Dependent Riccati Equation", IEEE-CYBER 2014, Hong Kong, China, June 4-7, 2014, accepted [76].

8. **Khamis, A.**;Ahmed M. Kamel; Naidu, D. S., "Nonlinear Optimal Tracking For Missile Gimbaled Seeker Using Finite-Horizon State Dependent Riccati Equation", IEEE-CYBER 2014, Hong Kong, China, June 4-7, 2014, accepted [77].

9. **Khamis, A.**; Naidu, D. S., "Experimental Validation for Real Time Control of DC Motor Using Novel Finite-Horizon Optimal Technique", IEEE-CYBER 2014, Hong Kong, China, June 4-7, 2014, accepted [75].

Chapter 2

Infinite-Horizon State Dependent Riccati Equation (SDRE) for Deterministic Systems

The need to improve performance in controlled systems leads to more and more accurate modeling of dynamical systems or plants. However, if a model is a good representation of the real system over a wide range operating points, it is most often nonlinear. Therefore, the ordinarily used linear control techniques are inadequate and it becomes necessary to use some other nonlinear control techniques. The competitive era of technological change has motivated the rapid development of nonlinear control theory for application to challenging, complex dynamical real-world problems [19].

There exist many nonlinear control design techniques, each has benefits and weaknesses. Most of them are limited in range of applicability, and use of certain nonlinear control technique for a specific system usually demands choosing between different factors, e.g., performance, robustness, optimality, and cost. Some of the well-known nonlinear control techniques are feedback linearization, adaptive control, nonlinear predictive control, sliding mode control, and approximating sequence of Riccati Equa-

tions. One of the highly promising and rapidly emerging techniques for nonlinear optimal controllers designing is the State Dependent Riccati Equation (SDRE) technique. Although there exist a number of other methods for stabilization of nonlinear systems, the SDRE approach involves imitating standard linear quadratic regulator (LQR) design for linear systems. The SDRE based techniques are among the few successful approaches that have important properties, such as applicability to a large class of nonlinear systems, allowing the controller designer to make a tradeoff between control effort and state errors, and its systematic formulation [23].

2.1 Algebraic State Dependent Riccati Equation Overview

State Dependent Riccati Equation (SDRE), also referred to as the Frozen Riccati Equation (FRE) [38], was first proposed by Pearson (1962), in addressing a state dependent formulation of nonlinear time-varying systems for nonlinear optimal control problems. Pearson suggested treating it as *an instantaneously* linear time invariant (LTI) system to approximate the nonlinear optimal control problem at *each instant of time*. Later, SDRE was expanded by Wernli and Cook (1975), and the intense start of real interest in the field did not come until the late 1990's when several studies were done by Mracek and Cloutier (1998) [32].

The SDRE has become a very attractive tool for the systematic design of nonlinear controllers, very common within the control community over the last decade, providing an extremely effective algorithm for nonlinear feedback control design by allowing nonlinearities in the system states while additionally offering great design flexibility through design matrices [19].

The SDRE method involves factorization of the nonlinear dynamics into product of a matrix-valued function (which depends on the states) and state vector. Thus, the SDRE algorithm captures the nonlinearities of the system, transforming the original

nonlinear system to a linear-like structure with state dependent coefficient (SDC) matrices, and minimizing a nonquadratic performance index with a quadratic-like structure [23]. The Riccati equation using the SDC matrices is then solved *online* to give the sub-optimum control law. Moreover, with enough sample points, the suboptimal solution can be made to be very close to the optimal solution of the original nonlinear system. The coefficients of this Riccati equation vary with each point in state space. The algorithm thus involves solving, at a given point in state space, a SDRE whose pointwise stabilizing solution during state evolution yields the SDRE nonlinear feedback control law.

As the SDRE depends only on *the current* state, the computation can be carried out *online*, in which case the SDRE is defined along the state trajectory. In addition, a primary advantage offered by SDRE to the control designer is the opportunity to make tradeoffs between control effort and state errors by tuning the SDC.

The process of factorizing a nonlinear system into a linear-like structure that contains SDC matrices is called extended linearization. It's well known that for single- variable (scalar) systems, the SDC parameterization is unique, On the other hand, in the multi variable case, the SDC parameterization is not unique. In fact, there are an infinite number of ways to bring a nonlinear system to SDC form.

For example, consider the two-dimensional nonlinear system in the form

$$\dot{\mathbf{x}}(t) = \mathbf{f}(\mathbf{x}) + \mathbf{B}(\mathbf{x})\mathbf{u}(t), \tag{2.1.1}$$

where $\mathbf{f}(\mathbf{x}) = [x_2, x_1^3]'$. We can write this system in the SDC form as

$$\dot{\mathbf{x}}(t) = \mathbf{A}(\mathbf{x})\mathbf{x}(t) + \mathbf{B}(\mathbf{x})\mathbf{u}(t), \tag{2.1.2}$$

with the obvious SDC parameterization $\mathbf{A_1}(\mathbf{x}) = \begin{bmatrix} 0 & 1 \\ x_1^2 & 0 \end{bmatrix}$. However, we can also find another SDC parameterizations:

$$\mathbf{A}(\mathbf{x}) = \mathbf{A_2}(\mathbf{x}) = \begin{bmatrix} -x_2 & 1+x_1 \\ x_1^2 & 0 \end{bmatrix}, \text{ or } \mathbf{A}(\mathbf{x}) = \mathbf{A_3}(\mathbf{x}) = \begin{bmatrix} \frac{x_2}{x_1} & 0 \\ x_1^2 & 0 \end{bmatrix}.$$

Because of the many available SDC parameterizations, as we design the optimal control law we must choose the one that is most appropriate for the system and control objectives of interest. To choose the one of the correct parameterizations for $\mathbf{A}(\mathbf{x})$ and $\mathbf{B}(\mathbf{x})$, one should consider that the matrices $\mathbf{A}(\mathbf{x})$ and $\mathbf{B}(\mathbf{x})$ must be chosen in such a way that the nonlinear system is *controllable* or at least *stabilizable*.

It is well known that the solution of the SDRE cannot be found analytically, except for very limited nonlinear systems. It is given that Taylor series and interpolation methods can be used to approximate the offline solution of the SDRE. However, it is still hard to solve the SDRE with these methods when the dynamics of the nonlinear system become very complex or of high-order.

2.2 Infinite-Horizon Regulation for Deterministic Nonlinear Systems

Consider the continuous-time, deterministic, full-state feedback, infinite-time horizon, nonlinear optimal regulation problem, where the system is having dynamics

$$\dot{\mathbf{x}}(t) = \mathbf{f}(\mathbf{x}) + \mathbf{B}(\mathbf{x})\mathbf{u}(t), \tag{2.2.1}$$

with state vector $\mathbf{x}(t) \in \Re^n$ and (unconstrained) input vector $\mathbf{u}(t) \in \Re^m$,such that $\mathbf{f} : \Re^n \to \Re^n$ and $\mathbf{B} : \Re^n \to \Re^{n\mathbf{x}m}$, with $\mathbf{B}(\mathbf{x}) \neq 0 \forall\ \mathbf{x}(t)$. In this context, the minimization of an infinite-time horizon performance criterion with a convex integrand, nonquadratic in $\mathbf{x}$ but quadratic in $\mathbf{u}$, is considered, given by

$$\mathbf{J}(\mathbf{x}, \mathbf{u}) = \frac{1}{2}\int_o^\infty \left[\mathbf{x}'(t)\mathbf{Q}(\mathbf{x})\mathbf{x}(t) + \mathbf{u}'(t)\mathbf{R}(\mathbf{x})\mathbf{u}(t)\right]\, dt. \tag{2.2.2}$$

The state and input weighting matrices (design parameters) are assumed to be state-dependent, such that $\mathbf{Q}(\mathbf{x}) : \Re^n \rightarrow \Re^{n\mathbf{x}n}$ and $\mathbf{R}(\mathbf{x}) : \Re^n \rightarrow \Re^{m\mathbf{x}m}$. Also $\mathbf{Q}(\mathbf{x})$ is a symmetric *positive semi-definite* matrix, and $\mathbf{R}(\mathbf{x})$ is a symmetric *positive definite* matrix. Moreover, $\mathbf{x}'(t)\mathbf{Q}(\mathbf{x})\mathbf{x}(t)$ is a measure of state-error accuracy and $\mathbf{u}'(t)\mathbf{R}(\mathbf{x})\mathbf{u}(t)$ is a measure of control effort [23].

Using SDC parameterization [32], the nonlinear system dynamics (2.2.1) can be converted into a linear-like structure which contains SDC matrices. Under the assumptions $\mathbf{f}(\mathbf{0}) = \mathbf{0}$, a continuous nonlinear matrix-valued function $\mathbf{A}(\mathbf{x})$ exists such that

$$\mathbf{f}(\mathbf{x}) = \mathbf{A}(\mathbf{x})\mathbf{x}(t), \tag{2.2.3}$$

where $\mathbf{A}(\mathbf{x}) \in \Re^{n\mathbf{x}n}$ is found by mathematical factorization and is non-unique when $n > 1$. Therefore, the nonlinear system (2.2.1) can now be represented in the SDC form

$$\dot{\mathbf{x}}(t) = \mathbf{A}(\mathbf{x})\mathbf{x}(t) + \mathbf{B}(\mathbf{x})\mathbf{u}(t), \quad \mathbf{x}(0) = \mathbf{x_0}, \tag{2.2.4}$$

which has a linear structure with SDC matrices $\mathbf{A}(\mathbf{x})$ and $\mathbf{B}(\mathbf{x})$.

2.2.1 Algebraic SDRE Regulation Controller Structure

The SDRE procedure uses *extended linearization* as the basic design concept in formulating the nonlinear optimal control problem (2.2.1) and (2.2.2). The basic linear control synthesis method in this case is the LQR method [4, 6]. Motivated by the LQR problem, which is characterized by *an algebraic* Riccati Equation (ARE), the algebraic SDRE feedback control is an extended linearization control method that provides a similar approach to the nonlinear regulation problem for the input-affine system (2.2.1) with cost functional (2.2.2). First, the following conditions must be met before starting the controller design [21]:

Condition 1: $\mathbf{f}(\mathbf{x})$ is a continuously differentiable vector-valued function of $\mathbf{x}(t)$.
Condition 2: The origin $\mathbf{x} = \mathbf{0}$ is an equilibrium point of the system with $\mathbf{u} = \mathbf{0}$.
Condition 3: $\mathbf{Q}(\mathbf{x})$ is a symmetric positive semi-definite matrix, and $\mathbf{R}(\mathbf{x})$ is a symmetric positive definite matrix.
Condition 4: $\mathbf{A}(\mathbf{x})$ and $\mathbf{B}(\mathbf{x})$ must be chosen in such a way that the nonlinear system is *controllable* or at least *stabilizable*.

By mimicking the LQR formulation, the optimal state-feedback controller is obtained in the form

$$\mathbf{u}(\mathbf{x}) = -\mathbf{K}(\mathbf{x})\mathbf{x}(t), \tag{2.2.5}$$

such that the nonlinear state-feedback gain $\mathbf{K}(\mathbf{x})$ for (approximately) minimizing (2.2.2) becomes

$$\mathbf{K}(\mathbf{x}) = \mathbf{R}^{-1}(\mathbf{x})\mathbf{B}'(\mathbf{x})\mathbf{P}(\mathbf{x}), \tag{2.2.6}$$

and hence the state-feedback controller can be written as

$$\mathbf{u}(\mathbf{x}) = -\mathbf{R}^{-1}(\mathbf{x})\mathbf{B}'(\mathbf{x})\mathbf{P}(\mathbf{x})\mathbf{x}(t). \tag{2.2.7}$$

Here, $\mathbf{P}(\mathbf{x})$ is the unique, symmetric, positive-definite solution of the continuous-time algebraic SDRE

$$\mathbf{P}(\mathbf{x})\mathbf{A}(\mathbf{x}) + \mathbf{A}'(\mathbf{x})\mathbf{P}(\mathbf{x}) - \mathbf{P}(\mathbf{x})\mathbf{B}(\mathbf{x})\mathbf{R}^{-1}(\mathbf{x})\mathbf{B}'(\mathbf{x})\mathbf{P}(\mathbf{x}) + \mathbf{Q}(\mathbf{x}) = 0. \tag{2.2.8}$$

The resulting algebraic SDRE-controlled trajectory (state) is the solution of the

closed-loop dynamics

$$\dot{\mathbf{x}}(t) = [\mathbf{A}(\mathbf{x}) - \mathbf{B}(\mathbf{x})\mathbf{R}^{-1}(\mathbf{x})\mathbf{B}'(\mathbf{x})\mathbf{P}(\mathbf{x})]\mathbf{x}(t). \tag{2.2.9}$$

The algebraic SDRE, strictly speaking it could be called State Dependent Algebraic Riccati Equation (SDARE), solution to the infinite-time horizon autonomous nonlinear regulator problem (2.2.1) and (2.2.2) is a true generalization of the infinite-time horizon *time-invariant* LQR problem, where all of the coefficient matrices are *state-dependent*. At each instant, the method treats the SDC matrices as being *constant*, and computes a control action by solving an LQ optimal control problem. The main advantage of the algebraic SDRE algorithm is its simplicity and its obvious efficiency, since there is no attempt to solve the Hamilton Jacobi Bellman (HJB) equation. That's applicable for nonlinear optimal control problems. When the coefficient and weighting matrices are constant, the nonlinear regulator problem converts to the LQR problem and the algebraic SDRE control method converts to the steady-state linear regulator.

Fig.2.1 shows a flow chart of the infinite-horizon algebraic SDRE regulator. At each sample time, the following procedure is accomplished. First, the current state vector $\mathbf{x}(t)$ is used to calculate numerical values for $\mathbf{A}(\mathbf{x})$ and $\mathbf{B}(\mathbf{x})$. Then, using the LQR equations, $\mathbf{P}(\mathbf{x})$ and $\mathbf{K}(\mathbf{x})$ are calculated. Control input $\mathbf{u}(\mathbf{x})$ is then calculated and applied to the system to calculate the state of the next step of time. This LQR procedure is then repeated at the next sample time. For the algebraic SDRE technique, the ARE is solved at every sample time for each new value of $\mathbf{A}(\mathbf{x})$ and $\mathbf{B}(\mathbf{x})$ at each step of time. This procedure views *the nonlinear* system to be approximated as a series of *linear* systems. Therefore, shorter time increments increase the accuracy of the control law, because the change in nonlinear dynamics over shorter time increments is more like a linear change. Because of its approximating nature, the algebraic SDRE technique is considered a suboptimal solution. However, with the proper choices for the $\mathbf{A}(\mathbf{x})$ and $\mathbf{B}(\mathbf{x})$ matrices, and with the proper amount of sample times, the algebraic SDRE technique can provide a very adequate optimal

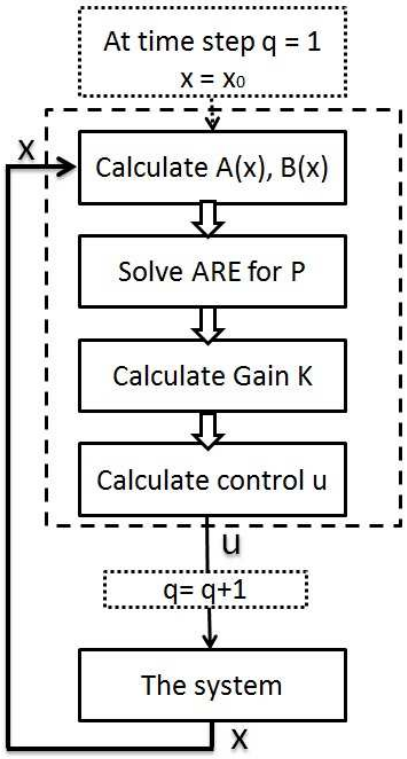

Figure 2.1: Flow Chart of Infinite-Horizon Algebraic SDRE Regulator

solution.

2.2.2 Infinite-Horizon Algebraic SDRE Regulation Simulation: Van der Pol's Oscillator

This section presents simulations with the infinite-horizon optimal regulator controller for Van der Pol's oscillator using algebraic SDRE. Consider the Van der Pol's oscillator nonlinear equations

$$\dot{x}_1 = x_2, \tag{2.2.10}$$

$$\dot{x}_2 = 1 - x_1^2 x_2 - x_1 + u, \tag{2.2.11}$$

with the equilibrium point of this system at $\mathbf{x_0} = (0, 0)'$. Note that $x_1 = x_1(t)$ and $x_2 = x_2(t)$.

The given nonlinear system can be written in the SDC form

$$\mathbf{A} = \begin{bmatrix} 0 & 1 \\ -1 & 1 - x_1^2 \end{bmatrix}, \quad \mathbf{B} = \begin{bmatrix} 0 \\ 1 \end{bmatrix}, \tag{2.2.12}$$

and the weighted matrices

$$\mathbf{R} = [1], \quad \mathbf{Q} = \begin{bmatrix} 50 & 0 \\ 0 & 50 \end{bmatrix}. \tag{2.2.13}$$

The simulations are performed for a time interval of 50 seconds with 500 time steps, the resulting states trajectories is shown in Fig. 2.2 and the optimal control is shown in Fig. 2.3. In Fig. 2.2, the solid line denotes state x_1, the doted line denotes state x_2 trajectory. Fig. 2.2 clearly illustrates of the infinite-horizon algebraic SDRE nonlinear regulator algorithm.

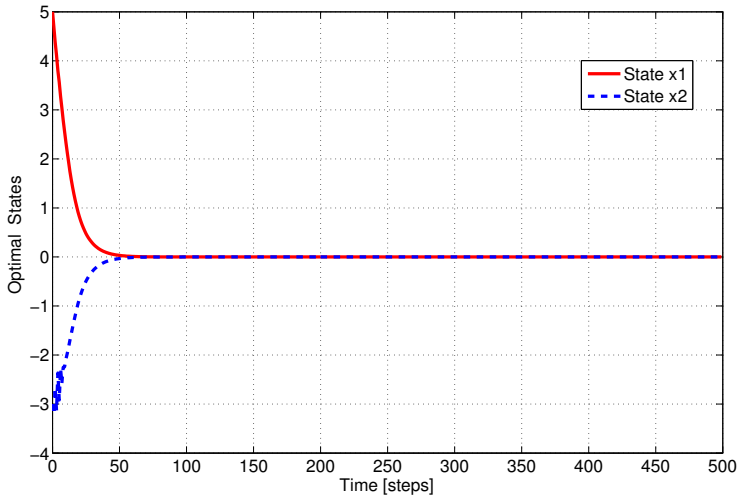

Figure 2.2: Optimal States for the Van der Pol's Oscillator

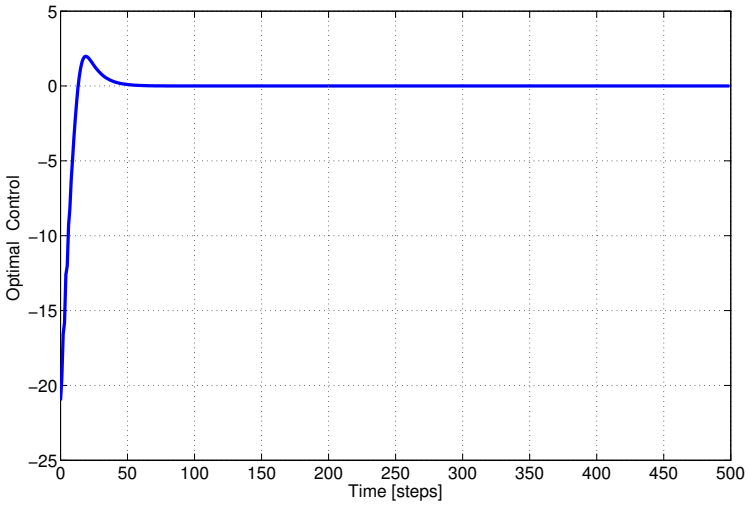

Figure 2.3: Optimal Control for the Van der Pol's Oscillator

2.3 Infinite-Horizon Tracking for Deterministic Nonlinear Systems

Consider the continuous-time, deterministic, full-state feedback, infinite-time horizon, nonlinear optimal tracking problem, where the system is having dynamics

$$\dot{\mathbf{x}}(t) = \mathbf{f}(\mathbf{x}) + \mathbf{B}(\mathbf{x})\mathbf{u}(t), \tag{2.3.1}$$

$$\mathbf{y}(t) = \mathbf{h}(\mathbf{x}), \tag{2.3.2}$$

with state vector $\mathbf{x}(t) \in \Re^n$, (unconstrained) input vector $\mathbf{u}(t) \in \Re^m$, and the output $\mathbf{y}(t) \in \Re^p$. Such that $\mathbf{f}(\mathbf{x}) : \Re^n \rightarrow \Re^n$, $\mathbf{B}(\mathbf{x}) : \Re^n \rightarrow \Re^{n\mathbf{x}m}$, and $\mathbf{h}(\mathbf{x}) : \Re^n \rightarrow \Re^{p\mathbf{x}n}$.

That nonlinear system can be expressed in a state-dependent like linear form, as:

$$\dot{\mathbf{x}}(t) = \mathbf{A}(\mathbf{x})\mathbf{x}(t) + \mathbf{B}(\mathbf{x})\mathbf{u}(t), \tag{2.3.3}$$

$$\mathbf{y}(t) = \mathbf{C}(\mathbf{x})\mathbf{x}(t), \tag{2.3.4}$$

where $\mathbf{f}(\mathbf{x}) = \mathbf{A}(\mathbf{x})\mathbf{x}(t)$, $\mathbf{h}(\mathbf{x}) = \mathbf{C}(\mathbf{x})\mathbf{x}(t)$. $\mathbf{A}(\mathbf{x}) \in \Re^{n\mathbf{x}n}$, $\mathbf{B}(\mathbf{x}) \in \Re^{n\mathbf{x}m}$, and

$\mathbf{C}(\mathbf{x}) \in \Re^{p\mathbf{x}n}$.

Let $\mathbf{z}(t) \in \Re^p$ be the desired output. The goal is to control the system (2.3.3, 2.3.4) so that the output $\mathbf{y}(t)$ follows, as close as possible, the commanded output $\mathbf{z}(t)$. This objective can be accomplished by using a state feedback control law that minimizes a cost function [98]:

$$\mathbf{J}(\mathbf{x}, \mathbf{u}) = \frac{1}{2} \int_0^\infty [\mathbf{e}'(t)\mathbf{Q}(\mathbf{x})\mathbf{e}(t) + \mathbf{u}'(\mathbf{x})\mathbf{R}(\mathbf{x})\mathbf{u}(\mathbf{x})] \, dt, \tag{2.3.5}$$

where $\mathbf{e}(t) = \mathbf{z}(t) - \mathbf{y}(t)$, $\mathbf{Q}(\mathbf{x})$ is a symmetric *positive semi-definite* matrix, and $\mathbf{R}(\mathbf{x})$ is a symmetric *positive definite* matrix. $\mathbf{e}'(t)\mathbf{Q}(\mathbf{x})\mathbf{e}(t)$ is a measure of tracking error accuracy and $\mathbf{u}'(\mathbf{x})\mathbf{R}(\mathbf{x})\mathbf{u}(\mathbf{x})$ is a measure of control effort [23].

2.3.1 Algebraic SDRE Tracking Controller Structure

The algebraic SDRE, strictly speaking it could be called State Dependent Algebraic Riccati Equation (SDARE), control theory has only been developed for the infinite-time non-linear optimal regulation (stabilization) problem, for which $\mathbf{z}(t) = 0$ and $\mathbf{C}(\mathbf{x}) = I_{n\mathbf{x}n}$. This is because the method requires solving the infinite-time algebraic Riccati equation. Unfortunately, the developed theory of the infinite-time LQ optimal tracking problem has hindered its application for solving *non-linear* trajectory tracking problems, unless an integral servomechanism is used [23], which increases the number of states and thus the computation time required for solving algebraic Riccati equations. Regardless of the developed theory of *infinite-time* LQ optimal tracking control, a good approximation can be developed for excessively large terminal time [20]. The derived results are approximate in nature and are valid for very large values of the terminal time. First, similar to Section 2.2.1, the following conditions must be met before starting the controller design [21]:

Condition 1: $\mathbf{f}(\mathbf{x})$ is a continuously differentiable vector-valued function of $\mathbf{x}(t)$.

Condition 2: The origin $\mathbf{x} = \mathbf{0}$ is an equilibrium point of the system with $\mathbf{u} = \mathbf{0}$.

Condition 3: $\mathbf{Q}(\mathbf{x})$ is a symmetric positive semi-definite matrix, and $\mathbf{R}(\mathbf{x})$ is a sym-

metric positive definite matrix.

Condition 4: $\mathbf{A}(\mathbf{x})$ and $\mathbf{B}(\mathbf{x})$ must be chosen in such a way that the nonlinear system is *controllable* or at least *stabilizable*. $\mathbf{A}(\mathbf{x})$ and $\mathbf{C}(\mathbf{x})$ must be chosen in such a way that the nonlinear system is *observable* or at least *detectable*.

By following the LQR formulation, the state-feedback controller is obtained in the form

$$\mathbf{u}(\mathbf{x}) = -\mathbf{R}^{-1}(\mathbf{x})\mathbf{B}'(\mathbf{x})[\mathbf{P}(\mathbf{x})\mathbf{x}(t) - \mathbf{g}(\mathbf{x})]. \tag{2.3.6}$$

$\mathbf{P}(\mathbf{x})$ is a positive-definite solution of the continuous-time algebraic SDRE

$$\mathbf{P}(\mathbf{x})\mathbf{A}(\mathbf{x}) + \mathbf{A}'(\mathbf{x})\mathbf{P}(\mathbf{x}) - \mathbf{P}(\mathbf{x})\mathbf{B}(\mathbf{x})\mathbf{R}^{-1}(\mathbf{x})\mathbf{B}'(\mathbf{x})\mathbf{P}(\mathbf{x}) + \mathbf{C}'(\mathbf{x})\mathbf{Q}(\mathbf{x})\mathbf{C}(\mathbf{x}) = 0, \tag{2.3.7}$$

and $\mathbf{g}(\mathbf{x})$ is a solution of the continuous-time state dependent non-homogeneous equation

$$\mathbf{g}(\mathbf{x}) = -\left([\mathbf{A}(\mathbf{x}) - \mathbf{B}(\mathbf{x})\mathbf{R}^{-1}(\mathbf{x})\mathbf{B}'(\mathbf{x})\mathbf{P}(\mathbf{x})]'\right)^{-1}\mathbf{C}'(\mathbf{x})\mathbf{Q}(\mathbf{x})\mathbf{z}(\mathbf{x}). \tag{2.3.8}$$

The resulting algebraic SDRE-derived trajectory is the solution of the closed-loop dynamics

$$\dot{\mathbf{x}}(t) = [\mathbf{A}(\mathbf{x}) - \mathbf{B}(\mathbf{x})\mathbf{R}^{-1}(\mathbf{x})\mathbf{B}'(\mathbf{x})\mathbf{P}(\mathbf{x})]\mathbf{x}(t) + \mathbf{B}(\mathbf{x})\mathbf{R}^{-1}(\mathbf{x})\mathbf{B}'(\mathbf{x})\mathbf{g}(\mathbf{x}). \tag{2.3.9}$$

Fig.2.4 shows a flow chart of the infinite-horizon algebraic SDRE tracking. At each sample time, the following procedure is accomplished. First, the current state vector $\mathbf{x}(t)$ is used to calculate numerical values for $\mathbf{A}(\mathbf{x})$, $\mathbf{B}(\mathbf{x})$, and $\mathbf{C}(\mathbf{x})$. Then, using the LQT equations, $\mathbf{P}(\mathbf{x})$ and $\mathbf{g}(\mathbf{x})$ are calculated. Control input $\mathbf{u}(\mathbf{x})$ is then calculated and applied to the system. This procedure is then repeated at the next sample time.

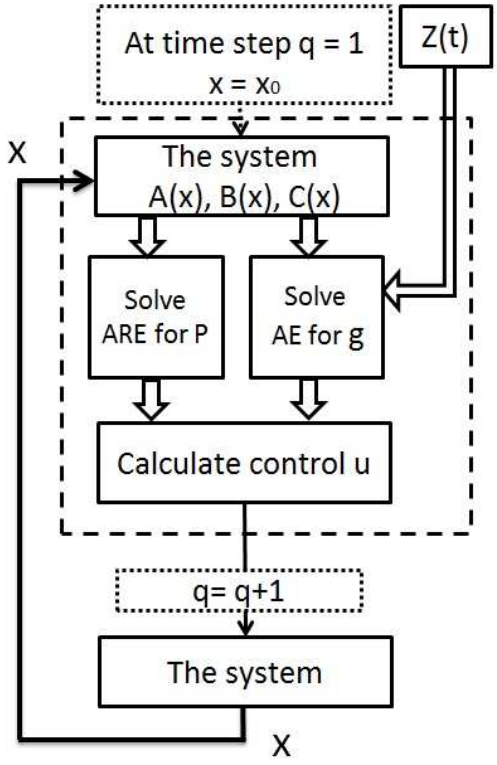

Figure 2.4: Flow Chart of Infinite-Horizon Algebraic SDRE Tracking

2.3.2 Infinite-Horizon Algebraic SDRE Tracking Simulation: Forced Damped Pendulum

This section presents simulations with the infinite-time horizon optimal tracking controller for forced damped pendulum with different reference (commanded) outputs. The dynamic equation for forced damped pendulum is:

$$ml^2\ddot{\theta} \quad = \quad -mglsin(\theta) - k\dot{\theta} + T, \tag{2.3.10}$$

where, θ is the angle of pendulum, l is the length of rod, m is the mass of pendulum, g is the gravitational constant, k is the damping (friction) constant, T is the driving torque.

The system nonlinear state equations can be written in the form:

$$\begin{aligned} \dot{x_1} &= x_2, && (2.3.11)\\ \dot{x_2} &= -\frac{g}{l}sin(x_1) - \frac{k}{ml^2}x_2 + \frac{1}{ml^2}u, && (2.3.12)\\ y &= x_1, && (2.3.13) \end{aligned}$$

where: $\theta = x_1$, $\dot{\theta} = x_2$, and $T = u$. Or in state dependent form:

$$\begin{aligned} \begin{bmatrix} \dot{x_1} \\ \dot{x_2} \end{bmatrix} &= \begin{bmatrix} 0 & 1 \\ \frac{-4.9sin(x_1)}{x_1} & -0.25 \end{bmatrix} \begin{bmatrix} x_1 \\ x_2 \end{bmatrix} + \begin{bmatrix} 0 \\ 0.25 \end{bmatrix} u, && (2.3.14)\\ y(t) &= \begin{bmatrix} 1 & 0 \end{bmatrix} \begin{bmatrix} x_1 \\ x_2 \end{bmatrix}, && (2.3.15) \end{aligned}$$

where $\mathbf{A} = \begin{bmatrix} 0 & 1 \\ -4.9sin(x_1)/x_1 & -0.25 \end{bmatrix}$, $\mathbf{B} = \begin{bmatrix} 0 \\ 0.25 \end{bmatrix}$, $\mathbf{C} = \begin{bmatrix} 1 & 0 \end{bmatrix}$.

Let Us select weighted matrices as

$$\mathbf{Q} = diag(100, 0), \quad \mathbf{R} = 0.01, \tag{2.3.16}$$

and, let the reference output as

$$z(t) = t^3 - t + 5. \tag{2.3.17}$$

The simulations are performed for 500 time steps and the resulting output trajectory is shown in Fig. 2.5, and the optimal control is shown in Fig. 2.6. In Fig. 2.5, the solid line denotes the actual output trajectory and the doted line denotes the reference output trajectory. Comparing trajectories in Fig. 2.5, it's clear that the infinite-horizon algebraic SDRE nonlinear tracking algorithm gives very good results

as the actual optimal output is making very good tracking to the reference output.

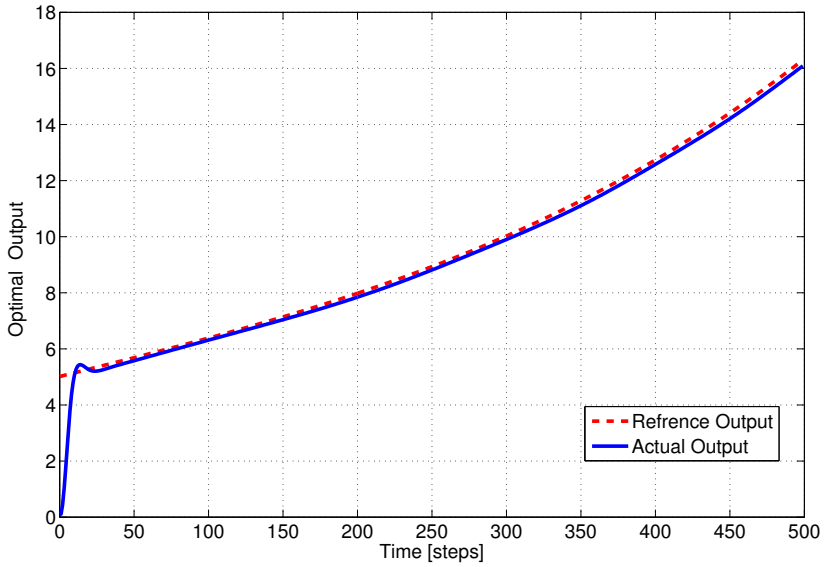

Figure 2.5: Optimal Output for Forced Damped Pendulum with Cubic Polynomial Reference

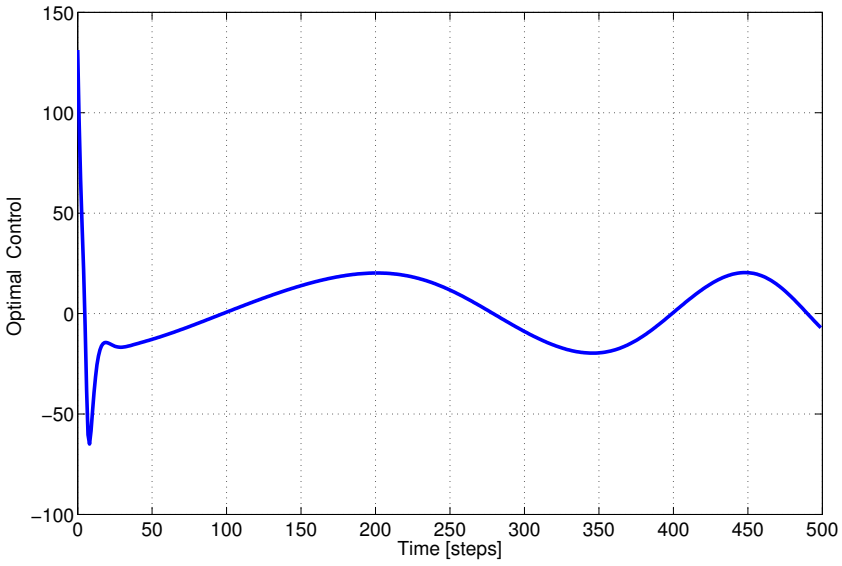

Figure 2.6: Optimal Control for Forced Damped Pendulum with Cubic Polynomial Reference

2.4 Conclusions

The Algebraic State Dependent Riccati Equation (SDRE) provide an extremely effective algorithm for nonlinear feedback control design by allowing nonlinearities in the system states while additionally offering great design flexibility through design matrices. The algebraic SDRE method involves factorization of the nonlinear dynamics into product of State Dependent Coefficient (SDC) matrices and state vector. Thus, the algebraic SDRE algorithm captures the nonlinearities of the system, transforming the original nonlinear system to a linear-like structure with SDC matrices, and minimizing a non-quadratic performance index with a quadratic-like structure. The Algebraic Riccati Equation (ARE) using the SDC matrices is then solved online to give the sub optimum control law, and with enough time sample points, the suboptimal solution can be made to be very close to optimal solution. As the algebraic SDRE depends only on the current state, the computation can be carried out online, in which case the algebraic SDRE is defined along the state trajectory. In addition, the main advantage of the algebraic SDRE is the flexibility to make tradeoffs between control effort and state errors by tuning the SDC.

Chapter 3

Infinite-Horizon Algebraic State Dependent Riccati Equation (SDRE) for Stochastic Systems

The estimation of states in a system is an essential problem for control. The estimated states might be needed to control the system, e.g. the aerospace engineer needs to estimate the velocity of a satellite in order to control its orbit, or the estimated state itself is the point of interest, e.g. to estimate the position of a satellite in order to schedule the future mission of that satellite [121]. Kalman filter is a well-known effective state estimator that estimates the unmeasured states corrupted with noise. The standard Kalman filter is limited only to *linear* systems. However, the Extended Kalman filter (EKF) estimates the *linearized* (using Taylor series) states of the original nonlinear system.

The need to improve performance in control systems leads to more accurate modeling. However, if a model is a good representation of the real system over a wide range of operating points, it is most often nonlinear. Therefore, the ordinarily used linear filter techniques become inadequate and it becomes necessary to explore some other

nonlinear filter techniques. Most of nonlinear filters deal with the nonlinear system after linearization, i.e first to linearize the nonlinear system in a small region around the operating point (using Taylor series), then to estimate the unmeasured linearized states. The key assumption is that the range of operation is small for the linearized model to be valid. As a result, the filter will only be effective in the small vicinity of the operating points, and the accuracy of this technique will decrease for large operating range of nonlinear systems [24].

3.1 Standard Kalman Filter

The Kalman filter is basically an optimal state estimator which uses the input and measured output corrupted with noise and minimizes the mean-squared error between the true value and estimated value of the state of a stochastic system composed of a process model and measurement model subjected to process and measurement noises, respectively. We first focus on the development of the continuous-time Kalman filter for linear systems subject to plant and measurement noises.

Consider the linear, continuous-time, stochastic system with dynamic model:

$$\dot{\mathbf{x}}(t) = \mathbf{A}(t)\mathbf{x}(t) + \mathbf{B}(t)\mathbf{u}(t) + \mathbf{B}_w(t)\mathbf{w}(t), \tag{3.1.1}$$

$$\mathbf{y}(t) = \mathbf{C}(t)\mathbf{x}(t) + \mathbf{v}(t), \tag{3.1.2}$$

where, $\mathbf{w}(t)$ and $\mathbf{v}(t)$ are process, and measurement (white, Gaussian) random noises with zero mean (i.e., $\bar{\mathbf{w}}(t) = \bar{\mathbf{v}}(t) = 0$) and covariances $\mathbf{Q}_w(t)$ and $\mathbf{R}_v(t)$, respectively, and assumed to be *uncorrelated* (see Fig. 3.1).

The estimated state $\hat{\mathbf{x}}(t)$ is given by

$$\dot{\hat{\mathbf{x}}}(t) = \mathbf{A}(t)\hat{\mathbf{x}}(t) + \mathbf{B}(t)\mathbf{u}(t) + \mathbf{K}_e(t)\left[\mathbf{y}(t) - \mathbf{C}(t)\hat{\mathbf{x}}(t)\right]; \tag{3.1.3}$$

$$\dot{\hat{\mathbf{x}}}(t) = \left[\mathbf{A}(t) - \mathbf{K}_e(t)\mathbf{C}(t)\right]\hat{\mathbf{x}}(t) + \mathbf{B}(t)\mathbf{u}(t) + \mathbf{K}_e(t)\mathbf{y}(t), \tag{3.1.4}$$

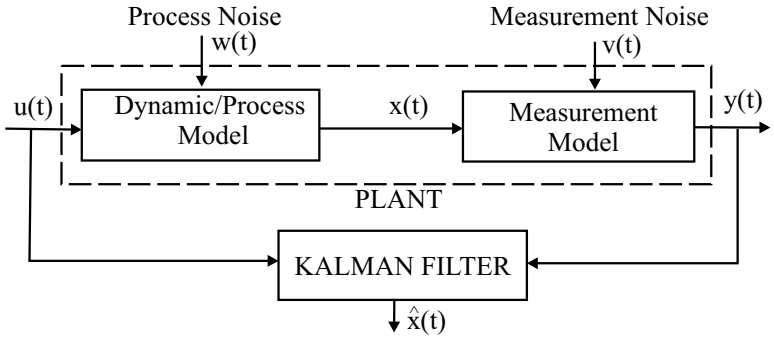

Figure 3.1: Summarized Linear Continuous-Time Kalman Filter

where, $\mathbf{K}_e(t)$ is the estimator gain, $\hat{\mathbf{x}}(t)$ is the *state estimate* with initial value

$$\mathcal{E}\{\mathbf{x}(t=0)\} = \bar{\mathbf{x}}(t_0) = \hat{\mathbf{x}}(t_0). \tag{3.1.5}$$

$\mathcal{E}$ stands for *expected, average or mean value* and considered intuitively equal to the *estimate*.

Let us define the error $\mathbf{e}(t)$ between the true or actual state $\mathbf{x}(t)$ and the state estimate $\hat{\mathbf{x}}(t)$ as

$$\mathbf{e}(t) = \mathbf{x}(t) - \hat{\mathbf{x}}(t), \tag{3.1.6}$$

$$\dot{\mathbf{e}}(t) = \dot{\mathbf{x}}(t) - \dot{\hat{\mathbf{x}}}(t). \tag{3.1.7}$$

Substituting (3.1.1) and (3.1.4) in (3.1.7)

$$\dot{\mathbf{e}}(t) = \mathbf{A}(t)\mathbf{e}(t) + \mathbf{K}_e(t)\mathbf{C}(t)\mathbf{e}(t) + \mathbf{B}_w(t)\mathbf{w}(t) - \mathbf{K}_e(t)\mathbf{v}(t); \tag{3.1.8}$$

$$\dot{\mathbf{e}}(t) = [\mathbf{A}(t) - \mathbf{K}_e(t)\mathbf{C}(t)]\,\mathbf{e}(t) + \mathbf{B}_{wk}(t)\mathbf{z}_{wk}(t), \tag{3.1.9}$$

where

$$\mathbf{B}_{wk}(t) = [\mathbf{B}_w(t) \quad -\mathbf{K}_e(t)], \quad \mathbf{z}_{wk} = [\mathbf{w}(t) \;\; \mathbf{v}(t)]'. \tag{3.1.10}$$

Using the results from [120] on propagation of state vector

$$\dot{\mathbf{x}}(t) = \mathbf{A}(t)\mathbf{x}(t) + \mathbf{B}(t)\mathbf{u}(t) + \mathbf{B}_w(t)\mathbf{w}(t), \tag{3.1.11}$$

and the corresponding state estimate error covariance $\mathbf{P}_e(t)$ can be calculated from

$$\dot{\mathbf{P}}_e(t) = \mathbf{A}(t)\mathbf{P}_e(t) + \mathbf{P}_e(t)\mathbf{A}'(t) + \mathbf{B}_w(t)\mathbf{Q}_w(t)\mathbf{B}'_w(t). \tag{3.1.12}$$

Now, using the result (3.1.12) for the error dynamics (3.1.9)

$$\begin{aligned}\dot{\mathbf{P}}_e(t) = {} & [\mathbf{A}(t) - \mathbf{K}_e(t)\mathbf{C}(t)]\,\mathbf{P}_e(t) + \mathbf{P}_e(t)\,[\mathbf{A}(t) - \mathbf{K}_e(t)\mathbf{C}(t)]' \\ & + [\mathbf{B}_w(t) \quad -\mathbf{K}_e(t)] \begin{bmatrix} \mathbf{Q}_w(t) \\ \mathbf{R}_v(t) \end{bmatrix} [\mathbf{B}_w(t) \quad -\mathbf{K}_e(t)]'; \qquad (3.1.13) \\ \dot{\mathbf{P}}_e(t) = {} & [\mathbf{A}(t) - \mathbf{K}_e(t)\mathbf{C}(t)]\,\mathbf{P}_e(t) + \mathbf{P}_e(t)\,[\mathbf{A}(t) - \mathbf{K}_e(t)\mathbf{C}(t)]' \\ & + [\mathbf{B}_w(t)\mathbf{Q}_w(t)\mathbf{B}'_w(t) + \mathbf{K}_e(t)\mathbf{R}_v(t)\mathbf{K}'_e(t), \qquad (3.1.14)\end{aligned}$$

where, $\mathbf{P}_e = \mathbf{P}_e(t) = \mathcal{E}\{[\mathbf{x}(t) - \hat{\mathbf{x}}(t)]\,[\mathbf{x}(t) - \hat{\mathbf{x}}(t)]'\}$ is to be solved in *forward* direction of time with initial condition

$$\mathbf{P}_{e0} = \mathbf{P}_e(t_0) = \mathcal{E}\{[\mathbf{x}(t_0) - \hat{\mathbf{x}}(t_0)]\,[\mathbf{x}(t_0) - \hat{\mathbf{x}}(t_0)]'\}. \tag{3.1.15}$$

We have the relation on $\mathbf{K}_e(t)$ for minimum error variance as

$$\mathbf{K}_e(t) = \mathbf{P}_e(t)\mathbf{C}'(t)\mathbf{R}_v^{-1}(t). \tag{3.1.16}$$

Using the optimal Kalman gain (3.1.16) in the covariance relation (3.1.14), we get

$$\dot{\mathbf{P}}_e(t) = \mathbf{A}(t)\mathbf{P}_e(t) + \mathbf{P}_e(t)\mathbf{A}'(t) - \mathbf{P}_e(t)\mathbf{C}'(t)\mathbf{R}_v^{-1}(t)\mathbf{C}(t)\mathbf{P}_e(t) + \mathbf{B}_w(t), \mathbf{Q}_w(t)\mathbf{B}'_w(t), \tag{3.1.17}$$

with initial condition $\mathbf{P}_e(t=0) = \mathbf{P}_{e0}$.

This is called the continuous-time differential Riccati equation (CDRE) arising in optimal state estimation. Fig. 3.2 shows a structure of the detailed standard linear continuous-time Kalman filter.

3.2 Infinite-Horizon Regulator for Nonlinear Stochastic Systems

3.2.1 Optimal Estimation

Let us suppose that the entire state $\mathbf{x}(t)$ is not available, but only the output $\mathbf{y}(t)$ is measurable. For the sake of convenience we reproduce the nonlinear system with noises in state dependent form

$$\dot{\mathbf{x}}(t) = \mathbf{A}(\mathbf{x})\mathbf{x}(t) + \mathbf{B}(\mathbf{x})\mathbf{u}(t) + \mathbf{B}_w(t)\mathbf{w}(t), \tag{3.2.1}$$

$$\mathbf{y}(t) = \mathbf{C}(\mathbf{x})\mathbf{x}(t) + \mathbf{v}(t), \tag{3.2.2}$$

where, $\mathbf{w}(t)$ and $\mathbf{v}(t)$ are process, and measurement (white, Gaussian, zero mean) random noises, respectively.

In order to find the best estimate $\hat{\mathbf{x}}(t)$ and the corresponding state estimator error covariance matrix $\mathbf{P}_e(\hat{\mathbf{x}}, t)$, we use the results of Section 3.1. At each time step, the

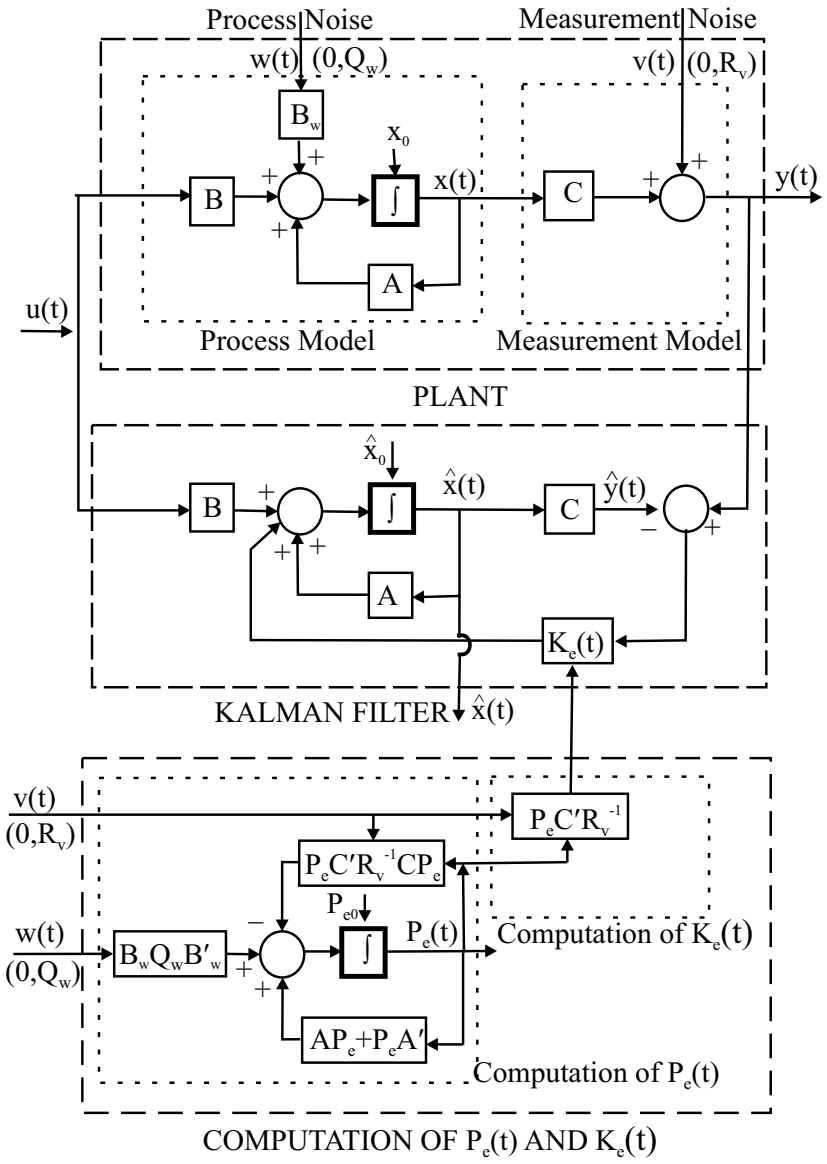

Figure 3.2: Detailed Linear Continuous-Time Kalman Filter

filter (estimate) equations are

$$\dot{\hat{\mathbf{x}}}(t) = \mathbf{A}(\hat{\mathbf{x}})\hat{\mathbf{x}}(t) + \mathbf{B}(\hat{\mathbf{x}})\mathbf{u}(t) + \mathbf{K}_e(\hat{\mathbf{x}}, t)[\mathbf{y}(t) - \mathbf{C}(\hat{\mathbf{x}})\hat{\mathbf{x}}(t)]; \tag{3.2.3}$$

$$\hat{\mathbf{x}}(t_0) = \bar{\mathbf{x}}(t_0),$$

where, $\mathbf{K}_e(\hat{\mathbf{x}}, t)$, the optimal Kalman estimator (filter) gain, is obtained as

$$\mathbf{K}_e(\hat{\mathbf{x}}, t) = \mathbf{P}_e(\hat{\mathbf{x}}, t)\mathbf{C}'(\hat{\mathbf{x}})\mathbf{R}_v^{-1}(t), \tag{3.2.4}$$

and $\mathbf{P}_e(\hat{\mathbf{x}}, t)$ is the solution of the matrix algebraic Riccati equation

$$\begin{aligned} 0 = \mathbf{A}(\hat{\mathbf{x}})\mathbf{P}_e(\hat{\mathbf{x}}, t) + \mathbf{P}_e(\hat{\mathbf{x}}, t)\mathbf{A}'(\hat{\mathbf{x}}) + \mathbf{B}_w(t)\mathbf{Q}_w(t)\mathbf{B}_w'(t) \\ -\mathbf{P}_e(\hat{\mathbf{x}}, t)\mathbf{C}'(\hat{\mathbf{x}})\mathbf{R}_v^{-1}(t)\mathbf{C}(\hat{\mathbf{x}})\mathbf{P}_e(\hat{\mathbf{x}}, t), \end{aligned} \tag{3.2.5}$$

where $\mathbf{P}_e(\hat{\mathbf{x}}, t_0) = \mathbf{P}_{e0}$.

Note that we used subscript e for matrices $\mathbf{P}_e$ and $\mathbf{K}_e$ above to denote that they refer to the *estimation* problem and we designate the matrices $\mathbf{P}_c$ and $\mathbf{K}_c$ with the subscript c to denote that they refer to the *control* problem in stochastic control systems. The minimization of J is equivalent to minimization of

$$J_a(\mathbf{x}, u) = \mathcal{E}\left\{\frac{1}{2}\int_o^\infty [\hat{\mathbf{x}}'(t)\mathbf{Q}(\hat{\mathbf{x}})\hat{\mathbf{x}}(t) + \mathbf{u}'(\hat{\mathbf{x}}, t)\mathbf{R}(\hat{\mathbf{x}})\mathbf{u}(\hat{\mathbf{x}}, t)dt\right\}. \tag{3.2.6}$$

3.2.2 Optimal Regulation

At each time step, using the results of nonlinear regulator obtained in Section 2.2.1 (except that the state is now the optimal estimate $\hat{\mathbf{x}}(t)$) we get

$$\mathbf{u}(\hat{\mathbf{x}}, t) = -\mathbf{R}^{-1}(\hat{\mathbf{x}})\mathbf{B}'(\hat{\mathbf{x}})\mathbf{P}_c(\hat{\mathbf{x}}, t)\hat{\mathbf{x}}(t), \tag{3.2.7}$$

or, in terms of the optimal feedback control gain $\mathbf{K}_c(\hat{\mathbf{x}}, t)$

$$\mathbf{u}(\hat{\mathbf{x}}, t) \;=\; -\mathbf{K}_c(\hat{\mathbf{x}}, t)\hat{\mathbf{x}}(t), \tag{3.2.8}$$

where, $\mathbf{K}_c(\hat{\mathbf{x}}, t) = \mathbf{R}^{-1}(\hat{\mathbf{x}})\mathbf{B}'(\hat{\mathbf{x}})\mathbf{P}_c(\hat{\mathbf{x}}, t)$, is the Kalman (controller) gain, and $\mathbf{P}_c(\hat{\mathbf{x}}, t)$ is the solution of the algebraic SDRE

$$\mathbf{P_c}(\hat{\mathbf{x}})\mathbf{A}(\hat{\mathbf{x}}) + \mathbf{A}'(\hat{\mathbf{x}})\mathbf{P_c}(\hat{\mathbf{x}}) - \mathbf{P_c}(\hat{\mathbf{x}})\mathbf{B}(\hat{\mathbf{x}})\mathbf{R}^{-1}(\hat{\mathbf{x}})\mathbf{B}'(\hat{\mathbf{x}})P_c(\hat{\mathbf{x}}) + \mathbf{Q}(\hat{\mathbf{x}}) = 0. \tag{3.2.9}$$

The entire algorithm of combined optimal *estimation* and *control* leading to nonlinear regulator problem is shown in Table 3.1, where we introduced the reference command $\mathbf{r}(t)$ for a more general treatment [99].

3.2.3 Infinite-Horizon Algebraic SDRE Regulation for Stochastic Systems Simulation: Van der Pol's Oscillator

This section presents simulations with the finite-time horizon, optimal regulator controller and noise cancellation for Van der Pol's oscillator. The dynamic equations of the Van der Pol's oscillator are

$$\dot{x_1} \;=\; x_2, \tag{3.2.10}$$

$$\dot{x_2} \;=\; (1 - {x_1}^2)x_2 - x_1 + u, \tag{3.2.11}$$

Table 3.1: Incomplete State Information Solution of Continuous-Time Regulator Problem

Statement of the Problem	
Given the process as $\dot{\mathbf{x}}(t) = \mathbf{A}(\mathbf{x})\mathbf{x}(t) + \mathbf{B}(\mathbf{x})\mathbf{u}(t) + \mathbf{B}_w(t)\mathbf{w}(t)$, the observation of the state as $\mathbf{y}(t) = \mathbf{C}(\mathbf{x})\mathbf{x}(t) + \mathbf{v}(t)$, the performance measure for estimate as $J(t) = \text{trace}\,[var[\tilde{\mathbf{x}}(t)]] + \text{trace}[\mathbf{P}_e(t)]$, the conditions as $\mathcal{E}[\mathbf{w}(t)] = 0, \quad \text{COV}[\mathbf{w}(t), \mathbf{w}(\tau)] = \mathbf{Q}_w(t)\delta(t-\tau), \quad \mathcal{E}[\mathbf{x}(t_0)] = \bar{\mathbf{x}}_0,$ $\text{VAR}[\mathbf{x}(t_0)] = \mathbf{P}_0; \quad \text{COV}[\mathbf{x}(t), \mathbf{w}(\tau)] = 0 \quad \text{for all } \tau > t,$ $E[\mathbf{v}(t)] = 0, \quad COV[\mathbf{v}(t), \mathbf{v}(\tau)] = \mathbf{R}_v(t)\delta(t-\tau),$ $COV[\mathbf{v}(t), \mathbf{w}(\tau)] = 0, \quad COV[\mathbf{v}(t), \mathbf{x}(\tau)] = 0 \text{ for all } t, \tau,$ and the performance measure for control as $\hat{J}(\mathbf{x}_0, t_0) = \mathcal{E}\left\{\frac{1}{2}\int_o^\infty [\mathbf{x}'(t)\mathbf{Q}(\mathbf{x})\mathbf{x}(t) + \mathbf{u}'(\mathbf{x})\mathbf{R}(\mathbf{x})\mathbf{u}(\mathbf{x})]\right\} dt$ find the optimal estimator and controller	
Solution of the Problem I: Optimal Estimator/Kalman Filter	
Step 1	At each time step, solve the matrix differential Riccati equation $0 = \mathbf{A}(\hat{\mathbf{x}})\mathbf{P}_e(\hat{\mathbf{x}}, t) + \mathbf{P}_e(\hat{\mathbf{x}}, t)\mathbf{A}'(\hat{\mathbf{x}}) + \mathbf{B}_w(t)\mathbf{Q}_w(t)\mathbf{B}_w'(t) -$ $\mathbf{P}_e(\hat{\mathbf{x}}, t)\mathbf{C}'(\hat{\mathbf{x}})\mathbf{R}_v^{-1}(t)\mathbf{C}(\hat{\mathbf{x}})\mathbf{P}_e(\hat{\mathbf{x}}, t); \quad \mathbf{P}_e(\hat{\mathbf{x}}, t_0) = \mathbf{P}_{e0}.$
Step 2	Using $\mathbf{P}_e(\hat{\mathbf{x}}, t)$ from Step 1, obtain the optimal estimator (filter) gain as $\mathbf{K}_e(\hat{\mathbf{x}}, t) = \mathbf{P}_e(\hat{\mathbf{x}}, t)\mathbf{C}'(\hat{\mathbf{x}})\mathbf{R}_v^{-1}(t).$
Step 3	Using $\mathbf{K}_e(\hat{\mathbf{x}}, t)$ from Step 2, solve the optimal state estimate $\hat{\mathbf{x}}(t)$ from $\dot{\hat{\mathbf{x}}}(t) = \mathbf{A}(\hat{\mathbf{x}})\hat{\mathbf{x}}(t) + \mathbf{B}(\hat{\mathbf{x}})\mathbf{u}(t) + \mathbf{K}_e(\hat{\mathbf{x}}, t)[\mathbf{y}(t) - \mathbf{C}(\hat{\mathbf{x}})\hat{\mathbf{x}}(t)]; \quad \hat{\mathbf{x}}(t_0) = \bar{\mathbf{x}}_0.$
Solution of the Problem II: Optimal Controller	
Step 4	At each time step, calculate the value of $\mathbf{P}_c(\hat{\mathbf{x}}, t)$ from the LQR equation $\mathbf{P_c}(\hat{\mathbf{x}}, \mathbf{t}) = \mathbf{P_{ss}}(\hat{\mathbf{x}}),$
Step 5	Using $\mathbf{P}_c(\hat{\mathbf{x}}, t)$ from Step 4, obtain the optimal controller gain as $\mathbf{K}_c(\hat{\mathbf{x}}, t) = \mathbf{R}^{-1}(\hat{\mathbf{x}})\mathbf{B}'(\hat{\mathbf{x}})\mathbf{P}_c(\hat{\mathbf{x}}, t).$
Step 6	Using $\mathbf{K}(\hat{\mathbf{x}}, t)$ from Step 5, obtain the closed-loop optimal control as $\mathbf{u}(\hat{\mathbf{x}}, t) = -\mathbf{K}_c(\hat{\mathbf{x}}, t)\hat{\mathbf{x}}(t).$

with the initial conditions

$$\mathbf{x_0} = [5, -3]'. \tag{3.2.12}$$

The selected weighted matrices are

$$\mathbf{Q} = diag(50, 50), \quad \mathbf{R} = 1. \tag{3.2.13}$$

The covariances of the noises have been taken as

$$\mathbf{Q_w} = diag(1, 1), \quad \mathbf{R_v} = 10. \tag{3.2.14}$$

The simulations are performed for a time interval of 30 seconds with 300 time steps and the resulting states trajectories is shown in Fig. 3.3 and Fig. 3.4, the resulting optimal control trajectory is shown in Fig. 3.5, the error between the actual and the estimated state is shown in Fig. 3.6.

Note that for the sake of validity of the proposed technique, a comparison between the *estimated* (with noise), and the *actual* (with filtered noise) states was done. The solid line denotes the estimated trajectory of the state, the dashed line denotes the actual trajectory. It can be noted that the algorithm gives very good results as the estimated state is very close to the actual state. As shown in Fig. 3.6 the error between the actual and the estimated state is very small, the average error for this example is 0.03%.

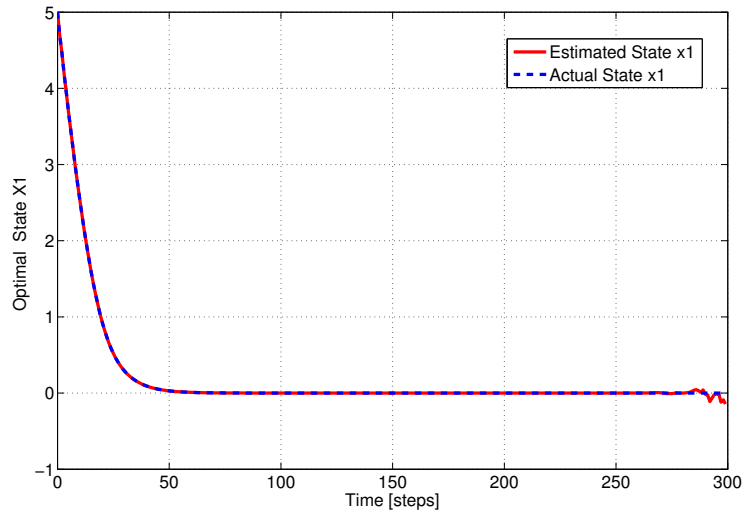

Figure 3.3: Optimal State x_1 for the Van der Pol's Oscillator

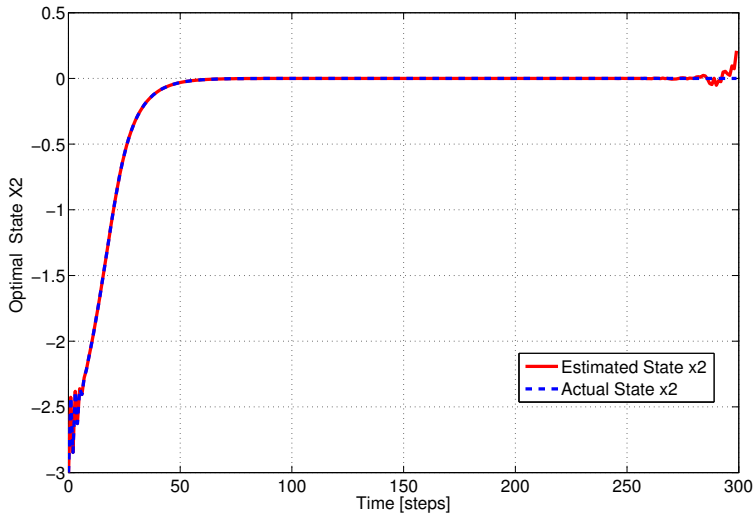

Figure 3.4: Optimal State x_2 for the Van der Pol's Oscillator

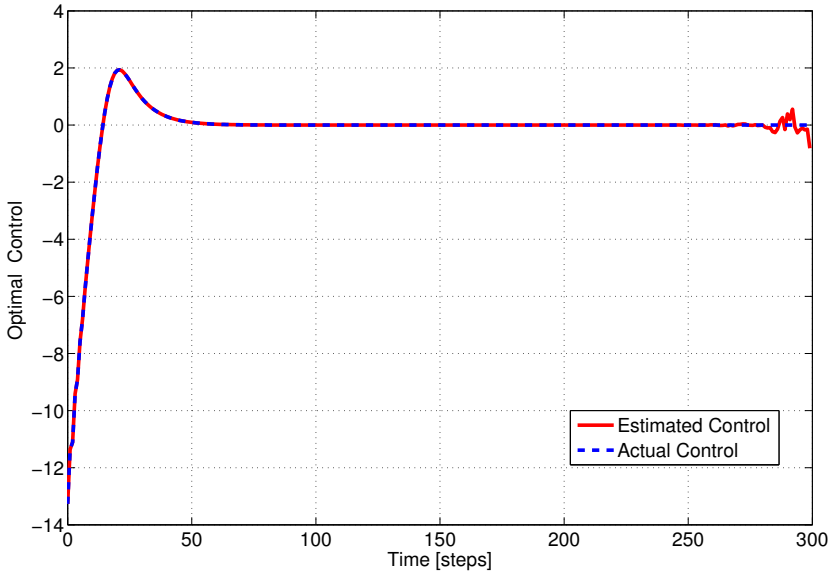

Figure 3.5: Optimal Control for the Van der Pol's Oscillator

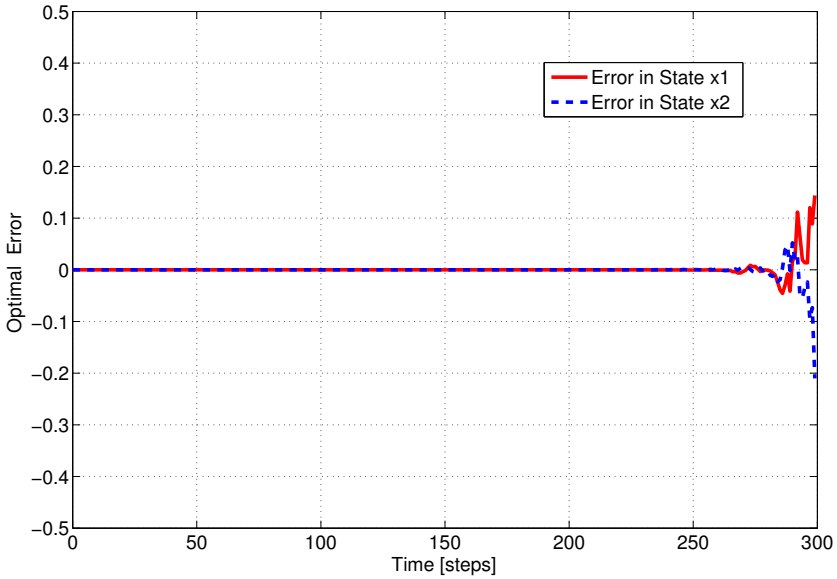

Figure 3.6: Error Signals for the Van der Pol's Oscillator

3.3 Infinite-Horizon Tracking for Nonlinear Stochastic Systems

3.3.1 Optimal Estimation

Let us reproduce the nonlinear system with noises in state dependent form

$$\dot{\mathbf{x}}(t) = \mathbf{A}(\mathbf{x})\mathbf{x}(t) + \mathbf{B}(\mathbf{x})\mathbf{u}(t) + \mathbf{B}_w(t)\mathbf{w}(t), \tag{3.3.1}$$

$$\mathbf{y}(t) = \mathbf{C}(\mathbf{x})\mathbf{x}(t) + \mathbf{v}(t), \tag{3.3.2}$$

where, $\mathbf{w}(t)$ and $\mathbf{v}(t)$ are process, and measurement (white, Gaussian) random noises with zero mean, respectively. In order to find the best estimate $\hat{\mathbf{x}}(t)$ and the corresponding covariance matrix $\mathbf{P}_e(\hat{\mathbf{x}}, t)$, we use the results of Section 3.1. At each time step, the *estimate* equations are

$$\dot{\hat{\mathbf{x}}}(t) = \mathbf{A}(\hat{\mathbf{x}})\hat{\mathbf{x}}(t) + \mathbf{B}(\hat{\mathbf{x}})\mathbf{u}(t) + \mathbf{K}_e(\hat{\mathbf{x}}, t)[\mathbf{y}(t) - \mathbf{C}(\hat{\mathbf{x}})\hat{\mathbf{x}}(t)], \;\; \hat{\mathbf{x}}(t_0) = \bar{\mathbf{x}}(t_0), \tag{3.3.3}$$

where, $\mathbf{K}_e(\hat{\mathbf{x}}, t)$, the optimal Kalman *estimator gain*, is obtained as

$$\mathbf{K}_e(\hat{\mathbf{x}}, t) = \mathbf{P}_e(\hat{\mathbf{x}}, t)\mathbf{C}'(\hat{\mathbf{x}})\mathbf{R}_v^{-1}(t), \tag{3.3.4}$$

and $\mathbf{P}_e(\hat{\mathbf{x}}, t)$ is the solution of the matrix algebraic Riccati equation

$$0 = \mathbf{A}(\hat{\mathbf{x}})\mathbf{P}_e(\hat{\mathbf{x}}, t) + \mathbf{P}_e(\hat{\mathbf{x}}, t)\mathbf{A}'(\hat{\mathbf{x}}) + \mathbf{B}_w(t)\mathbf{Q}_w(t)\mathbf{B}'_w(t)$$
$$-\mathbf{P}_e(\hat{\mathbf{x}}, t)\mathbf{C}'(\hat{\mathbf{x}})\mathbf{R}_v^{-1}(t)\mathbf{C}(\hat{\mathbf{x}})\mathbf{P}_e(\hat{\mathbf{x}}, t), \tag{3.3.5}$$

where $\mathbf{P}_e(\hat{\mathbf{x}}, t_0) = \mathbf{P}_{e0}$.

The minimization of the cost function J is equivalent to minimization of

$$J_a(\mathbf{x}, u) = \mathcal{E}\left\{\frac{1}{2}\int_0^\infty [\hat{\mathbf{e}}'(t)\mathbf{Q}(\hat{\mathbf{x}})\hat{\mathbf{e}}(t) + \mathbf{u}'(\hat{\mathbf{x}}, t)\mathbf{R}(\hat{\mathbf{x}})\mathbf{u}(\hat{\mathbf{x}}, t)dt\right\}, \tag{3.3.6}$$

where $\hat{\mathbf{e}}(t) = \mathbf{z}(t) - \mathbf{C}(\hat{\mathbf{x}})\hat{\mathbf{x}}(t)$.

3.3.2 Optimal Tracking

At each time step, using the results of nonlinear tracking obtained in Section 2.3.1 (except that the state is now the optimal estimate $\hat{\mathbf{x}}(t)$) we get

$$\mathbf{u}(\hat{\mathbf{x}}, t) = -\mathbf{R}^{-1}(\hat{\mathbf{x}})\mathbf{B}'(\hat{\mathbf{x}})[\mathbf{P}_c(\hat{\mathbf{x}}, t)\hat{\mathbf{x}}(t) - \mathbf{g}(\hat{\mathbf{x}}, t)], \tag{3.3.7}$$

where, $\mathbf{P_c}(\mathbf{x})$ is a positive-definite solution of the continuous-time algebraic SDRE

$$\mathbf{P_c}(\hat{\mathbf{x}})\mathbf{A}(\hat{\mathbf{x}}) + \mathbf{A}'(\hat{\mathbf{x}})\mathbf{P_c}(\hat{\mathbf{x}}) - \mathbf{P_c}(\hat{\mathbf{x}})\mathbf{B}(\hat{\mathbf{x}})\mathbf{R}^{-1}(\hat{\mathbf{x}})\mathbf{B}'(\hat{\mathbf{x}})\mathbf{P_c}(\hat{\mathbf{x}}) + \mathbf{C}'(\hat{\mathbf{x}})\mathbf{Q}(\hat{\mathbf{x}})\mathbf{C}(\hat{\mathbf{x}}) = 0, \tag{3.3.8}$$

and $\mathbf{g}(\mathbf{x})$ is a solution of the continuous-time state dependent non-homogeneous equation

$$\mathbf{g}(\hat{\mathbf{x}}) = -\left([\mathbf{A}(\hat{\mathbf{x}}) - \mathbf{B}(\hat{\mathbf{x}})\mathbf{R}^{-1}(\hat{\mathbf{x}})\mathbf{B}'(\hat{\mathbf{x}})\mathbf{P}_c(\hat{\mathbf{x}})]'\right)^{-1}\mathbf{C}'(\hat{\mathbf{x}})\mathbf{Q}(\hat{\mathbf{x}})z(\hat{\mathbf{x}}), \tag{3.3.9}$$

The entire algorithm of the combined optimal *estimation* and *control* leading to non-linear tracking problem is shown in Table 3.2.

Table 3.2: Incomplete State Information Solution of Continuous-Time Tracking Problem

Statement of the Problem	
Given the process as $\dot{\mathbf{x}}(t) = \mathbf{A}(\mathbf{x})\mathbf{x}(t) + \mathbf{B}(\mathbf{x})\mathbf{u}(t) + \mathbf{B}_w(t)\mathbf{w}(t)$, the observation of the state as $\mathbf{y}(t) = \mathbf{C}(\mathbf{x})\mathbf{x}(t) + \mathbf{v}(t)$, the performance measure for estimate as $J(t) = \text{trace}\left[var[\tilde{\mathbf{x}}(t)]\right] + \text{trace}[\mathbf{P}_e(t)]$, the conditions as $\mathcal{E}[\mathbf{w}(t)] = 0, \quad \text{COV}[\mathbf{w}(t), \mathbf{w}(\tau)] = \mathbf{Q}_w(t)\delta(t-\tau), \quad \mathcal{E}[\mathbf{x}(t_0)] = \bar{\mathbf{x}}_0,$ $\text{VAR}[\mathbf{x}(t_0)] = \mathbf{P}_0; \quad \text{COV}[\mathbf{x}(t), \mathbf{w}(\tau)] = 0 \quad \text{for all } \tau > t,$ $E[\mathbf{v}(t)] = 0, \quad COV[\mathbf{v}(t), \mathbf{v}(\tau)] = \mathbf{R}_v(t)\delta(t-\tau),$ $COV[\mathbf{v}(t), \mathbf{w}(\tau)] = 0, \quad COV[\mathbf{v}(t), \mathbf{x}(\tau)] = 0 \text{ for all } t, \tau,$ and the performance measure for control as $\hat{J}(\mathbf{x}_0, t_0) = \mathcal{E}\left\{\frac{1}{2}\int_0^\infty \left[\mathbf{e}'(t)\mathbf{Q}(\mathbf{x})\mathbf{e}(t) + \mathbf{u}'(\mathbf{x})\mathbf{R}(\mathbf{x})\mathbf{u}(\mathbf{x})\right]\right\} dt$ find the optimal estimator and controller	
Solution of the Problem I: Optimal Estimator/Kalman Filter	
Step 1	At each time step, solve the matrix differential Riccati equation $0 = \mathbf{A}(\hat{\mathbf{x}})\mathbf{P}_e(\hat{\mathbf{x}}, t) + \mathbf{P}_e(\hat{\mathbf{x}}, t)\mathbf{A}'(\hat{\mathbf{x}}) + \mathbf{B}_w(t)\mathbf{Q}_w(t)\mathbf{B}'_w(t) -$ $\mathbf{P}_e(\hat{\mathbf{x}}, t)\mathbf{C}'(\hat{\mathbf{x}})\mathbf{R}_v^{-1}(t)\mathbf{C}(\hat{\mathbf{x}})\mathbf{P}_e(\hat{\mathbf{x}}, t); \quad \mathbf{P}_e(\hat{\mathbf{x}}, t_0) = \mathbf{P}_{e0}.$
Step 2	Using $\mathbf{P}_e(\hat{\mathbf{x}}, t)$ from Step 1, obtain the optimal estimator (filter) gain as $\mathbf{K}_e(\hat{\mathbf{x}}, t) = \mathbf{P}_e(\hat{\mathbf{x}}, t)\mathbf{C}'(\hat{\mathbf{x}})\mathbf{R}_v^{-1}(t).$
Step 3	Using $\mathbf{K}_e(\hat{\mathbf{x}}, t)$ from Step 2, solve the optimal state estimate $\hat{\mathbf{x}}(t)$ from $\dot{\hat{\mathbf{x}}}(t) = \mathbf{A}(\hat{\mathbf{x}})\hat{\mathbf{x}}(t) + \mathbf{B}(\hat{\mathbf{x}})\mathbf{u}(t) + \mathbf{K}_e(\hat{\mathbf{x}}, t)[\mathbf{y}(t) - \mathbf{C}(\hat{\mathbf{x}})\hat{\mathbf{x}}(t)]; \quad \hat{\mathbf{x}}(t_0) = \bar{\mathbf{x}}_0.$
Solution of the Problem II: Optimal Controller	
Step 4	At each time step, calculate the value of $\mathbf{P}_c(\hat{\mathbf{x}})$ from the equation $\mathbf{P_c}(\hat{\mathbf{x}})\mathbf{A}(\hat{\mathbf{x}}) + \mathbf{A}'(\hat{\mathbf{x}})\mathbf{P_c}(\hat{\mathbf{x}}) - \mathbf{P}(\hat{\mathbf{x}})_\mathbf{c}\mathbf{B}(\hat{\mathbf{x}})\mathbf{R}^{-1}(\hat{\mathbf{x}})\mathbf{B}'(\hat{\mathbf{x}})\mathbf{P_c}(\hat{\mathbf{x}}) + \mathbf{C}'(\hat{\mathbf{x}})\mathbf{Q}(\hat{\mathbf{x}})\mathbf{C}(\hat{\mathbf{x}}) = 0,$
Step 5	Calculate the value of $\mathbf{g}(\mathbf{x})$ from the equation $\mathbf{g}(\hat{\mathbf{x}}) = -\left([\mathbf{A}(\hat{\mathbf{x}}) - \mathbf{B}(\hat{\mathbf{x}})\mathbf{R}^{-1}(\hat{\mathbf{x}})\mathbf{B}'(\hat{\mathbf{x}})\mathbf{P_c}(\hat{\mathbf{x}})]'\right)^{-1}\mathbf{C}'(\hat{\mathbf{x}})\mathbf{Q}(\hat{\mathbf{x}})\mathbf{z}(\hat{\mathbf{x}})$
Step 6	Obtain the closed-loop optimal control as $\mathbf{u}(\hat{\mathbf{x}}, t) = -\mathbf{R}^{-1}(\hat{\mathbf{x}})\mathbf{B}'(\hat{\mathbf{x}})[\mathbf{P}_c(\hat{\mathbf{x}}, t)\hat{\mathbf{x}}(t) - \mathbf{g}(\hat{\mathbf{x}}, t)].$

3.3.3 Infinite-Horizon Algebraic SDRE Tracking for Stochastic Systems Simulation: Inverted Pendulum

For numerical simulation and analysis, the developed estimation and optimal tracking technique is implemented for noise cancellation for an inverted pendulum controlled by DC motor, as shown in Fig. 3.7.

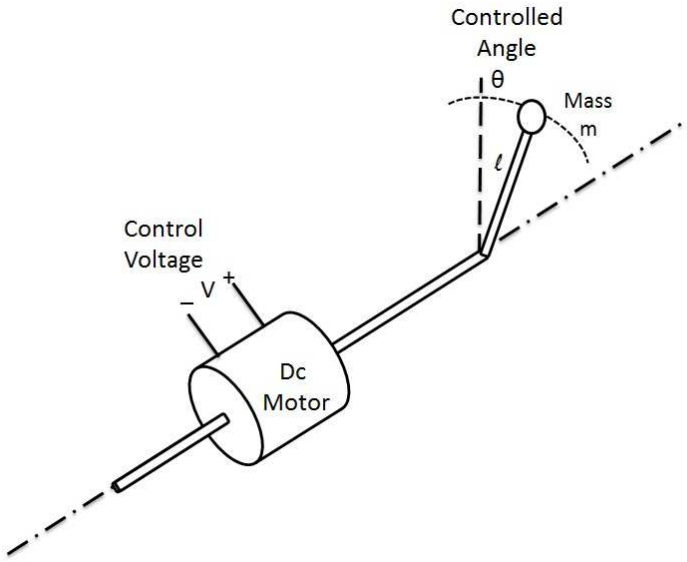

Figure 3.7: Inverted Pendulum Controlled by DC Motor

The dynamic equations for system

$$V(t) = L\frac{di(t)}{dt} + Ri(t) + k_b\frac{d\theta(t)}{dt}, \tag{3.3.10}$$

$$ml^2\frac{d^2\theta(t)}{dt^2} = -mglsin(\theta(t)) - k_m i(t), \tag{3.3.11}$$

where, V is the control voltage, L is the motor inductance, i is the current through the motor winding, R the motor winding resistance, k_b the motor's back electro magnetic force constant, θ the angle of pendulum, m the mass of pendulum, l the length of rod, g the gravitational constant, and k_m the damping (friction) constant.

The nonlinear state equations for the system are written in the state dependent

form

$$\begin{bmatrix} \dot{x_1} \\ \dot{x_2} \\ \dot{x_3} \end{bmatrix} = \begin{bmatrix} 0 & 1 & 0 \\ \frac{g}{l}\frac{sin(x_1)}{x_1} & 0 & \frac{k_m}{ml^2} \\ 0 & -\frac{k_b}{L} & \frac{R}{L} \end{bmatrix} \begin{bmatrix} x_1 \\ x_2 \\ x_3 \end{bmatrix} + \begin{bmatrix} 0 \\ 0 \\ \frac{1}{L} \end{bmatrix} u, \tag{3.3.12}$$

where: $\theta = x_1$, $\dot{\theta} = x_2$, $i = x_3$, and $V = u$.

Let the selected weighted matrices be

$$\mathbf{Q} = diag(100, 0, 0), \quad \mathbf{R} = 0.07, \quad \mathbf{F} = diag(1, 1, 1). \tag{3.3.13}$$

The covariances of the noises have been taken as

$$\mathbf{Q_w} = diag(0.2, 0.2, 0.2), \quad \mathbf{R_v} = 10. \tag{3.3.14}$$

The simulations are performed for a time interval of 30 seconds with 300 time steps and the resulting angle trajectories is shown in Fig. 3.8, where the dash-dot line denotes the *reference* angle trajectory, the dashed line denotes the *actual* angle, and the solid line denotes the *estimated* angle. The optimal control voltage is shown in Fig. 3.9, where the solid line denotes the estimated optimal control and the doted line denotes the actual optimal control signal. The error between the actual and the estimated angle is shown in Fig. 3.10.

Comparing these trajectories in Fig. 3.8, it's clear that the proposed methodology gives very good results as the estimated optimal angle is making a very good tracking

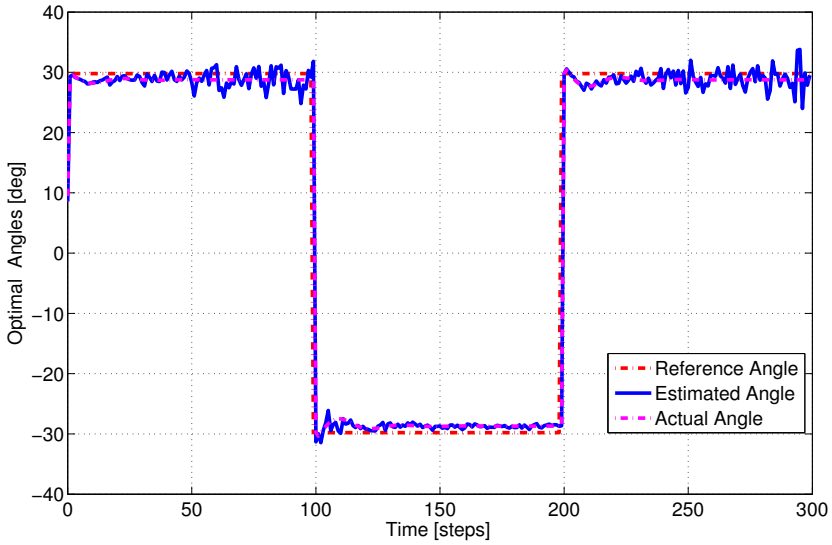

Figure 3.8: Angle Trajectories for Inverted Pendulum Controlled by DC Motor

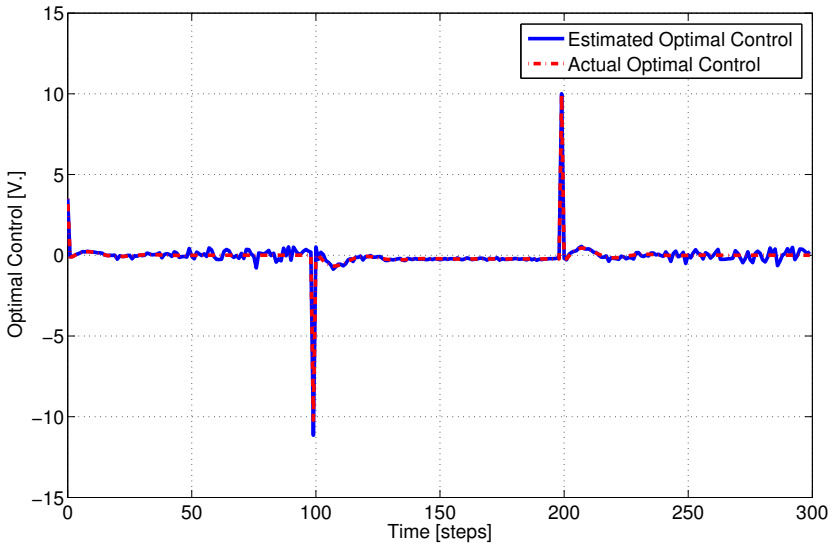

Figure 3.9: Optimal Control for Inverted Pendulum Controlled by DC Motor

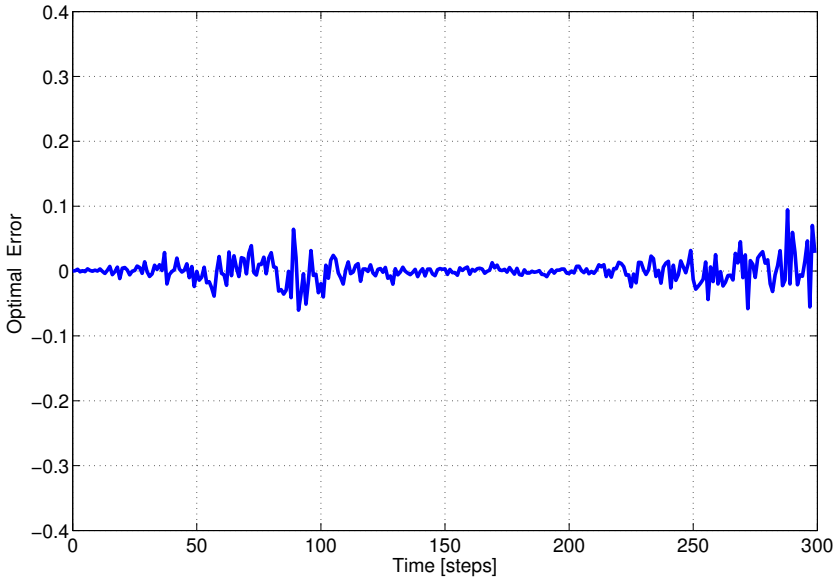

Figure 3.10: Optimal Error for Inverted Pendulum Controlled by DC Motor

to the reference angle, and also the estimated trajectory is very close to the actual output trajectory. As shown in Fig. 3.10 the error between the actual and the estimated motor angle is very small, the average error for this example is 0.02%.

3.4 Conclusions

Most of existing estimation techniques relies on applying *the linear* estimation techniques to the *linearized* systems, which can be effective only in the small vicinity of the operating point. This chapter presents an efficient online technique used for infinite-horizon nonlinear stochastic regulator and tracking problems.

The idea of the proposed technique is to integrate the Kalman filter algorithm and the infinite-horizon SDRE technique. Kalman filter is used to estimate the unmeasured states which are corrupted with noises in the nonlinear model. Unlike the

ordinary methods which deal with the linearized system, this technique will estimate the unmeasured states of the nonlinear system directly, and this will make the proposed technique effective for wide range of operating points.

Chapter 4

Finite-Horizon Differential State Dependent Riccati Equation (SDRE) for Deterministic Systems

The infinite-horizon optimal control for nonlinear systems was discussed in Chapter 2. In infinite-horizon optimal nonlinear control problem, the differential Riccati equation (DRE) is converted to an algebraic Riccati equation (ARE) which is easy to be solved. Finite-horizon optimal control of nonlinear systems is a challenging problem in the control field due to the complexity of time-dependency of the Hamilton Jacobi Bellman (HJB) differential equation. Also, in the finite-horizon SDRE problems, the solution of the SDRE is time dependent and a differential equation, rather than an algebraic equation in infinite-horizon SDRE.

From the literature, the available methods for this purpose can be classified to

classical and intelligent methods. One approach in the classical methods is to calculate the open loop solution through some numerical methods and then use predictive techniques for closing the control loop [89, 65]. The drawback of this technique is mainly the dependency of the solution to the pre-specified initial conditions (IC) and time-to-go. On the other hand, the intelligent methods are based on *offline* training of the weights and online usage of the neural network for calculation of the control. But, this method cannot be used if resulted trajectory lies out of the neural network trained domain [27, 52, 55, 142].

4.1 Lyapunov Equation Approach for Differential SDRE

Inspired by the great potential of the algebraic SDRE for regulation and tracking of *infinite-horizon* nonlinear systems [20, 29], this chapter presents the differential SDRE, strictly speaking it could be called State Dependent Differential Riccati Equation (SDDRE), technique for *finite-horizon* optimal control of nonlinear systems based on a change of variable [104], that converts the differential Riccati equation (DRE) to a linear differential Lyapunov equation (DLE) [101], and evaluating the coefficients of the resulted equation based on the current state values at each time step and freezing these coefficients from current time to the next time step. Then, the Lyapunov equation is solved in a closed form at each step during online implementation. The use of Lyapunov-type equations in solving optimal problems is given in [136]. Because the

solution is based on the differential Lyapunov equation, we call the new method the Lyapunov equation approach.

4.1.1 Supporting Theorems

In this section, the relation between the proposed technique and the exact optimal solution to the finite-horizon problem will be discussed. This is done through the following Theorems [56]

4.1.1.1 Theorem 1

The solution to the optimal control of the nonlinear finite-horizon problem can be approximated to an optimal solution given through finite-horizon differential SDRE. Given the nonlinear system in the form

$$\dot{\mathbf{x}}(t) = \mathbf{f}(\mathbf{x}) + \mathbf{g}(\mathbf{x})\mathbf{u}(t), \tag{4.1.1}$$

which is expressed in a state-dependent like linear form, as:

$$\dot{\mathbf{x}}(t) = \mathbf{A}(\mathbf{x})\mathbf{x}(t) + \mathbf{B}(\mathbf{x})\mathbf{u}(t), \tag{4.1.2}$$

where $\mathbf{f}(\mathbf{x}) = \mathbf{A}(\mathbf{x})\mathbf{x}(t)$, and $\mathbf{B}(\mathbf{x}) = \mathbf{g}(\mathbf{x})$.

The solution to the optimal control of nonlinear system (4.1.2) subject to the cost

function

$$\mathbf{J}(\mathbf{x},\mathbf{u}) = \frac{1}{2}\mathbf{x}'(t_f)\mathbf{F}\mathbf{x}(t_f) + \frac{1}{2}\int_{t_0}^{t_f} [\mathbf{x}'(t)\mathbf{Q}(\mathbf{x})\mathbf{x}(t) + \mathbf{u}'(\mathbf{x})\mathbf{R}(\mathbf{x})\mathbf{u}(\mathbf{x})]\, dt, \quad (4.1.3)$$

where $\mathbf{Q}(\mathbf{x})$ and $\mathbf{F}$ are symmetric *positive semi-definite* matrices, and $\mathbf{R}(\mathbf{x})$ is a symmetric *positive definite* matrix, is given by

$$\mathbf{u}(\mathbf{x},t) = -\mathbf{R}^{-1}(\mathbf{x})\mathbf{B}'(\mathbf{x})[\mathbf{P}(\mathbf{x},t)\mathbf{x}(t) + \Pi], \quad (4.1.4)$$

where

$$\Pi = \frac{1}{2}[\mathbf{x}'\mathbf{P}_{x_1}\mathbf{x} \;\; \mathbf{x}'\mathbf{P}_{x_2}\mathbf{x} \;\; \ldots \;\; \mathbf{x}'\mathbf{P}_{x_n}\mathbf{x}]', \quad \mathbf{P}_{x_i} = \frac{\partial \mathbf{P}(\mathbf{x},t)}{\partial x_i}. \quad (4.1.5)$$

$\mathbf{P}(\mathbf{x},t)$ is a symmetric positive definite solution to the equation

$$-\dot{\mathbf{P}}(\mathbf{x},t) = \mathbf{P}(\mathbf{x},t)\mathbf{A}(\mathbf{x}) + \mathbf{A}'(\mathbf{x})\mathbf{P}(\mathbf{x},t) - \mathbf{P}(\mathbf{x},t)\mathbf{B}(\mathbf{x})\mathbf{R}^{-1}(\mathbf{x})\mathbf{B}'(\mathbf{x})\mathbf{P}(\mathbf{x},t)$$
$$+\mathbf{Q}(\mathbf{x}) + \Omega, \quad (4.1.6)$$

with the final condition $\mathbf{P}(\mathbf{x},t_f) = \mathbf{F}$, where

$$\Omega = \frac{1}{4}\sum_{i=1}^{n}\sum_{j=1}^{n} \mathbf{P}_{x_i}\mathbf{x}[\mathbf{B}(\mathbf{x})\mathbf{R}^{-1}(\mathbf{x})\mathbf{B}'(\mathbf{x})]_{ij}\mathbf{x}'\mathbf{P}_{x_j}, \quad (4.1.7)$$

and $[\;\;]_{ij}$ is the *ith* element of the *jth* row of that matrix.

Proof :

The desired finite-horizon optimal control is given by the partial differential HJB equation [83]

$$-\mathbf{J}_t(\mathbf{x},t) = \mathbf{J}'_x(\mathbf{x},t)\mathbf{A}(\mathbf{x})\mathbf{x} + \frac{1}{2}\mathbf{x}'\mathbf{Q}(\mathbf{x})\mathbf{x} - \frac{1}{2}\mathbf{J}'_x(\mathbf{x},t)\mathbf{B}(\mathbf{x})\mathbf{R}^{-1}(\mathbf{x})\mathbf{B}'(\mathbf{x})\mathbf{J}_x(\mathbf{x},t), \quad (4.1.8)$$

with the final condition $\mathbf{J}(\mathbf{x},t_f) = \frac{1}{2}\mathbf{x}'(t)\mathbf{F}\mathbf{x}(t)$, where $\mathbf{J}(\mathbf{x},t)$ represents the optimal cost function and subscript t and x denote the corresponding partial derivatives, $\mathbf{J}_t$ and $\mathbf{J}_x$, respectively, of $\mathbf{J}$, the optimal control is given by

$$\mathbf{u}(\mathbf{x},t) = -\mathbf{R}^{-1}(\mathbf{x})\mathbf{B}'(\mathbf{x})\mathbf{J}_x(\mathbf{x},t). \quad (4.1.9)$$

$\mathbf{J}(\mathbf{x},t)$ is a positive definite matrix can be written in the form

$$\mathbf{J}(\mathbf{x},t) = \frac{1}{2}\mathbf{x}'(t)\mathbf{P}(\mathbf{x},t)\mathbf{x}(t), \quad (4.1.10)$$

which leads to

$$\mathbf{J}_t(\mathbf{x},t) = \frac{1}{2}\mathbf{x}'\mathbf{P}_t(\mathbf{x},t)\mathbf{x}, \quad \mathbf{J}_x(\mathbf{x},t) = \mathbf{P}(\mathbf{x},t)\mathbf{x} + \Pi. \quad (4.1.11)$$

Substituting (4.1.11) and (4.1.11) in (4.1.8)

$$-\frac{1}{2}\mathbf{x}'\mathbf{P}_t(\mathbf{x},t)\mathbf{x} = (\mathbf{P}(\mathbf{x},t)\mathbf{x} + \Pi)'\mathbf{A}(\mathbf{x})\mathbf{x} + \frac{1}{2}\mathbf{x}'\mathbf{Q}(\mathbf{x})\mathbf{x} - \frac{1}{2}(\mathbf{P}(\mathbf{x},t)\mathbf{x} + \Pi)'\mathbf{B}(\mathbf{x})\mathbf{R}^{-1}\mathbf{B}'(\mathbf{x})(\mathbf{P}(\mathbf{x},t)\mathbf{x} + \Pi), \quad (4.1.12)$$

which is rearranged in the form

$$-\frac{1}{2}\mathbf{x}'\mathbf{P}_t(\mathbf{x},t)\mathbf{x} = \mathbf{x}'\left[\mathbf{P}(\mathbf{x},t)\mathbf{A}(\mathbf{x}) + \frac{1}{2}\mathbf{Q}(\mathbf{x}) - \frac{1}{2}\mathbf{P}(\mathbf{x},t)\mathbf{B}(\mathbf{x})\mathbf{R}^{-1}\mathbf{B}'(\mathbf{x})\mathbf{P}(\mathbf{x},t)\right]\mathbf{x}$$
$$+\Pi'\left[\mathbf{A}(\mathbf{x})\mathbf{x} - \mathbf{B}(\mathbf{x})\mathbf{R}^{-1}\mathbf{B}'(\mathbf{x})\left(\mathbf{P}(\mathbf{x},t)\mathbf{x} + \frac{1}{2}\Pi\right)\right]. \tag{4.1.13}$$

Substituting (4.1.4) in (4.1.2)

$$\dot{\mathbf{x}}(t) \;=\; \mathbf{A}(\mathbf{x})\mathbf{x} - \mathbf{B}(\mathbf{x})\mathbf{R}^{-1}\mathbf{B}'(\mathbf{x})[\mathbf{P}(\mathbf{x},t)\mathbf{x} + \Pi], \tag{4.1.14}$$

Substituting (4.1.14) in (4.1.13)

$$-\frac{1}{2}\mathbf{x}'\mathbf{P}_t(\mathbf{x},t)\mathbf{x} = \mathbf{x}'\left[\mathbf{P}(\mathbf{x},t)\mathbf{A}(\mathbf{x}) + \frac{1}{2}\mathbf{Q}(\mathbf{x}) - \frac{1}{2}\mathbf{P}(\mathbf{x},t)\mathbf{B}(\mathbf{x})\mathbf{R}^{-1}\mathbf{B}'(\mathbf{x})\mathbf{P}(\mathbf{x},t)\right]\mathbf{x}$$
$$+\Pi'\dot{\mathbf{x}} + \frac{1}{2}\Pi'\mathbf{B}(\mathbf{x})\mathbf{R}^{-1}\mathbf{B}'(\mathbf{x})\Pi. \tag{4.1.15}$$

Multiplying the transpose of (4.1.5) by $\dot{\mathbf{x}}(t)$

$$\Pi'\dot{\mathbf{x}} = \frac{1}{2}\sum_{i=1}^{n}\left(\mathbf{x}'\mathbf{P}_{x_i}\mathbf{x}\right)\dot{x}_i = \frac{1}{2}\mathbf{x}'\left(\sum_{i=1}^{n}\mathbf{P}_{x_i}\dot{x}_i\right)\mathbf{x}. \tag{4.1.16}$$

From (4.1.15) and (4.1.16)

$$-\frac{1}{2}\mathbf{x}'(\mathbf{P}_t + \sum_{i=1}^{n}\mathbf{P}_{x_i}\dot{x}_i)\mathbf{x} = \mathbf{x}'\left[\mathbf{P}\mathbf{A}(\mathbf{x}) + \frac{1}{2}\mathbf{Q} - \frac{1}{2}\mathbf{P}\mathbf{B}(\mathbf{x})\mathbf{R}^{-1}\mathbf{B}'(\mathbf{x})\mathbf{P}\right]\mathbf{x}$$
$$+\frac{1}{2}\Pi'\mathbf{B}(\mathbf{x})\mathbf{R}^{-1}\mathbf{B}'(\mathbf{x})\Pi. \tag{4.1.17}$$

Calculating the total derivative of P as

$$\dot{\mathbf{P}} = \mathbf{P}_t + \sum_{i=1}^{n} \mathbf{P}_{x_i} \dot{x}_i, \tag{4.1.18}$$

and since

$$\Pi' \mathbf{B}(\mathbf{x}) \mathbf{R}^{-1} \mathbf{B}'(\mathbf{x}) \Pi = \frac{1}{4} \mathbf{x}' \left(\sum_{i=1}^{n} \sum_{j=1}^{n} \mathbf{P}_{x_i} \mathbf{x} [\mathbf{B}(\mathbf{x}) \mathbf{R}^{-1} \mathbf{B}'(\mathbf{x})]_{ij} \mathbf{x}' \mathbf{P}_{x_j} \right) \mathbf{x}. \tag{4.1.19}$$

Substituting from (4.1.18) and (4.1.19) in (4.1.17)

$$-\frac{1}{2} \mathbf{x}' \dot{\mathbf{P}}(\mathbf{x}, t) \mathbf{x} = \mathbf{x}' \left(\mathbf{P}(\mathbf{x}, t) \mathbf{A}(\mathbf{x}) + \frac{1}{2} \mathbf{Q}(\mathbf{x}) - \frac{1}{2} \mathbf{P}(\mathbf{x}, t) \mathbf{B}(\mathbf{x}) \mathbf{R}^{-1} \mathbf{B}'(\mathbf{x}) \mathbf{P}(\mathbf{x}, t) + \frac{1}{2} \Omega \right) \mathbf{x}. \tag{4.1.20}$$

It follows that (4.1.20) should hold good for any value of $\mathbf{x}$. This clearly means that the function $\mathbf{P}(\mathbf{x}, t)$ should satisfy the matrix differential Riccati equation

$$-\dot{\mathbf{P}}(\mathbf{x}, t) = \mathbf{P}(\mathbf{x}, t) \mathbf{A}(\mathbf{x}) + \mathbf{A}'(\mathbf{x}) \mathbf{P}(\mathbf{x}, t) + \mathbf{Q} - \mathbf{P}(\mathbf{x}, t) \mathbf{B}(\mathbf{x}) \mathbf{R}^{-1} \mathbf{B}'(\mathbf{x}) \mathbf{P}(\mathbf{x}, t) + \Omega, \tag{4.1.21}$$

with the final condition

$$\mathbf{P}(\mathbf{x}, t_f) = \mathbf{F}. \tag{4.1.22}$$

This proves that solving (4.1.6) solves the HJB equation (4.1.8) and gives the optimal solution to the nonlinear finite-horizon problem.

Performing some approximations by neglecting terms Ω in (4.1.6) and Π in (4.1.4),

which leads to the optimal control given by [56]

$$\mathbf{u}(\mathbf{x},t) = -\mathbf{R}^{-1}(\mathbf{x})\mathbf{B}'(\mathbf{x})\mathbf{P}(\mathbf{x},t)\mathbf{x}(t), \tag{4.1.23}$$

resulted from solving the differential SDRE

$$-\dot{\mathbf{P}}(\mathbf{x},t) = \mathbf{P}(\mathbf{x},t)\mathbf{A}(\mathbf{x}) + \mathbf{A}'(\mathbf{x})\mathbf{P}(\mathbf{x},t) - \mathbf{P}(\mathbf{x},t)\mathbf{B}(\mathbf{x})\mathbf{R}^{-1}(\mathbf{x})\mathbf{B}'(\mathbf{x})\mathbf{P}(\mathbf{x},t) + \mathbf{Q}(\mathbf{x}). \tag{4.1.24}$$

Using this approximation, the control will be approximated to be optimal control.

4.1.1.2 Theorem 2

The approximated optimal control given through finite-horizon differential SDRE in (4.1.23) resulted from solving the DRE (4.1.24) for the positive definite matrix $\mathbf{P}(\mathbf{x},t)$, makes the nonlinear system (4.1.2) a globally stable system.

Proof :

Selecting the Lyapunov function

$$-\mathbf{V}(\mathbf{x},t) = \mathbf{x}'\mathbf{P}(\mathbf{x},t)\mathbf{x}, \tag{4.1.25}$$

where $\mathbf{P}(\mathbf{x},t)$ is the symmetric positive definite matrix, and taking the total derivative of $\mathbf{V}(\mathbf{x},t)$ leads to

$$-\dot{\mathbf{V}}(\mathbf{x},t) = \dot{\mathbf{x}}'\mathbf{P}\mathbf{x},t)\mathbf{x} + \mathbf{x}'\dot{\mathbf{P}}(\mathbf{x},t)\mathbf{x} + \mathbf{x}'\mathbf{P}(\mathbf{x},t)\dot{\mathbf{x}}. \tag{4.1.26}$$

Substituting from (4.1.23) in (4.1.2)

$$\dot{\mathbf{x}}(t) = \mathbf{A}(\mathbf{x})\mathbf{x} - \mathbf{B}(\mathbf{x})\mathbf{R}^{-1}\mathbf{B}'(\mathbf{x})\mathbf{P}(\mathbf{x},t)\mathbf{x}. \tag{4.1.27}$$

Substituting from (4.1.24) and (4.1.27) in (4.1.26)

$$-\dot{\mathbf{V}}(\mathbf{x},t) = \dot{\mathbf{x}}'[-\mathbf{P}(\mathbf{x},t)\mathbf{B}(\mathbf{x})\mathbf{R}^{-1}(\mathbf{x})\mathbf{B}'(\mathbf{x})\mathbf{P}(\mathbf{x},t) - \mathbf{Q}]\mathbf{x}. \tag{4.1.28}$$

Since $\mathbf{Q}(\mathbf{x})$ is a symmetric positive *semi-definite* matrix, and $\mathbf{P}(\mathbf{x},t)$ and $\mathbf{R}(\mathbf{x})$ are symmetric *positive definite* matrices, it's clear that $\mathbf{V}(\mathbf{x},t)$ is *a positive definite* matrix and the total derivative $\dot{\mathbf{V}}(\mathbf{x},t)$ is *a negative definite* matrix. Hence, the finite-horizon differential SDRE method is *globally stable*.

4.2 Finite-Horizon Regulator for Deterministic Nonlinear Systems

4.2.1 Problem Formulation

The *nonlinear* system considered in this chapter is in the form:

$$\dot{\mathbf{x}}(t) = \mathbf{f}(\mathbf{x}) + \mathbf{g}(\mathbf{x})\mathbf{u}(t), \tag{4.2.1}$$

$$\mathbf{y}(t) = \mathbf{h}(\mathbf{x}). \tag{4.2.2}$$

This nonlinear system can be expressed in a state-dependent *linear*-like form

$$\dot{\mathbf{x}}(t) = \mathbf{A}(\mathbf{x})\mathbf{x}(t) + \mathbf{B}(\mathbf{x})\mathbf{u}(t), \tag{4.2.3}$$

$$\mathbf{y}(t) = \mathbf{C}(\mathbf{x})\mathbf{x}(t), \tag{4.2.4}$$

where $\mathbf{f}(\mathbf{x}) = \mathbf{A}(\mathbf{x})\mathbf{x}(t)$, $\mathbf{B}(\mathbf{x}) = \mathbf{g}(\mathbf{x})$, and $\mathbf{h}(\mathbf{x}) = \mathbf{C}(\mathbf{x})\mathbf{x}(t)$.

The goal is to find a state feedback optimal control law of the form $\mathbf{u}(\mathbf{x}) = -\mathbf{K}\mathbf{x}(t)$, that minimizes a cost function given by [98]

$$\mathbf{J}(\mathbf{x}, \mathbf{u}) = \frac{1}{2}\mathbf{x}'(t_f)\mathbf{F}\mathbf{x}(t_f) + \frac{1}{2}\int_{t_0}^{t_f} \left[\mathbf{x}'(t)\mathbf{Q}(\mathbf{x})\mathbf{x}(t) + \mathbf{u}'(\mathbf{x})\mathbf{R}(\mathbf{x})\mathbf{u}(\mathbf{x})\right] dt, \tag{4.2.5}$$

where $\mathbf{Q}(\mathbf{x})$ and $\mathbf{F}$ are symmetric *positive semi-definite* matrices, and $\mathbf{R}(\mathbf{x})$ is a symmetric *positive definite* matrix. Moreover, $\mathbf{x}'\mathbf{Q}(\mathbf{x})\mathbf{x}$ is a measure of state accuracy and $\mathbf{u}'(\mathbf{x})\mathbf{R}(\mathbf{x})\mathbf{u}(\mathbf{x})$ is a measure of control effort.

4.2.2 Solution for Finite-Horizon Differential SDRE Regulator

To minimize the above cost function (4.2.5), a state feedback control law is given as

$$\mathbf{u}(\mathbf{x}) = -\mathbf{K}\mathbf{x}(t) = -\mathbf{R}^{-1}(\mathbf{x})\mathbf{B}'(\mathbf{x})\mathbf{P}(\mathbf{x})\mathbf{x}(t), \tag{4.2.6}$$

where $\mathbf{P}(\mathbf{x}, t)$ is a symmetric, positive-definite solution of the differential SDRE, strictly speaking it could be called State Dependent Differential Riccati Equation

(SDDRE), of the form

$$-\dot{\mathbf{P}}(\mathbf{x}) = \mathbf{P}(\mathbf{x})\mathbf{A}(\mathbf{x}) + \mathbf{A}'(\mathbf{x})\mathbf{P}(\mathbf{x}) - \mathbf{P}(\mathbf{x})\mathbf{B}(\mathbf{x})\mathbf{R}^{-1}(\mathbf{x})\mathbf{B}'(\mathbf{x})\mathbf{P}(\mathbf{x}) + \mathbf{Q}(\mathbf{x}), \quad (4.2.7)$$

with the final condition

$$\mathbf{P}(\mathbf{x}, t_f) = \mathbf{F}. \quad (4.2.8)$$

The resulting differential SDRE-controlled trajectory becomes the solution of the state-dependent closed-loop dynamics

$$\dot{\mathbf{x}}(t) = [\mathbf{A}(\mathbf{x}) - \mathbf{B}(\mathbf{x})\mathbf{R}^{-1}(\mathbf{x})\mathbf{B}'(\mathbf{x})\mathbf{P}(\mathbf{x})]\mathbf{x}(t). \quad (4.2.9)$$

As the differential SDRE is a function of $(\mathbf{x}, t)$, we do not know the value of the states ahead of present time step. Consequently, the state dependent coefficients can not be calculated to solve (4.2.7) with the final condition (4.2.8) by backward integration from t_f to t_0. To overcome this problem, *an approximate* analytical approach is used [56, 101, 104], which converts the original *nonlinear* differential Ricatti equation to *a linear* differential Lyapunov equation, which can be solved in closed form at each time step. In order to solve the DRE (4.2.7), one can follow the following steps at each time step [74]:

1. Solve the ARE to calculate the steady state value $\mathbf{P}_{\mathbf{ss}}(\mathbf{x})$

$$\mathbf{P}_{\mathbf{ss}}(\mathbf{x})\mathbf{A}(\mathbf{x}) + \mathbf{A}'(\mathbf{x})\mathbf{P}_{\mathbf{ss}}(\mathbf{x}) - \mathbf{P}_{\mathbf{ss}}(\mathbf{x})\mathbf{B}(\mathbf{x})\mathbf{R}^{-1}(\mathbf{x})\mathbf{B}'(\mathbf{x})\mathbf{P}_{\mathbf{ss}}(\mathbf{x}) + \mathbf{Q}(\mathbf{x}) = 0 \quad (4.2.10)$$

2. Use changing-of-variables procedure and assume that

$$\mathbf{K}(\mathbf{x},\mathbf{t}) = [\mathbf{P}(\mathbf{x},\mathbf{t}) - \mathbf{P_{ss}}(\mathbf{x})]^{-1}. \tag{4.2.11}$$

3. Calculate the value of $\mathbf{A_{cl}}(\mathbf{x})$ as

$$\mathbf{A_{cl}}(\mathbf{x}) = \mathbf{A}(\mathbf{x}) - \mathbf{B}(\mathbf{x})\mathbf{R^{-1}}\mathbf{B'}(\mathbf{x})\mathbf{P_{ss}}(\mathbf{x}). \tag{4.2.12}$$

4. Calculate the value of $\mathbf{D}$ by solving the algebraic Lyapunov equation [44]

$$\mathbf{A_{cl}}\mathbf{D} + \mathbf{D}\mathbf{A'_{cl}} - \mathbf{B}\mathbf{R}^{-1}\mathbf{B'} = 0. \tag{4.2.13}$$

5. Solve the differential Lyapunov equation

$$\dot{\mathbf{K}}(\mathbf{x},t) = \mathbf{K}(\mathbf{x},t)\mathbf{A'_{cl}}(\mathbf{x}) + \mathbf{A_{cl}}(\mathbf{x})\mathbf{K}(\mathbf{x},t) - \mathbf{B}(\mathbf{x})\mathbf{R}^{-1}\mathbf{B'}(\mathbf{x}). \tag{4.2.14}$$

The solution of (4.2.14), as shown by [12], is given by

$$\mathbf{K}(\mathbf{x},t) = \mathbf{e}^{\mathbf{A_{cl}(t-t_f)}}(\mathbf{K}(\mathbf{x},t_f) - \mathbf{D})\mathbf{e}^{\mathbf{A_{cl}}'\mathbf{(t-t_f)}} + \mathbf{D}. \tag{4.2.15}$$

6. Use change-of-variables procedure to calculate the value of $\mathbf{P}(\mathbf{x},\mathbf{t})$ from (4.2.11)

$$\mathbf{P}(\mathbf{x},t) = \mathbf{K}^{-1}(\mathbf{x},t) + \mathbf{P_{ss}}(t). \tag{4.2.16}$$

7. Finally, calculate the value of the optimal control $\mathbf{u}(\mathbf{x}, t)$ as

$$\mathbf{u}(\mathbf{x}, t) = -\mathbf{R}^{-1}\mathbf{B}'(\mathbf{x})\mathbf{P}(\mathbf{x}, t)\mathbf{x}(t). \tag{4.2.17}$$

Fig.4.1 summarizes the overview of the flow chart of finite-horizon differential SDRE regulation technique. Basically, $\mathbf{P}(\mathbf{x}, t)$, instead of solving backward in time from (4.2.7), we now obtain $\mathbf{P}(\mathbf{x}, t)$ from (4.2.16) in terms of $\mathbf{K}(\mathbf{x}, t)$, (4.2.15), the analytical solution of the linear differential Lyapunov equation (DLE) (4.2.14), which itself requires the solution of the ARE (4.2.10), and the solution of algebraic Lyapunov equation (4.2.13).

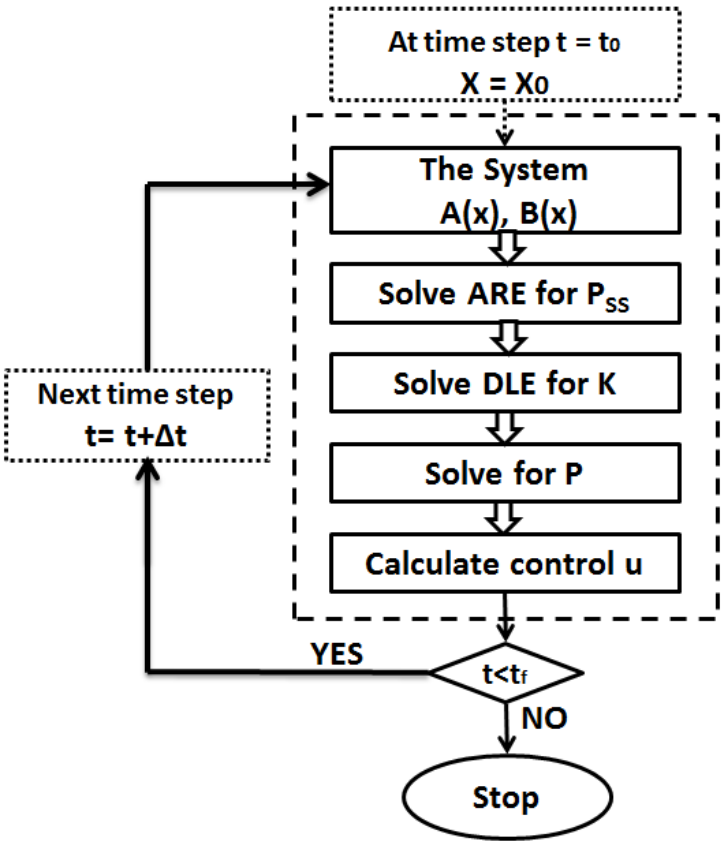

Figure 4.1: Flow Chart for Finite-Horizon Differential SDRE Regulation Technique

At least for linear systems, if $t_0 \ll t_f$, the solution of the DRE convergences to that of ARE, and $\mathbf{K}(\mathbf{x},t) = [\mathbf{P}(\mathbf{x},t) - \mathbf{P_{ss}}(\mathbf{x})]^{-1}$ becomes singular. To avoid that, *the negative definite* solution of the ARE can be calculated instead of *the positive definite* solution, and in this case $[\mathbf{P}(\mathbf{x},t) - \mathbf{P_{ss}}(\mathbf{x})]$ is guaranteed to be *the positive definite*, hence, its inverse always exists. This approach works for nonlinear case as well [104]. For calculation of *the negative definite* solution of the ARE, it suffices to flip the sign of matrix $\mathbf{A}(\mathbf{x})$ and solve the ARE for *the positive definite* solution, then by using *the negative* of $\mathbf{P_{ss}}(\mathbf{x})$, *the negative definite* solution of the original ARE cab be obtained [104].

Note : It is easily seen that this technique with finite-horizon differential SDRE can be used for linear systems and the resulting differential SDRE becomes the standard DRE [98].

4.2.3 Finite-Horizon Differential SDRE Regulation Simulation

To support the effectiveness of the proposed technique, this section presents simulations with the finite-horizon optimal regulator controller for linear and nonlinear systems.

4.2.3.1 Linear System Example : Aircraft

Consider the continuous-time F-16 aircraft plant [127, 135]

$$\begin{bmatrix} \dot{x_1} \\ \dot{x_2} \\ \dot{x_3} \end{bmatrix} = \begin{bmatrix} -1.01887 & 0.90506 & -0.00215 \\ 0.82225 & -1.07741 & -0.17555 \\ 0 & 0 & -1 \end{bmatrix} \begin{bmatrix} x_1 \\ x_2 \\ x_3 \end{bmatrix} + \begin{bmatrix} 0 \\ 0 \\ -1 \end{bmatrix} u, \quad (4.2.18)$$

with the initial conditions

$$\mathbf{x_0} = [15, -13, -12]'. \quad (4.2.19)$$

The selected weighted matrices are

$$\mathbf{Q} = diag(100, 100, 100), \quad \mathbf{R} = 1, \quad \mathbf{F} = diag(1, 1, 1). \quad (4.2.20)$$

The simulations are performed for final time of 10 seconds. The optimal states trajectories is shown in Fig. 4.2, where the solid line denotes state x_1, the dashed line denotes state x_2, and the dashed doted line denotes state x_3. The optimal control is shown in Fig. 4.3. From the simulation results, it is clear that the proposed finite-horizon differential SDRE technique for nonlinear systems is able to solve the optimal regulation problem of linear systems.

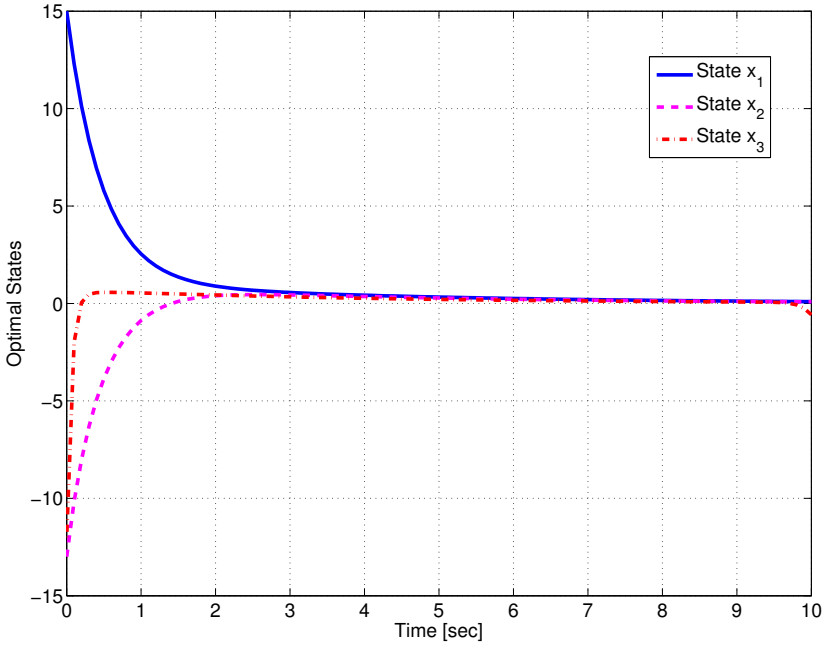

Figure 4.2: Optimal States for the F-16 Aircraft

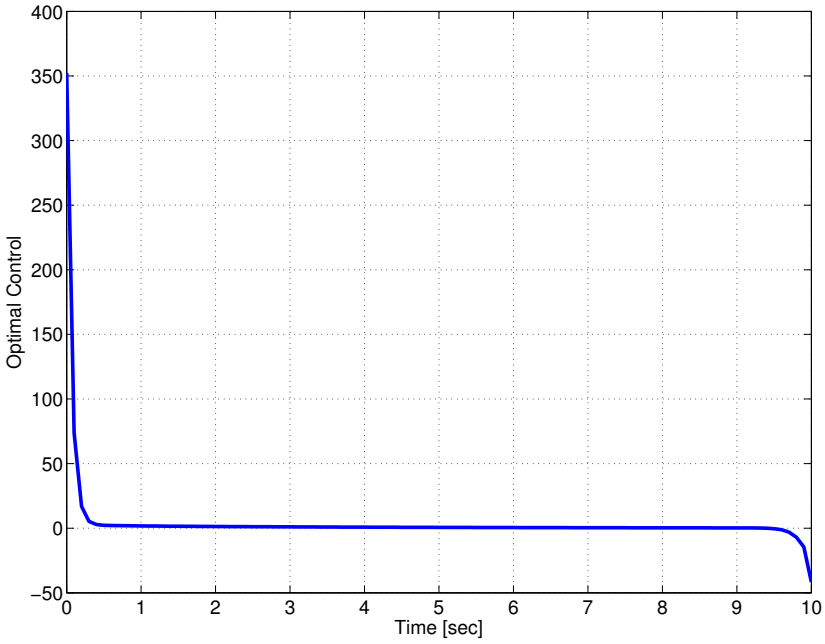

Figure 4.3: Optimal Control for the F-16 Aircraft

4.2.3.2 Nonlinear System Example: Input-Affine Nonlinear System

Consider the following affine in control input nonlinear system [135, 141]

$$\dot{x_1}(t) = -x_1(t) + x_2(t), \tag{4.2.21}$$

$$\dot{x_2}(t) = -0.5x_1(t) - 0.5x_2(t)\left[1 - \left(cos(2x_1(t)) + 2\right)^2\right] + u(t)cos(2x_1(t)), \tag{4.2.22}$$

with the initial conditions

$$\mathbf{x_0} = [2, -1]'. \tag{4.2.23}$$

The system can be rewritten in the state dependent form

$$\begin{bmatrix} \dot{x_1} \\ \dot{x_2} \end{bmatrix} = \begin{bmatrix} -1 & 1 \\ -0.5 & -0.5\left[1 - (cos(2x_1) + 2)^2\right] \end{bmatrix} \begin{bmatrix} x_1 \\ x_2 \end{bmatrix} + \begin{bmatrix} 0 \\ cos(2x_1) \end{bmatrix} u. \tag{4.2.24}$$

Let the selected weighted matrices are

$$\mathbf{Q} = diag(50, 10), \quad \mathbf{R} = 0.1, \quad \mathbf{F} = diag(1, 1). \tag{4.2.25}$$

The simulations are performed for final time of 12 seconds. The optimal states trajectories is shown in Fig. 4.4, and the optimal control is shown in Fig. 4.5. It is shown in the simulation example that the finite-horizon differential SDRE has been able to understand the limitation on the time and apply the control such that the states error at the final time is very small.

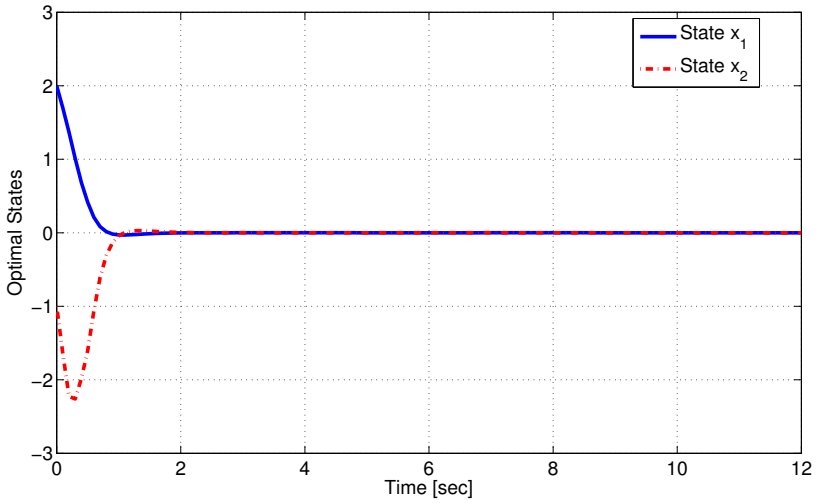

Figure 4.4: Optimal States for the Nonlinear System

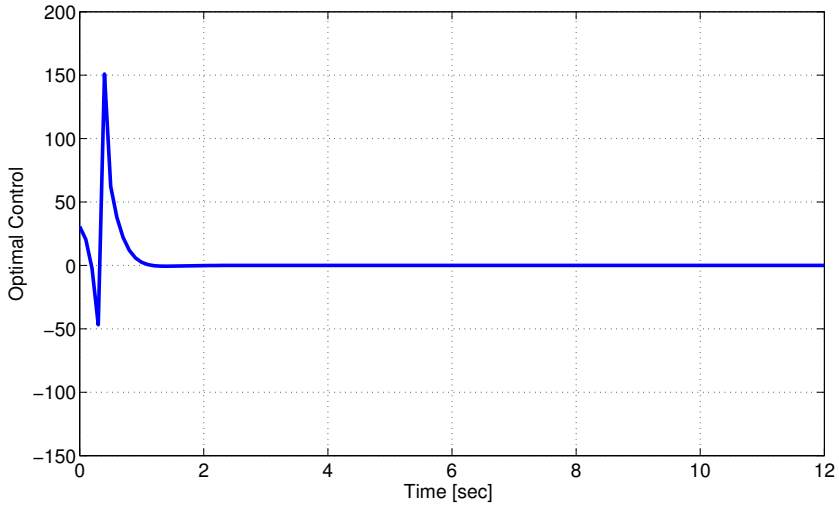

Figure 4.5: Optimal Control for the Nonlinear System

4.3 Finite-Horizon Tracking for Deterministic Nonlinear Systems

4.3.1 Problem Formulation

Consider the nonlinear system given by (4.2.1) and (4.2.2), which can be re-described in the form (4.2.3) and (4.2.4), and let $\mathbf{z}(t)$ be the *desired*, or reference output.

The goal is to find a state feedback, control law that minimizes a cost function given by

$$\mathbf{J}(\mathbf{x},\mathbf{u}) = \frac{1}{2}\mathbf{e}'(t_f)\mathbf{F}\mathbf{e}(t_f) + \frac{1}{2}\int_{t_0}^{t_f} [\mathbf{e}'(t)\mathbf{Q}(\mathbf{x})\mathbf{e}(t) + \mathbf{u}'(\mathbf{x})\mathbf{R}(\mathbf{x})\mathbf{u}(\mathbf{x})]\, dt, \qquad (4.3.1)$$

where the error $\mathbf{e}(t) = \mathbf{z}(t) - \mathbf{y}(t)$.

4.3.2 Solution for Finite-Horizon Tracking using Differential SDRE

To minimize the cost function (4.3.1), a feedback control law is given as

$$\mathbf{u}(\mathbf{x}) = -\mathbf{R}^{-1}\mathbf{B}'(\mathbf{x})[\mathbf{P}(\mathbf{x})\mathbf{x} - \mathbf{g}(\mathbf{x})], \qquad (4.3.2)$$

where $\mathbf{P}(\mathbf{x})$ is a symmetric, positive-definite solution of the differential SDRE of the form

$$-\dot{\mathbf{P}}(\mathbf{x}) = \mathbf{P}(\mathbf{x})\mathbf{A}(\mathbf{x}) + \mathbf{A}'(\mathbf{x})\mathbf{P}(\mathbf{x}) - \mathbf{P}(\mathbf{x})\mathbf{B}(\mathbf{x})\mathbf{R}^{-1}\mathbf{B}'(\mathbf{x})\mathbf{P}(\mathbf{x}) + \mathbf{C}'(\mathbf{x})\mathbf{Q}(\mathbf{x})\mathbf{C}(\mathbf{x}), \qquad (4.3.3)$$

with the final condition

$$\mathbf{P}(\mathbf{x}, t_f) = \mathbf{C}'(t_f)\mathbf{F}\mathbf{C}(t_f), \tag{4.3.4}$$

and $\mathbf{g}(\mathbf{x})$ is a solution of the state-dependent non-homogeneous vector differential equation

$$\dot{\mathbf{g}}(\mathbf{x}) = -[\mathbf{A}(\mathbf{x}) - \mathbf{B}(\mathbf{x})\mathbf{R}^{-1}(\mathbf{x})\mathbf{B}'(\mathbf{x})\mathbf{P}(\mathbf{x})]'\mathbf{g}(\mathbf{x}) - \mathbf{C}'(\mathbf{x})\mathbf{Q}(\mathbf{x})\mathbf{z}(\mathbf{x}), \tag{4.3.5}$$

with the final condition

$$\mathbf{g}(\mathbf{x}, t_f) = \mathbf{C}'(t_f)\mathbf{F}\mathbf{z}(t_f). \tag{4.3.6}$$

The resulting differential SDRE-controlled trajectory becomes the solution of the state-dependent closed-loop dynamics

$$\dot{\mathbf{x}}(t) = [\mathbf{A}(\mathbf{x}) - \mathbf{B}(\mathbf{x})\mathbf{R}^{-1}(\mathbf{x})\mathbf{B}'(\mathbf{x})\mathbf{P}(\mathbf{x})]\mathbf{x}(t) + \mathbf{B}(\mathbf{x})\mathbf{R}^{-1}(\mathbf{x})\mathbf{B}'(\mathbf{x})\mathbf{g}(\mathbf{x}). \tag{4.3.7}$$

Similar to Section 4.2.2, an approximate analytical approach is used and the DRE (4.3.3), and the non-homogeneous differential equation (4.3.5), can be solved in the following steps at each time step:

1. Solve for $\mathbf{P}(\mathbf{x}, \mathbf{t})$ similar to the differential SDRE regulator problem in Section 4.2.2, steps from 1 to 6.

2. Calculate the steady state value $\mathbf{g_{ss}}(\mathbf{x})$ from the equation

$$\mathbf{g_{ss}}(\mathbf{x}) = [\mathbf{A}(\mathbf{x}) - \mathbf{B}(\mathbf{x})\mathbf{R}^{-1}(\mathbf{x})\mathbf{B}'(\mathbf{x})\mathbf{P_{ss}}(\mathbf{x})]'^{-1}\mathbf{C}'(\mathbf{x})\mathbf{Q}(\mathbf{x})\mathbf{z}(\mathbf{x}). \tag{4.3.8}$$

3. Use change-of-variables technique and assume that

$$\mathbf{K_g}(\mathbf{x}, t) = [\mathbf{g}(\mathbf{x}, t) - \mathbf{g_{ss}}(\mathbf{x})]. \tag{4.3.9}$$

4. Solve the differential equation

$$\mathbf{K_g}(\mathbf{x}, t) = \mathbf{e}^{-(\mathbf{A}-\mathbf{B}\mathbf{R}^{-1}\mathbf{B}'\mathbf{P})'(\mathbf{t}-\mathbf{t_f})}[\mathbf{g}(\mathbf{x}, t_f) - \mathbf{g_{ss}}(\mathbf{x})]. \tag{4.3.10}$$

5. Use changing-of-variables procedure to calculate the value of $\mathbf{g}(\mathbf{x}, t)$

$$\mathbf{g}(\mathbf{x}, t) = \mathbf{K_g}(\mathbf{x}, t) + \mathbf{g_{ss}}(\mathbf{x}). \tag{4.3.11}$$

6. Calculate the value of the optimal control $\mathbf{u}(\mathbf{x}, t)$ as

$$\mathbf{u}(\mathbf{x}, t) = -\mathbf{R}^{-1}(\mathbf{x})\mathbf{B}'(\mathbf{x})[\mathbf{P}(\mathbf{x}, t)\mathbf{x}(t) - \mathbf{g}(\mathbf{x}, t)]. \tag{4.3.12}$$

Fig.4.6 summarizes the overview of the flow chart of finite-horizon differential SDRE tracking technique

Note : As in the regulation, the technique with finite-horizon differential SDRE can be used for linear systems and the differential SDRE becomes the standard DRE [98].

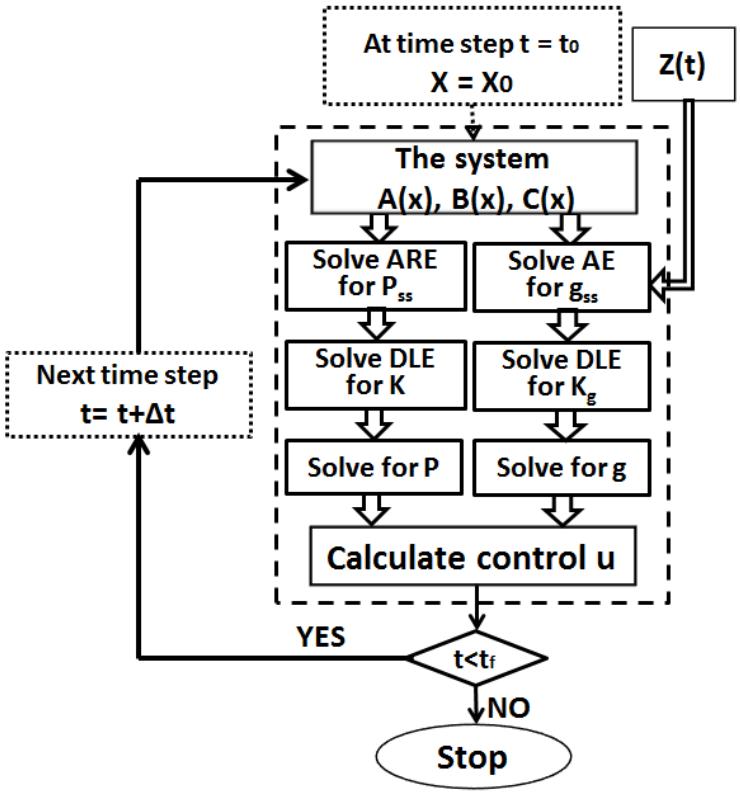

Figure 4.6: Flow Chart for the Finite-Horizon Differential SDRE Tracking Technique

4.3.3 Finite-Horizon Differential SDRE Tracking Simulation

In this section, simulations with the finite-time horizon optimal tracking controller for linear and nonlinear systems are presented.

4.3.3.1 Linear System Example : Smart Prosthetic Hand

Consider the two-link thumb of a smart prosthetic hand [26]. The links in kinematics are modeled as rigid bodies, as shown in Fig. 4.7, and the properties of rigid body displacement take a central place in kinematics [64]. Figure 4.8 shows the illustration of two-link thumb. L_1^t and L_2^t are the lengths of the links 1 and 2 of the thumb, respectively; q_1^t and q_2^t are the angles of joints 1 and 2 of the thumb.

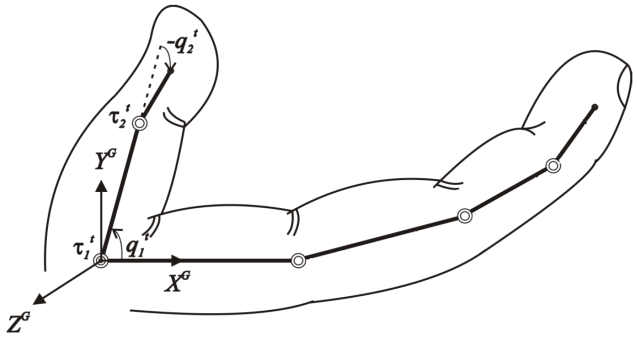

Figure 4.7: Schematic Diagram of Thumb

The various parameters [128] relating to desired trajectory and the two-link thumb selected for the simulations are given in Table 4.1

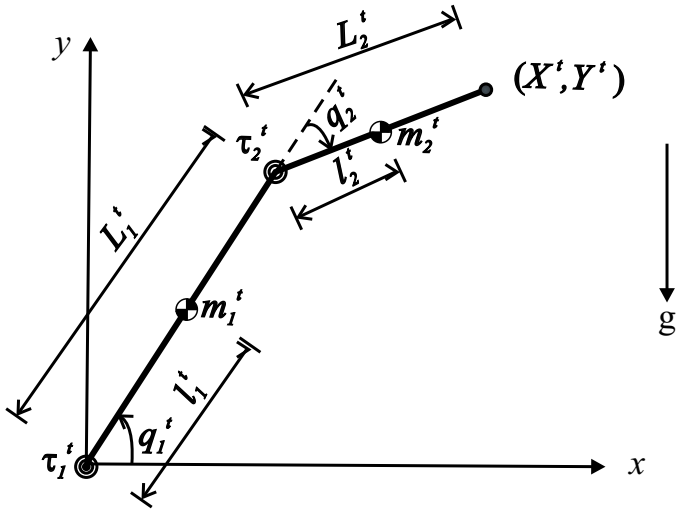

Figure 4.8: Illustration of Two-Link Thumb [26]

Table 4.1: Parameter Selection of Thumb

Parameters	Values
Time (t_0, t_f)	0, 20 (sec)
Desired Initial Position (X_0^t, Y_0^t)	0.035, 0.060 (m)
Desired Final Position (X_f^t, Y_f^t)	0.0495, 0.060 (m)
Desired Initial Velocity ($\dot{X}_0^t$, $\dot{Y}_0^t$)	0, 0 (m/s)
Desired Final Velocity ($\dot{X}_f^t$, $\dot{Y}_f^t$)	0, 0 (m/s)
Length (L_1^t, L_2^t)	0.040, 0.040 (m)
p3 inMass (m_1^t, m_2^t)	0.043, 0.031 (kg)
p3 inInertia (I_{zz1}^t, I_{zz2}^t)	6.002×10^{-6}, 4.327×10^{-6} (kg-m^2)

Matrices **A**, **B**, and **C** of thumb are chosen as

$$\mathbf{A} = \begin{bmatrix} 0 & 0 & 1 & 0 \\ 0 & 0 & 0 & 1 \\ 0 & 0 & 0 & 0 \\ 0 & 0 & 0 & 0 \end{bmatrix}, \tag{4.3.13}$$

$$\mathbf{B} = \begin{bmatrix} 0 & 0 & 0 & 1 \\ 0 & 0 & 1 & 0 \end{bmatrix}', \quad \mathbf{C} = \begin{bmatrix} 1 & 0 & 0 & 0 \\ 0 & 1 & 0 & 0 \end{bmatrix}, \tag{4.3.14}$$

and the selected weighted matrices are

$$\mathbf{Q} = diag(100, 100, 10, 10), \quad \mathbf{R} = diag(0.1, 0.1), \quad \mathbf{F} = diag(1, 1, 1, 1). \qquad (4.3.15)$$

The simulations are performed for final time of 10 seconds and the resulting angle trajectory is shown in Fig. 4.9, the solid blue line denotes *the actual* angle of joint 1 of thumb using finite-horizon differential SDRE controller, the dashed red line denotes *the desired* angle of joint 1 of thumb, the solid green line denotes *the actual* angle of joint 2 of thumb, the dashed green line denotes *the desired* angle of joint 2 of thumb. It's clear that the proposed methodology gives very good result as the actual angles is making almost ideal tracking to the desired angles. The tracking angles errors are shown in Fig. 4.10.

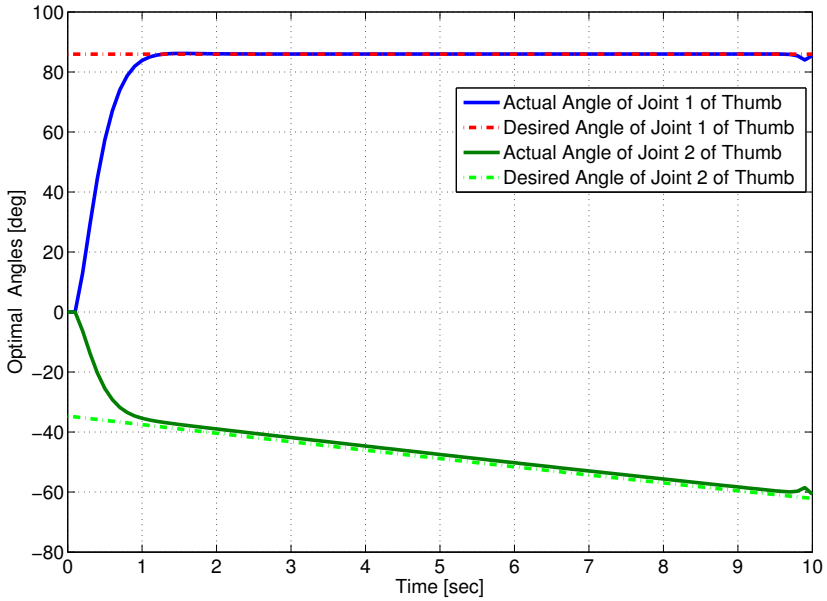

Figure 4.9: Joint Angles of Thumb

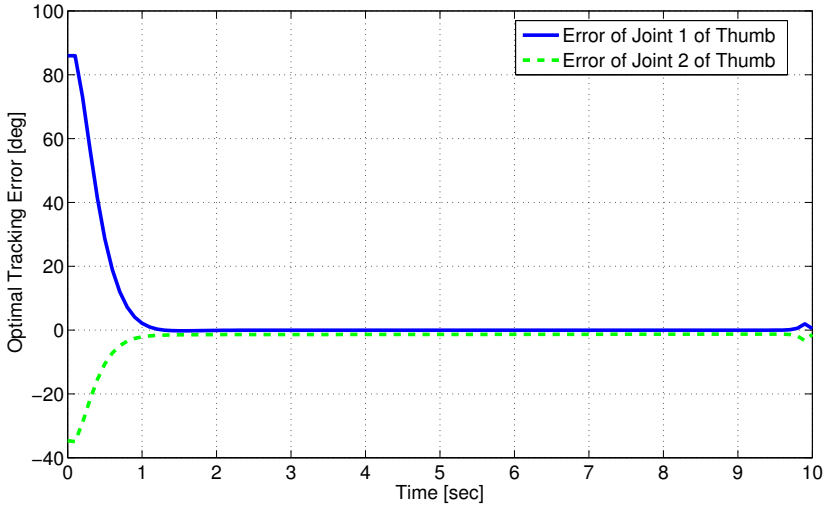

Figure 4.10: Tracking Error of Thumb

4.3.3.2 Nonlinear System Example : Permanent Magnet Synchronous Motor

The mathematical model of a surface mounted permanent magnet synchronous motor (PMSM) based on $d-q$ axis can be expressed as [111]

$$J\frac{d\omega}{dt} = P\psi_f i_q - B\omega, \tag{4.3.16}$$

$$L\frac{di_q}{dt} = -Ri_q + LP\omega i_d - P\psi_f\omega + u_q, \tag{4.3.17}$$

$$L\frac{di_d}{dt} = -Ri_d + LP\omega i_q + u_d, \tag{4.3.18}$$

where, R is stator resistance, L is stator winding inductance, P is pole pairs, ψ_f is rotor permanent magnet flux linkage, J is moment inertia, B is viscous friction coefficient, i_d and i_q , u_d and u_q are $d-q$ axis stator current and voltage respectively,

ω is the motor mechanical velocity.

The nonlinear equations of the system can be written as

$$\dot{x_1} = -0.8x_1 + 720x_2, \tag{4.3.19}$$

$$\dot{x_2} = -80x_1 - 185x_2 - 4x_1x_3 + 100u_1, \tag{4.3.20}$$

$$\dot{x_3} = -185x_3 - 4x_1x_2 + 100u_2, \tag{4.3.21}$$

$$y = x_1, \tag{4.3.22}$$

where: $\omega = x_1$, $i_q = x_2$, $i_d = x_3$, $u_q = u_1$, $u_d = u_2$, and the motor parameters are showed in Table 4.2

The system nonlinear equations can be rewritten in the state dependent form

$$\begin{bmatrix} \dot{x_1} \\ \dot{x_2} \\ \dot{x_3} \end{bmatrix} = \begin{bmatrix} -0.8 & 720 & 0 \\ -80 & -185 & -4x_1 \\ 0 & -4x_1 & -185 \end{bmatrix} \begin{bmatrix} x_1 \\ x_2 \\ x_3 \end{bmatrix} + \begin{bmatrix} 0 & 0 \\ 100 & 0 \\ 0 & 100 \end{bmatrix} \begin{bmatrix} u_1 \\ u_2 \end{bmatrix}. \tag{4.3.23}$$

Let the desired motor speed be

$$z(t) = \begin{cases} 300 \ \ rpm \quad \text{for} \quad t < 3, \\ 50 \ \ rpm \quad \text{for} \quad 3 < t < 10, \end{cases} \tag{4.3.24}$$

and the selected weighted matrices be

$$\mathbf{Q} = diag(2000, 2000, 2000), \quad \mathbf{R} = diag(1, 1), \quad \mathbf{F} = diag(1, 1, 1). \tag{4.3.25}$$

Table 4.2: PMSM Parameters

Parameter	Nominal value
R	1.65Ω
L	$0.0092H$
J	$0.001kg.m^2$
P	4
ψ_f	$0.18Wb$
B	$0.0008N.m.sec/rad$

The simulations are performed for final time of 10 seconds and the resulting motor speed trajectory is shown in Fig. 4.11, and the optimal control is shown in Fig. 4.12. In Fig. 4.11, the solid line denotes *the actual* motor speed trajectory, and the dashed line denotes *the desired* speed.

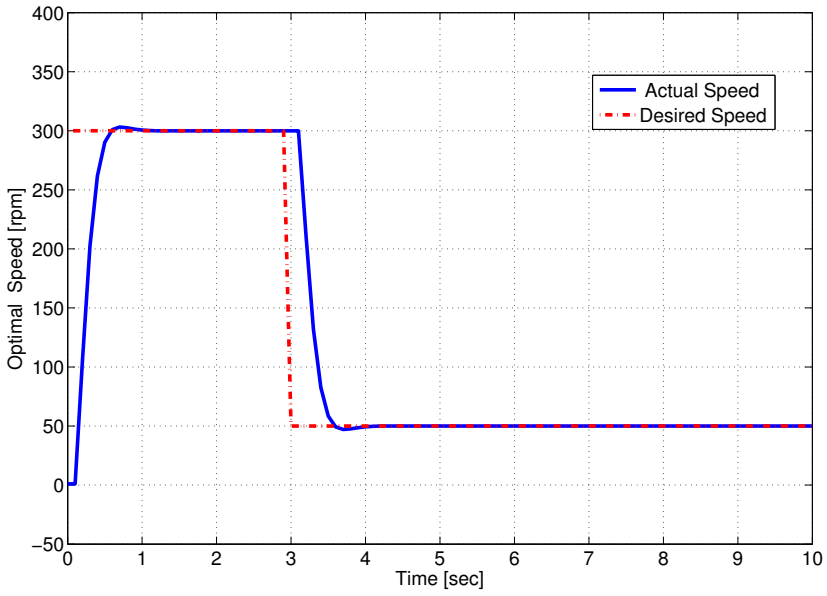

Figure 4.11: Optimal speed for PMSM

Comparing these trajectories in Fig. 4.11, it's clear that the finite-horizon differential SDRE nonlinear tracking algorithm gives very good results as the actual optimal

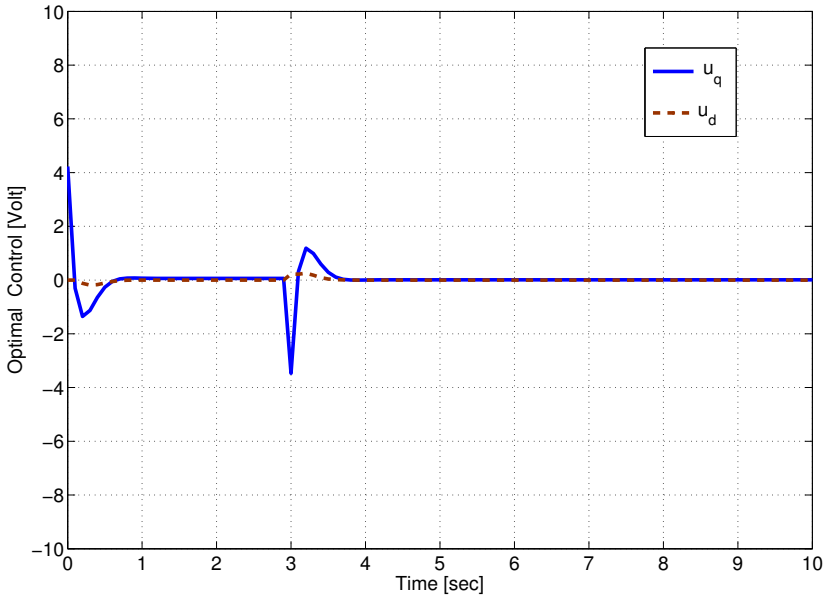

Figure 4.12: Optimal Control for PMSM

speed is making very good tracking to the desired one, and the developed algorithm is able to solve the differential SDRE finite-horizon nonlinear tracking problem.

4.4 Conclusions

Finite-horizon optimal control of nonlinear systems is a challenging problem in the control field due to the complexity of time-dependency of the Hamilton Jacobi Bellman (HJB) differential equation. The available methods for this purpose have drawbacks in terms of the dependency of the solution to the pre-specified initial conditions and the lack existence of the optimal solution under all conditions.

This chapter presents a novel and computationally efficient online technique used for finite-horizon nonlinear regulating and tracking problems. This technique based on change of variables that converts the differential Riccati equation to a linear Lyapunov

equation. During online implementation, the Lyapunov equation is solved in a closed form at the given time step.

Chapter 5

Finite-Horizon Differential State Dependent Riccati Equation (SDRE) for Stochastic Systems

Kalman filter is an effective minimum variance linear state estimator that estimates the system states corrupted with white process and measurement noise. The standard Kalman filter is limited only to *linear* systems. Most real-world systems are *nonlinear*, in which case standard Kalman filters are not applicable [121]. Therefore, it becomes necessary to use some other nonlinear filter techniques. The Extended Kalman filter (EKF) is the most widely applied state estimation algorithm for nonlinear systems. The EKF relies on *linearization* of the nonlinear system (using Taylor series expansion) near the region close to the operating point [114]. In linearization, we assume that the range of operation is small. Consequently, the EKF will only be

effective in the small neighborhood of the operating points, and the accuracy of this technique will decrease for large operating range of nonlinear systems.

5.1 Finite-Horizon Regulation for Stochastic Nonlinear Systems

5.1.1 Optimal Estimation

Suppose that the entire state $\mathbf{x}(t)$ is not available, but only the output $\mathbf{y}(t)$ is measurable. Let us reproduce the nonlinear system with noises in state dependent form

$$\dot{\mathbf{x}}(t) = \mathbf{A}(\mathbf{x})\mathbf{x}(t) + \mathbf{B}(\mathbf{x})\mathbf{u}(t) + \mathbf{B}_w(t)\mathbf{w}(t), \tag{5.1.1}$$

$$\mathbf{y}(t) = \mathbf{C}(\mathbf{x})\mathbf{x}(t) + \mathbf{v}(t), \tag{5.1.2}$$

where, $\mathbf{w}(t)$ and $\mathbf{v}(t)$ are process, and measurement (white, Gaussian, zero mean) random noises, respectively.

In order to find the best estimate $\hat{\mathbf{x}}(t)$ and the corresponding covariance matrix $\mathbf{P}_e(\hat{\mathbf{x}}, t)$, we use the results of Section 3.1 from Chapter 3 . At each time step, the state estimate equations are

$$\dot{\hat{\mathbf{x}}}(t) = \mathbf{A}(\hat{\mathbf{x}})\hat{\mathbf{x}}(t) + \mathbf{B}(\hat{\mathbf{x}})\mathbf{u}(t) + \mathbf{K}_e(\hat{\mathbf{x}}, t)[\mathbf{y}(t) - \mathbf{C}(\hat{\mathbf{x}})\hat{\mathbf{x}}(t)]; \tag{5.1.3}$$

$$\hat{\mathbf{x}}(t_0) = \bar{\mathbf{x}}(t_0),$$

where, $\mathbf{K}_e(\hat{\mathbf{x}}, t)$, the optimal Kalman estimator gain, is obtained as

$$\mathbf{K}_e(\hat{\mathbf{x}}, t) \;=\; \mathbf{P}_e(\hat{\mathbf{x}}, t)\mathbf{C}'(\hat{\mathbf{x}})\mathbf{R}_v^{-1}(t), \tag{5.1.4}$$

and $\mathbf{P}_e(\hat{\mathbf{x}}, t)$ is the solution of the matrix differential Riccati equation

$$\dot{\mathbf{P}}_e(\hat{\mathbf{x}}, t) = \mathbf{A}(\hat{\mathbf{x}})\mathbf{P}_e(\hat{\mathbf{x}}, t) + \mathbf{P}_e(\hat{\mathbf{x}}, t)\mathbf{A}'(\hat{\mathbf{x}}) + \mathbf{B}_w(t)\mathbf{Q}_w(t)\mathbf{B}_w'(t) - \mathbf{P}_e(\hat{\mathbf{x}}, t)\mathbf{C}'(\hat{\mathbf{x}})\mathbf{R}_v^{-1}(t)\mathbf{C}(\hat{\mathbf{x}})\mathbf{P}_e(\hat{\mathbf{x}}, t), \tag{5.1.5}$$

is to be solved in *forward* direction with initial condition $\mathbf{P}_e(\hat{\mathbf{x}}, t_0) = \mathbf{P}_{e0}$ for any real-time implementation, whereas the standard differential Riccati equation, arising in the control problem, is to be solved in *backward* direction with a given final condition. The minimization of J is equivalent to minimization of

$$J_a(\mathbf{x}, u) = \mathcal{E}\left\{\frac{1}{2}\hat{\mathbf{x}}'(t_f)\mathbf{F}\hat{\mathbf{x}}(t_f) + \frac{1}{2}\int_{t_0}^{t_f}[\hat{\mathbf{x}}'(t)\mathbf{Q}(\hat{\mathbf{x}})\hat{\mathbf{x}}(t) + \mathbf{u}'(\hat{\mathbf{x}}, t)\mathbf{R}(\hat{\mathbf{x}})\mathbf{u}(\hat{\mathbf{x}}, t)dt\right\}. \tag{5.1.6}$$

5.1.2 Optimal Regulation

At each time step, using the results of finite-horizon nonlinear regulator obtained in Chapter 4 except that the state is now the optimal estimate $\hat{\mathbf{x}}(t)$

$$\mathbf{u}(\hat{\mathbf{x}}, t) = -\mathbf{R}^{-1}(\hat{\mathbf{x}})\mathbf{B}'(\hat{\mathbf{x}})\mathbf{P}_c(\hat{\mathbf{x}}, t)\hat{\mathbf{x}}(t) = -\mathbf{K}_c(\hat{\mathbf{x}}, t)\hat{\mathbf{x}}(t), \tag{5.1.7}$$

where, $\mathbf{K}_c(\hat{\mathbf{x}}, t) = \mathbf{R}^{-1}(\hat{\mathbf{x}})\mathbf{B}'(\hat{\mathbf{x}})\mathbf{P}_c(\hat{\mathbf{x}}, t)$, is the Kalman *controller* gain and $\mathbf{P}_c(\hat{\mathbf{x}}, t)$ is the solution of the finite-horizon, differential SDRE obtained in Section 4.2 from

Chapter 4.

The entire algorithm of combined *estimation* and *control* leading to nonlinear regulator problem is shown in the following steps:

5.1.2.1 Optimal Estimator/Kalman Filter

- At each time step, solve the differential matrix Riccati equation

$$\dot{\mathbf{P}}_e(\hat{\mathbf{x}},t) = \mathbf{A}(\hat{\mathbf{x}})\mathbf{P}_e(\hat{\mathbf{x}},t) + \mathbf{P}_e(\hat{\mathbf{x}},t)\mathbf{A}'(\hat{\mathbf{x}}) + \mathbf{B}_w(t)\mathbf{Q}_w(t)\mathbf{B}'_w(t) - \mathbf{P}_e(\hat{\mathbf{x}},t)\mathbf{C}'(\hat{\mathbf{x}})\mathbf{R}_v^{-1}(t)\mathbf{C}(\hat{\mathbf{x}})\mathbf{P}_e(\hat{\mathbf{x}},t), \quad (5.1.8)$$

  in the forward direction with the initial condition $\mathbf{P}_e(\hat{\mathbf{x}},t_0) = \mathbf{P}_{e0}$.

- Obtain the optimal estimator (filter) gain as

$$\mathbf{K}_e(\hat{\mathbf{x}},t) = \mathbf{P}_e(\hat{\mathbf{x}},t)\mathbf{C}'(\hat{\mathbf{x}})\mathbf{R}_v^{-1}(t). \quad (5.1.9)$$

- Solve for the optimal state estimate $\hat{\mathbf{x}}(t)$ from

$$\dot{\hat{\mathbf{x}}}(t) = \mathbf{A}(\hat{\mathbf{x}})\hat{\mathbf{x}}(t) + \mathbf{B}(\hat{\mathbf{x}})\mathbf{u}(t) + \mathbf{K}_e(\hat{\mathbf{x}},t)[\mathbf{y}(t) - \mathbf{C}(\hat{\mathbf{x}})\hat{\mathbf{x}}(t)], \quad (5.1.10)$$

  with the initial condition $\hat{\mathbf{x}}(t_0) = \bar{\mathbf{x}}_0$.

5.1.2.2 Optimal Controller for Regulation

- Solve algebraic Riccati equation (ARE) to calculate the steady state value $\mathbf{P_{ss}}(\hat{\mathbf{x}})$

$$\mathbf{P_{ss}}(\hat{\mathbf{x}})\mathbf{A}(\hat{\mathbf{x}}) + \mathbf{A}'(\hat{\mathbf{x}})\mathbf{P_{ss}}(\hat{\mathbf{x}}) - \mathbf{P_{ss}}(\hat{\mathbf{x}})\mathbf{B}(\hat{\mathbf{x}})\mathbf{R}^{-1}(\hat{\mathbf{x}})\mathbf{B}'(\hat{\mathbf{x}})\mathbf{P_{ss}}\hat{\mathbf{x}} + \mathbf{Q}(\hat{\mathbf{x}}) = 0. \quad (5.1.11)$$

- Use change-of-variables procedure and assume that

$$\mathbf{K}(\hat{\mathbf{x}}, t) = [\mathbf{P_c}(\hat{\mathbf{x}}, t) - \mathbf{P_{ss}}(\hat{\mathbf{x}})]^{-1}. \quad (5.1.12)$$

- Calculate the value of $\mathbf{A_{cl}}(\hat{\mathbf{x}})$ from the equation

$$\mathbf{A_{cl}}(\hat{\mathbf{x}}) = \mathbf{A}(\hat{\mathbf{x}}) - \mathbf{B}(\hat{\mathbf{x}})\mathbf{R}^{-1}\mathbf{B}'(\hat{\mathbf{x}})\mathbf{P_{ss}}(\hat{\mathbf{x}}) \quad (5.1.13)$$

.

- Calculate the value of $\mathbf{D}$ by Solving the algebraic Lyapunov equation [44]

$$\mathbf{A_{cl}}\mathbf{D} + \mathbf{D}\mathbf{A}'_{\mathbf{cl}} - \mathbf{B}\mathbf{R}^{-1}\mathbf{B}' = \mathbf{0}. \quad (5.1.14)$$

- Solve the differential Lyapunov equation

$$\dot{\mathbf{K}}(\hat{\mathbf{x}}, t) = \mathbf{K}(\hat{\mathbf{x}}, t)\mathbf{A}'_{\mathbf{cl}}(\hat{\mathbf{x}}) + \mathbf{A_{cl}}(\hat{\mathbf{x}})\mathbf{K}(\hat{\mathbf{x}}, t) - \mathbf{B}(\hat{\mathbf{x}})\mathbf{R}^{-1}\mathbf{B}'(\hat{\mathbf{x}}). \quad (5.1.15)$$

The solution of (5.1.15) is given by [12]

$$\mathbf{K}(\hat{\mathbf{x}},t) = \mathbf{e}^{\mathbf{A_{cl}(t-t_f)}}(\mathbf{K}(\hat{\mathbf{x}},t_f) - \mathbf{D})\mathbf{e}^{\mathbf{A_{cl}}'\mathbf{(t-t_f)}} + \mathbf{D}. \tag{5.1.16}$$

- Calculate the value of $\mathbf{P_c}(\hat{\mathbf{x}},t)$ from

$$\mathbf{P_c}(\hat{\mathbf{x}},t) = \mathbf{K}^{-1}(\hat{\mathbf{x}},t) + \mathbf{P_{ss}}(\hat{\mathbf{x}}). \tag{5.1.17}$$

- Finally, calculating the value of the optimal control $\mathbf{u}(\hat{\mathbf{x}},t)$ as

$$\mathbf{u}(\hat{\mathbf{x}},t) = -\mathbf{R}^{-1}(\hat{\mathbf{x}})\mathbf{B}'(\hat{\mathbf{x}})\mathbf{P_c}(\hat{\mathbf{x}},t)\hat{\mathbf{x}}(t). \tag{5.1.18}$$

The summary of the nonlinear regulator problem is shown in Fig. 5.1, and the overview of the process of finite-horizon differential SDRE regulation technique for stochastic systems is summarized in Fig.5.2.

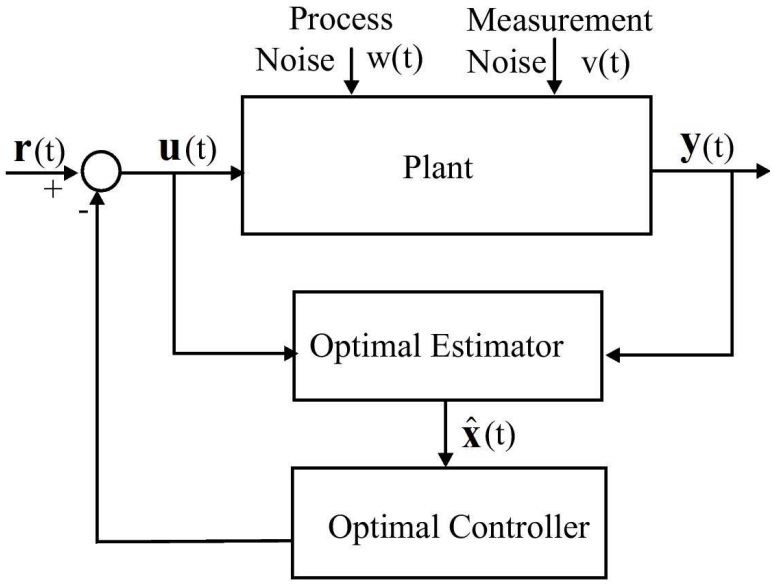

Figure 5.1: Summary of Continuous-Time Nonlinear Regulator

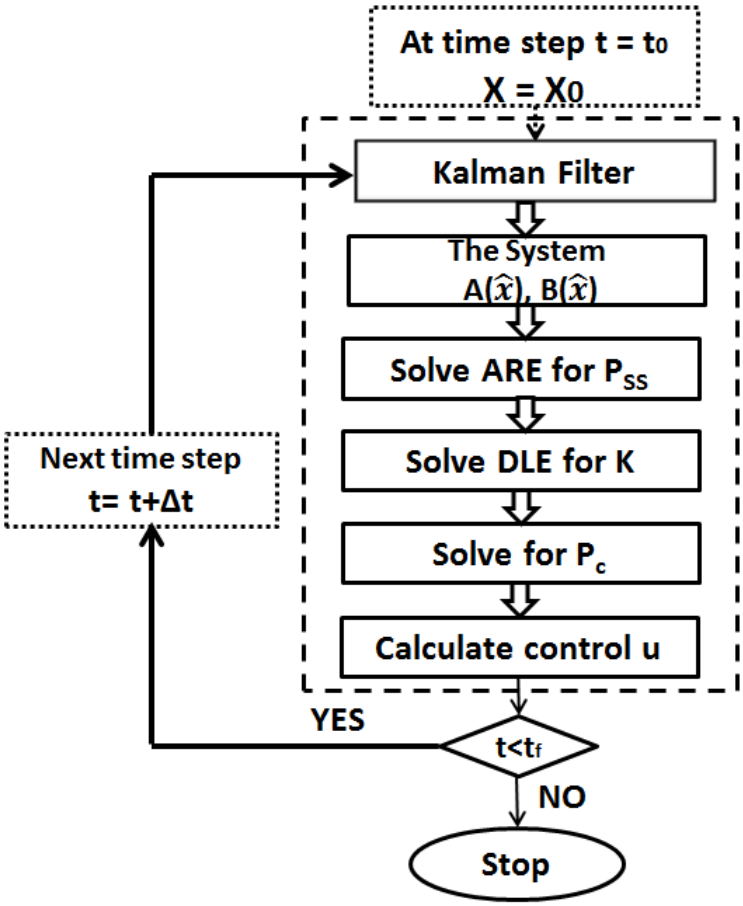

Figure 5.2: Flow Chart of Finite-Horizon Differential SDRE Regulation Technique for Stochastic Systems

Table 5.1: Procedure Summary of Continuous-Time Regulator Problem: Incomplete State Information

Statement of the Problem	
Given the process as $\dot{\mathbf{x}}(t) = \mathbf{A}(\mathbf{x})\mathbf{x}(t) + \mathbf{B}(\mathbf{x})\mathbf{u}(t) + \mathbf{B}_w(t)\mathbf{w}(t)$, the observation of the state as $\mathbf{y}(t) = \mathbf{C}(\mathbf{x})\mathbf{x}(t) + \mathbf{v}(t)$, the performance measure for estimate as $J(t) = \text{trace}\,[var[\tilde{\mathbf{x}}(t)]] + \text{trace}[\mathbf{P}_e(t)]$, the conditions as $\mathcal{E}[\mathbf{w}(t)] = 0, \quad \text{COV}[\mathbf{w}(t), \mathbf{w}(\tau)] = \mathbf{Q}_w(t)\delta(t-\tau), \quad \mathcal{E}[\mathbf{x}(t_0)] = \bar{\mathbf{x}}_0,$ $\text{VAR}[\mathbf{x}(t_0)] = \mathbf{P}_0; \quad \text{COV}[\mathbf{x}(t), \mathbf{w}(\tau)] = 0 \quad \text{for all } \tau > t,$ $E[\mathbf{v}(t)] = 0, \quad COV[\mathbf{v}(t), \mathbf{v}(\tau)] = \mathbf{R}_v(t)\delta(t-\tau),$ $COV[\mathbf{v}(t), \mathbf{w}(\tau)] = 0, \quad COV[\mathbf{v}(t), \mathbf{x}(\tau)] = 0 \text{ for all } t, \tau,$ and the performance measure for control as $\hat{J}(\mathbf{x}_0, t_0) = \mathcal{E}\left\{\frac{1}{2}\mathbf{x}'(t_f)\mathbf{F}\mathbf{x}(t_f) + \frac{1}{2}\int_{t_0}^{t_f}\left[\mathbf{x}'(t)\mathbf{Q}(\mathbf{x})\mathbf{x}(t) + \mathbf{u}'(\mathbf{x})\mathbf{R}(\mathbf{x})\mathbf{u}(\mathbf{x})\right]\right\} dt$ find the optimal estimator and controller	
Solution of the Problem I: Optimal Estimator/Kalman Filter	
Step 1	At each time step, solve the matrix differential Riccati equation $\dot{\mathbf{P}}_e(\hat{\mathbf{x}}, t) = \mathbf{A}(\hat{\mathbf{x}})\mathbf{P}_e(\hat{\mathbf{x}}, t) + \mathbf{P}_e(\hat{\mathbf{x}}, t)\mathbf{A}'(\hat{\mathbf{x}}) + \mathbf{B}_w(t)\mathbf{Q}_w(t)\mathbf{B}_w'(t) -$ $\mathbf{P}_e(\hat{\mathbf{x}}, t)\mathbf{C}'(\hat{\mathbf{x}})\mathbf{R}_v^{-1}(t)\mathbf{C}(\hat{\mathbf{x}})\mathbf{P}_e(\hat{\mathbf{x}}, t); \quad \mathbf{P}_e(\hat{\mathbf{x}}, t_0) = \mathbf{P}_{e0}.$
Step 2	Using $\mathbf{P}_e(\hat{\mathbf{x}}, t)$ from Step 1, obtain the optimal estimator (filter) gain as $\mathbf{K}_e(\hat{\mathbf{x}}, t) = \mathbf{P}_e(\hat{\mathbf{x}}, t)\mathbf{C}'(\hat{\mathbf{x}})\mathbf{R}_v^{-1}(t).$
Step 3	Using $\mathbf{K}_e(\hat{\mathbf{x}}, t)$ from Step 2, solve the optimal state estimate $\hat{\mathbf{x}}(t)$ from $\dot{\hat{\mathbf{x}}}(t) = \mathbf{A}(\hat{\mathbf{x}})\hat{\mathbf{x}}(t) + \mathbf{B}(\hat{\mathbf{x}})\mathbf{u}(t) + \mathbf{K}_e(\hat{\mathbf{x}}, t)[\mathbf{y}(t) - \mathbf{C}(\hat{\mathbf{x}})\hat{\mathbf{x}}(t)]; \quad \hat{\mathbf{x}}(t_0) = \bar{\mathbf{x}}_0.$
Solution of the Problem II: Optimal Controller	
Step 4	At each time step, calculate the value of $\mathbf{P}_c(\hat{\mathbf{x}}, t)$ from the equation $\mathbf{P_c}(\hat{\mathbf{x}}, \mathbf{t}) = \mathbf{K^{-1}}(\hat{\mathbf{x}}, \mathbf{t}) + \mathbf{P_{ss}}(\hat{\mathbf{x}})$, with $K(\hat{\mathbf{x}}, t)$ is the solution differential Lyapunov equation.
Step 5	Using $\mathbf{P}_c(\hat{\mathbf{x}}, t)$ from Step 4, obtain the optimal controller gain as $\mathbf{K}_c(\hat{\mathbf{x}}, t) = \mathbf{R}^{-1}(\hat{\mathbf{x}})\mathbf{B}'(\hat{\mathbf{x}})\mathbf{P}_c(\hat{\mathbf{x}}, t).$
Step 6	Using $\mathbf{K}(\hat{\mathbf{x}}, t)$ from Step 5, obtain the closed-loop optimal control as $\mathbf{u}(\hat{\mathbf{x}}, t) = -\mathbf{K}_c(\hat{\mathbf{x}}, t)\hat{\mathbf{x}}(t).$

The entire algorithm of combined estimation and control leading to nonlinear regulator problem is shown in Table 5.1.

5.1.3 Finite-Horizon Differential SDRE Regulation for Stochastic Systems Simulation : Crane System

This section presents simulations with the finite-time horizon optimal regulator controller and noise cancellation for a nonlinear crane system [58]. The aim of the control design is to control the swinging of a crane as quickly as possible, (see Fig. 5.3). The crane is described as follows

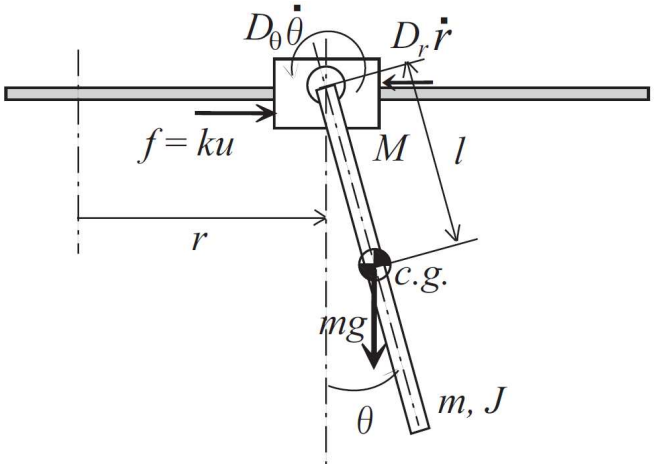

Figure 5.3: Crane System [84]

$$\begin{bmatrix} M+m & -mlcos(\theta) \\ -mlcos(\theta) & J+ml^2 \end{bmatrix} \begin{bmatrix} \ddot{r} \\ \ddot{\theta} \end{bmatrix} = \begin{bmatrix} -D_r\dot{r} - ml\dot{\theta}sin(\theta) + ku \\ -D_\theta\dot{\theta} - mglsin(\theta) \end{bmatrix}, \quad (5.1.19)$$

where M is the mass of cart, k is torque coefficient, J is moment of inertia, l is the length of pendulum, m is the mass of pendulum, D_r is friction coefficient between rail and cart, D_θ is friction coefficient between cart and pendulum, and g is the gravitational acceleration.

Introducing $\mathbf{x} = [\ \theta \quad r \quad \dot{\theta} \quad \dot{r}\ ]'$ as the state vector, we obtain the system state equations

$$\dot{x_1} = x_3, \tag{5.1.20}$$

$$\dot{x_2} = x_4, \tag{5.1.21}$$

$$\begin{aligned}\dot{x_3} = \frac{1}{\alpha(x_1)}\{&mlcos(x_1)\left(-D_r x_4 - mlx_3^2 sin(x_1)\right) \\ &+(M+m)(-D_\theta x_3 - mlgsin(x_1)) + mlkucos(x_1)\},\end{aligned} \tag{5.1.22}$$

$$\begin{aligned}\dot{x_4} = \frac{1}{\alpha(x_1)}\{&(J+ml^2)\left(-D_r x_4 - mlx_3^2 sin(x_1)\right) \\ &+mlcos(x_1)(-D_\theta x_3 - mlgsin(x_1)) + (J+ml^2)ku\},\end{aligned} \tag{5.1.23}$$

where $\alpha(x_1) = (J+ml^2)(M+m) - m^2l^2cos^2(x_1)$.

The nonlinear model for the crane can be rewritten in state dependent form with the State Dependent Coefficient (SDC) matrices

$$\mathbf{A}(\mathbf{x}) = \frac{1}{\alpha(x_1)}\begin{bmatrix} 0 & 0 & \alpha(x_1) & 0 \\ 0 & 0 & 0 & \alpha(x_1) \\ a_{31}(x) & 0 & a_{33}(x) & a_{34}(x) \\ a_{41}(x) & 0 & a_{43}(x) & a_{44} \end{bmatrix}, \tag{5.1.24}$$

$$\mathbf{B}(\mathbf{x}) = \frac{1}{\alpha(x_1)}\begin{bmatrix} 0 \\ 0 \\ b3(x) \\ b4 \end{bmatrix}, \tag{5.1.25}$$

where

$$a_{31}(x) = -(M+m)mlgsin(x_1), \tag{5.1.26}$$

$$a_{33}(x) = -m^2l^2x_3cos(x_1)sin(x_1) - (M+m)D_\theta, \tag{5.1.27}$$

$$a_{34}(x) = mlD_rcos(x_1), \tag{5.1.28}$$

$$a_{41}(x) = -m^2l^2gcos(x_1)sin(x_1), \tag{5.1.29}$$

$$a_{43}(x) = (J+ml^2)mlx_3sin(x_1) - mlD_\theta cos(x_1), \tag{5.1.30}$$

$$a_{44} = (J+ml^2)D_r, \tag{5.1.31}$$

$$b_3(x) = mlkcos(x_1), \tag{5.1.32}$$

$$b_4 = (J+ml^2)k, \tag{5.1.33}$$

The various parameters of the crane system are given in Table 5.2,

Table 5.2: Parameter of the Crane System

Parameters	Values
M	1.96 [kg]
k	0.98 [N/V]
J	0.000447 [kg-m2]
l	0.125 [m]
m	0.045 [kg]
D_r	16.3 [kg/sec]
D_θ	0.00402 [kg-m2/sec]
g	9.8 [m/sec2]

with the initial conditions

$$\mathbf{x_0} = [\pi/4, 0, 0, 0]'. \tag{5.1.34}$$

The selected weighted matrices are

$$\mathbf{Q} = diag(100, 1, 1, 1), \quad \mathbf{R} = 0.01, \quad \mathbf{F} = diag(1, 1, 1, 1). \tag{5.1.35}$$

The covariances of the noises have been taken as

$$\mathbf{Q_w} = diag(2, 1, 2, 1), \qquad \mathbf{R_v} = 1. \tag{5.1.36}$$

The simulations are performed for final time of 10 seconds and the resulting crane angle trajectories is shown in Fig. 5.4, and the optimal control trajectories is shown in Fig. 5.5.

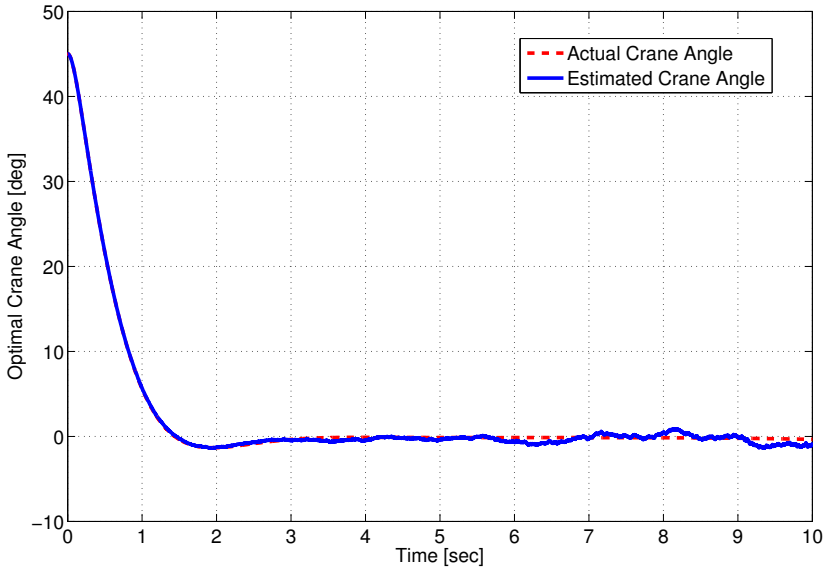

Figure 5.4: Optimal Crane Angles

Note that for sake of validity of the purposed technique, a comparison between *the estimated* (with noise) and *the actual* (without noise) angle was done. In Fig.

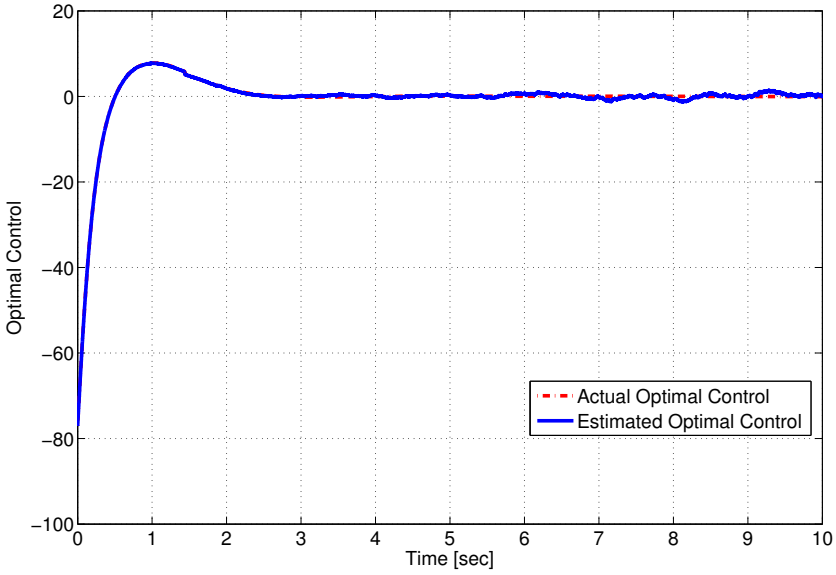

Figure 5.5: Optimal Crane Control

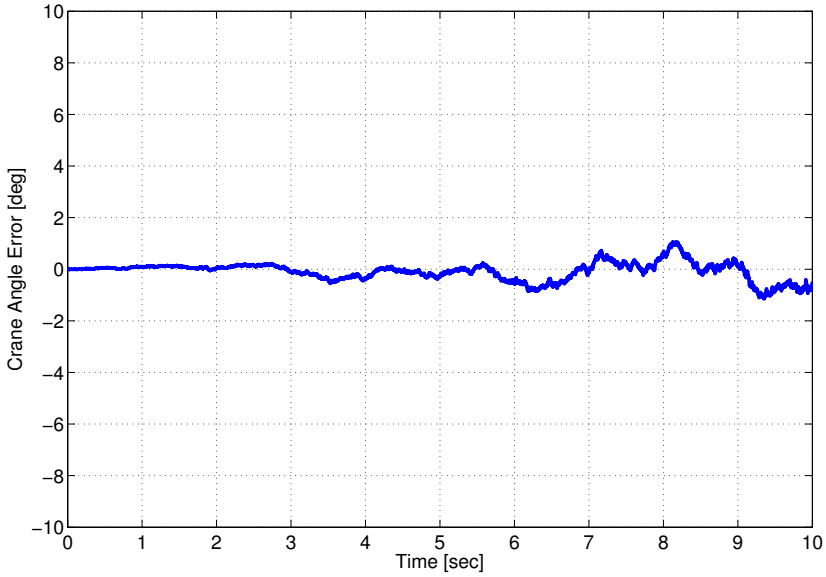

Figure 5.6: Crane Angle Error

5.4, the solid line denotes *the estimated* trajectory of the crane angle, the dashed line denotes *the actual* trajectory. It can be noted that the proposed method gives very good results as the estimated angle is very close to the actual state. As shown in Fig. 5.6 the error between the actual and the estimated state is very small, the average error for this example is 0.3%.

5.2 Finite-Horizon Tracking for Stochastic Nonlinear Systems

5.2.1 Optimal Estimation

Let us reproduce the nonlinear system with process and measurement noises in state dependent form

$$\dot{\mathbf{x}}(t) = \mathbf{A}(\mathbf{x})\mathbf{x}(t) + \mathbf{B}(\mathbf{x})\mathbf{u}(t) + \mathbf{B}_w(t)\mathbf{w}(t), \tag{5.2.1}$$

$$\mathbf{y}(t) = \mathbf{C}(\mathbf{x})\mathbf{x}(t) + \mathbf{v}(t). \tag{5.2.2}$$

In order to find the best estimate $\hat{\mathbf{x}}(t)$ and the corresponding covariance matrix $\mathbf{P}_e(\hat{\mathbf{x}}, t)$, we use the results of Section 3.1 from Chapter 3. At each time step, the estimate equation is

$$\dot{\hat{\mathbf{x}}}(t) = \mathbf{A}(\hat{\mathbf{x}})\hat{\mathbf{x}}(t) + \mathbf{B}(\hat{\mathbf{x}})\mathbf{u}(t) + \mathbf{K}_e(\hat{\mathbf{x}}, t)[\mathbf{y}(t) - \mathbf{C}(\hat{\mathbf{x}})\hat{\mathbf{x}}(t)]; \tag{5.2.3}$$

$$\hat{\mathbf{x}}(t_0) = \bar{\mathbf{x}}(t_0),$$

where, $\mathbf{K}_e(\hat{\mathbf{x}}, t)$, the optimal Kalman estimator gain, is obtained as

$$\mathbf{K}_e(\hat{\mathbf{x}}, t) = \mathbf{P}_e(\hat{\mathbf{x}}, t)\mathbf{C}'(\hat{\mathbf{x}})\mathbf{R}_v^{-1}(t), \tag{5.2.4}$$

and $\mathbf{P}_e(\hat{\mathbf{x}}, t)$ is the solution of the matrix differential Riccati equation

$$\begin{aligned}\dot{\mathbf{P}}_e(\hat{\mathbf{x}}, t) = \mathbf{A}(\hat{\mathbf{x}})\mathbf{P}_e(\hat{\mathbf{x}}, t) + \mathbf{P}_e(\hat{\mathbf{x}}, t)\mathbf{A}'(\hat{\mathbf{x}}) + \mathbf{B}_w(t)\mathbf{Q}_w(t)\mathbf{B}_w'(t) \\ -\mathbf{P}_e(\hat{\mathbf{x}}, t)\mathbf{C}'(\hat{\mathbf{x}})\mathbf{R}_v^{-1}(t)\mathbf{C}(\hat{\mathbf{x}})\mathbf{P}_e(\hat{\mathbf{x}}, t),\end{aligned} \tag{5.2.5}$$

where $\mathbf{P}_e(\hat{\mathbf{x}}, t_0) = \mathbf{P}_{e0}$.

The minimization of J is equivalent to minimization of

$$J_a(\mathbf{x}, u) = \mathcal{E}\left\{\frac{1}{2}\hat{\mathbf{e}}'(t_f)\mathbf{F}\hat{\mathbf{e}}(t_f) + \frac{1}{2}\int_{t_0}^{t_f}[\hat{\mathbf{e}}'(t)\mathbf{Q}(\hat{\mathbf{x}})\hat{\mathbf{e}}(t) + \mathbf{u}'(\hat{\mathbf{x}}, t)\mathbf{R}(\hat{\mathbf{x}})\mathbf{u}(\hat{\mathbf{x}}, t)dt\right\}, \tag{5.2.6}$$

where the estimated error $\hat{\mathbf{e}}(t) = \mathbf{z}(t) - \mathbf{C}(\hat{\mathbf{x}})\hat{\mathbf{x}}(t)$.

5.2.2 Optimal Tracking

At each time step, using the results of finite-horizon nonlinear tracking obtained in Chapter 4 except that the state is now the optimal estimate $\hat{\mathbf{x}}(t)$

$$\mathbf{u}(\hat{\mathbf{x}}, t) = -\mathbf{R}^{-1}(\hat{\mathbf{x}})\mathbf{B}'(\hat{\mathbf{x}})[\mathbf{P}_c(\hat{\mathbf{x}}, t)\hat{\mathbf{x}}(t) - \mathbf{g}(\hat{\mathbf{x}}, t)], \tag{5.2.7}$$

where, $\mathbf{P}_c(\hat{\mathbf{x}}, t)$ and $\mathbf{g}(\hat{\mathbf{x}}, t)$ are the solutions of the finite-horizon differential SDRE problem obtained in Section 4.3 from Chapter 4.

The entire algorithm of combined estimation and control leading to nonlinear tracking problem is shown in the following steps:

5.2.2.1 Optimal Estimator/Kalman Filter

- At each time step, solve the differential matrix Riccati equation

$$\dot{\mathbf{P}}_e(\hat{\mathbf{x}},t) = \mathbf{A}(\hat{\mathbf{x}})\mathbf{P}_e(\hat{\mathbf{x}},t) + \mathbf{P}_e(\hat{\mathbf{x}},t)\mathbf{A}'(\hat{\mathbf{x}}) + \mathbf{B}_w(t)\mathbf{Q}_w(t)\mathbf{B}_w'(t) - \mathbf{P}_e(\hat{\mathbf{x}},t)\mathbf{C}'(\hat{\mathbf{x}})\mathbf{R}_v^{-1}(t)\mathbf{C}(\hat{\mathbf{x}})\mathbf{P}_e(\hat{\mathbf{x}},t), \quad (5.2.8)$$

  in the forward direction with the initial condition $\mathbf{P}_e(\hat{\mathbf{x}},t_0) = \mathbf{P}_{e0}$.

- Obtain the optimal estimator (filter) gain as

$$\mathbf{K}_e(\hat{\mathbf{x}},t) = \mathbf{P}_e(\hat{\mathbf{x}},t)\mathbf{C}'(\hat{\mathbf{x}})\mathbf{R}_v^{-1}(t). \quad (5.2.9)$$

- Solve for the optimal state estimate $\hat{\mathbf{x}}(t)$ from

$$\dot{\hat{\mathbf{x}}}(t) = \mathbf{A}(\hat{\mathbf{x}})\hat{\mathbf{x}}(t) + \mathbf{B}(\hat{\mathbf{x}})\mathbf{u}(t) + \mathbf{K}_e(\hat{\mathbf{x}},t)[\mathbf{y}(t) - \mathbf{C}(\hat{\mathbf{x}})\hat{\mathbf{x}}(t)], \quad (5.2.10)$$

  with the initial condition $\hat{\mathbf{x}}(t_0) = \bar{\mathbf{x}}_0$.

5.2.2.2 Optimal Controller for Tracking

- Solve for $\mathbf{P}(\hat{\mathbf{x}},t)$ similar to the differential SDRE regulator problem in Section 5.1.2

- Calculate the steady state value $\mathbf{g_{ss}}(\hat{\mathbf{x}})$ from the equation

$$\mathbf{g_{ss}}(\hat{\mathbf{x}}) = [\mathbf{A}(\hat{\mathbf{x}}) - \mathbf{B}(\hat{\mathbf{x}})\mathbf{R}^{-1}(\hat{\mathbf{x}})\mathbf{B}'(\hat{\mathbf{x}})\mathbf{P_{ss}}(\hat{\mathbf{x}})]'^{-1}\mathbf{C}'(\hat{\mathbf{x}})\mathbf{Q}(\hat{\mathbf{x}})\mathbf{z}(\hat{\mathbf{x}}). \quad (5.2.11)$$

- Use change-of-variables procedure and assume that

$$\mathbf{K_g}(\hat{\mathbf{x}}, t) = [\mathbf{g}(\hat{\mathbf{x}}, t) - \mathbf{g_{ss}}(\hat{\mathbf{x}})]. \quad (5.2.12)$$

- Solve differential equation to obtain

$$\mathbf{K_g}(\hat{\mathbf{x}}, t) = \mathbf{e}^{-(\mathbf{A}-\mathbf{B}\mathbf{R}^{-1}\mathbf{B}'\mathbf{P})'(\mathbf{t}-\mathbf{t_f})}[\mathbf{g}(\hat{\mathbf{x}}, t_f) - \mathbf{g_{ss}}(\hat{\mathbf{x}})]. \quad (5.2.13)$$

- Calculate the value of $\mathbf{g}(\hat{\mathbf{x}}, t)$ from

$$\mathbf{g}(\hat{\mathbf{x}}, t) = \mathbf{K_g}(\hat{\mathbf{x}}, t) + \mathbf{g_{ss}}(\hat{\mathbf{x}}). \quad (5.2.14)$$

- Calculate the value of the optimal control $\mathbf{u}(\hat{\mathbf{x}}, t)$ as

$$\mathbf{u}(\hat{\mathbf{x}}, t) = -\mathbf{R}^{-1}(\hat{\mathbf{x}})\mathbf{B}'(\hat{\mathbf{x}})[\mathbf{P}_c(\hat{\mathbf{x}}, t)\hat{\mathbf{x}}(t) - \mathbf{g}(\hat{\mathbf{x}}, t)]. \quad (5.2.15)$$

The summary of the nonlinear tracking problem is shown in Fig. 5.7. Here, we see that the original plant is subjected to process noise $\mathbf{w}(t)$ and measurement noise $\mathbf{v}(t)$.

Fig.5.8 summarizes the overview of the process of finite-horizon differential SDRE tracking technique for stochastic systems.

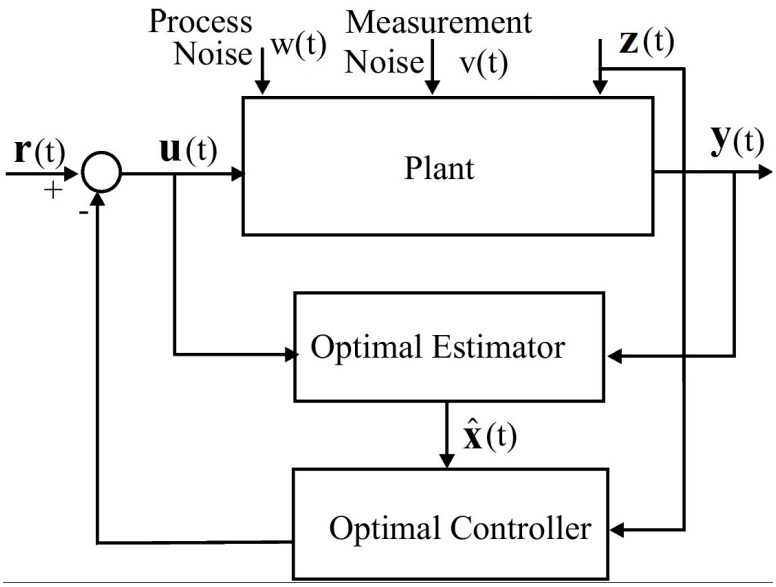

Figure 5.7: Summary of Continuous-Time Nonlinear Tracking

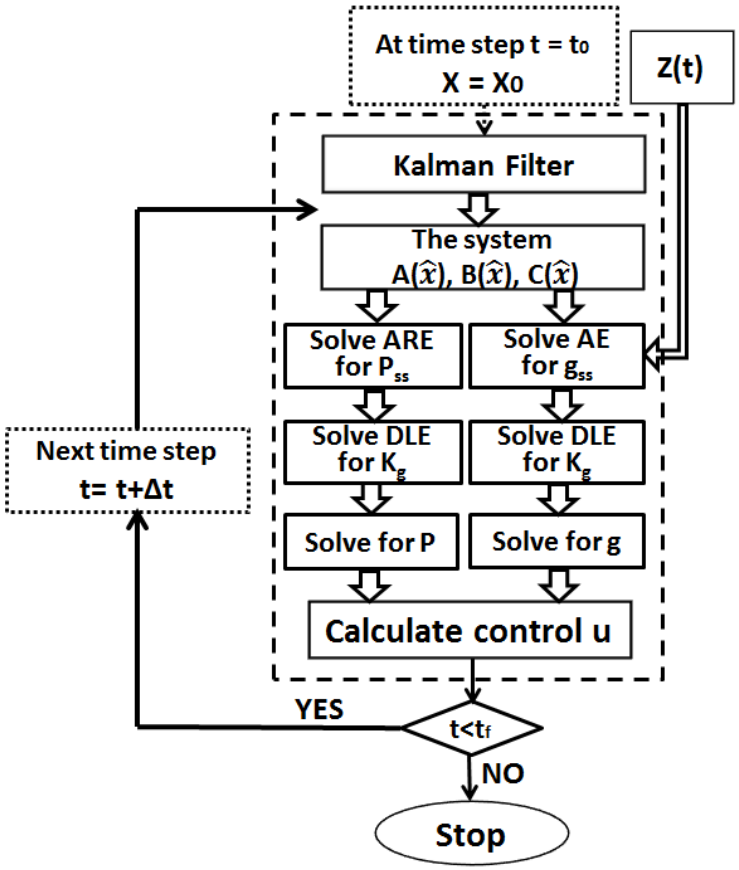

Figure 5.8: Flow Chart of Finite-Horizon Differential SDRE Tracking Technique for Stochastic Systems

Table 5.3: Procedure Summary of Continuous-Time Tracking Problem: Incomplete State Information

Statement of the Problem	
Given the process as $\dot{\mathbf{x}}(t) = \mathbf{A}(\mathbf{x})\mathbf{x}(t) + \mathbf{B}(\mathbf{x})\mathbf{u}(t) + \mathbf{B}_w(t)\mathbf{w}(t)$, the observation of the state as $\mathbf{y}(t) = \mathbf{C}(\mathbf{x})\mathbf{x}(t) + \mathbf{v}(t)$, the performance measure for estimate as $J(t) = \text{trace}\,[var[\tilde{\mathbf{x}}(t)]] + \text{trace}[\mathbf{P}_e(t)]$, the conditions as $\mathcal{E}[\mathbf{w}(t)] = 0, \quad \text{COV}[\mathbf{w}(t), \mathbf{w}(\tau)] = \mathbf{Q}_w(t)\delta(t-\tau), \quad \mathcal{E}[\mathbf{x}(t_0)] = \bar{\mathbf{x}}_0,$ $\text{VAR}[\mathbf{x}(t_0)] = \mathbf{P}_0; \quad \text{COV}[\mathbf{x}(t), \mathbf{w}(\tau)] = 0 \quad \text{for all } \tau > t,$ $E[\mathbf{v}(t)] = 0, \quad COV[\mathbf{v}(t), \mathbf{v}(\tau)] = \mathbf{R}_v(t)\delta(t-\tau),$ $COV[\mathbf{v}(t), \mathbf{w}(\tau)] = 0, \quad COV[\mathbf{v}(t), \mathbf{x}(\tau)] = 0 \text{ for all } t, \tau,$ and the performance measure for control as $\hat{J}(\mathbf{x}_0, t_0) = \mathcal{E}\left\{\frac{1}{2}\mathbf{x}'(t_f)\mathbf{F}\mathbf{x}(t_f) + \frac{1}{2}\int_{t_0}^{t_f}\left[\mathbf{x}'(t)\mathbf{Q}(\mathbf{x})\mathbf{x}(t) + \mathbf{u}'(\mathbf{x})\mathbf{R}(\mathbf{x})\mathbf{u}(\mathbf{x})\right]\right\} dt$ find the optimal estimator and controller	
Solution of the Problem I: Optimal Estimator/Kalman Filter	
Step 1	At each time step, solve the matrix differential Riccati equation $\dot{\mathbf{P}}_e(\hat{\mathbf{x}}, t) = \mathbf{A}(\hat{\mathbf{x}})\mathbf{P}_e(\hat{\mathbf{x}}, t) + \mathbf{P}_e(\hat{\mathbf{x}}, t)\mathbf{A}'(\hat{\mathbf{x}}) + \mathbf{B}_w(t)\mathbf{Q}_w(t)\mathbf{B}_w'(t) -$ $\mathbf{P}_e(\hat{\mathbf{x}}, t)\mathbf{C}'(\hat{\mathbf{x}})\mathbf{R}_v^{-1}(t)\mathbf{C}(\hat{\mathbf{x}})\mathbf{P}_e(\hat{\mathbf{x}}, t); \quad \mathbf{P}_e(\hat{\mathbf{x}}, t_0) = \mathbf{P}_{e0}.$
Step 2	Using $\mathbf{P}_e(\hat{\mathbf{x}}, t)$ from Step 1, obtain the optimal estimator (filter) gain as $\mathbf{K}_e(\hat{\mathbf{x}}, t) = \mathbf{P}_e(\hat{\mathbf{x}}, t)\mathbf{C}'(\hat{\mathbf{x}})\mathbf{R}_v^{-1}(t)$.
Step 3	Using $\mathbf{K}_e(\hat{\mathbf{x}}, t)$ from Step 2, solve the optimal state estimate $\hat{\mathbf{x}}(t)$ from $\dot{\hat{\mathbf{x}}}(t) = \mathbf{A}(\hat{\mathbf{x}})\hat{\mathbf{x}}(t) + \mathbf{B}(\hat{\mathbf{x}})\mathbf{u}(t) + \mathbf{K}_e(\hat{\mathbf{x}}, t)[\mathbf{y}(t) - \mathbf{C}(\hat{\mathbf{x}})\hat{\mathbf{x}}(t)]; \quad \hat{\mathbf{x}}(t_0) = \bar{\mathbf{x}}_0.$
Solution of the Problem II: Optimal Controller	
Step 4	At each time step, calculate the value of $\mathbf{P}_c(\hat{\mathbf{x}}, t)$ from the equation $\mathbf{P_c}(\hat{\mathbf{x}}, \mathbf{t}) = \mathbf{K^{-1}}(\hat{\mathbf{x}}, \mathbf{t}) + \mathbf{P_{ss}}(\hat{\mathbf{x}})$, with $K(\hat{\mathbf{x}}, t)$ is the solution differential Lyapunov equation (5.1.15) .
Step 5	Calculate the value of $\mathbf{g}(\mathbf{x}, t)$ from the equation $\mathbf{g}(\hat{\mathbf{x}}, t) = \mathbf{K_g}(\hat{\mathbf{x}}, t) + \mathbf{g_{ss}}(\hat{\mathbf{x}})$ with $K_g(\hat{\mathbf{x}}, t)$ is the solution differential equation (5.2.13) .
Step 6	Obtain the closed-loop optimal control as $\mathbf{u}(\hat{\mathbf{x}}, t) = -\mathbf{R^{-1}}(\hat{\mathbf{x}})\mathbf{B}'(\hat{\mathbf{x}})[\mathbf{P}_c(\hat{\mathbf{x}}, t)\hat{\mathbf{x}}(t) - \mathbf{g}(\hat{\mathbf{x}}, t)]$.

The entire algorithm of combined estimation and control leading to nonlinear tracking problem is shown in Table 5.3.

5.2.3 Finite-Horizon Differential SDRE Tracking for Stochastic Systems Simulation : Solar Generator System

For numerical simulation and analysis, the developed optimal estimation and tracking technique for stochastic systems is implemented for noise cancellation for the nonlinear electrical circuit with the solar generator and DC motor drive system [69]. The nonlinear circuit is presented in Fig. 5.9. In the time $t = 0$ the switch W is closed and the circuit is in a transient state.

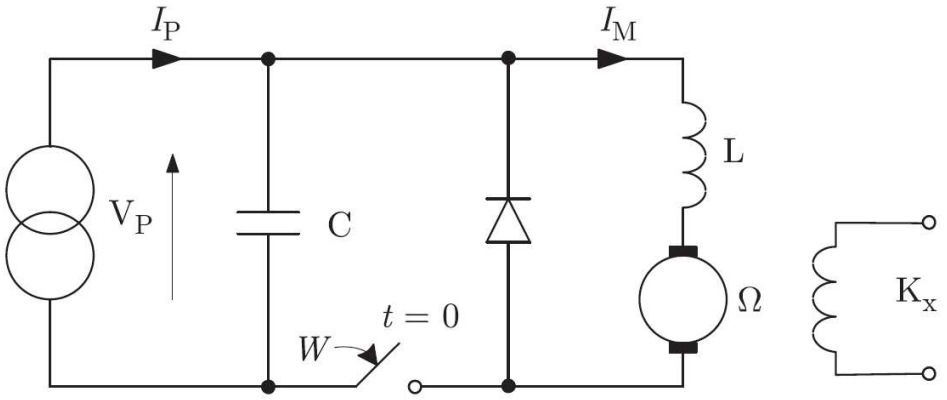

Figure 5.9: An Electric Circuit Containing Solar Generator and DC Motor [69]

The transient state of the nonlinear circuit is described by the following set of equations [11, 68]

$$\dot{x_1} = -a_1 x_1 + a_2 x_2, \tag{5.2.16}$$

$$\dot{x_2} = -a_3 x_1 - a_4 x_2 + a_5 x_3, \tag{5.2.17}$$

$$\dot{x_3} = -a_6 x_2 - a_7 e^{a x_3} + u, \tag{5.2.18}$$

where $x_1 = \Omega$ represents the DC motor rotational speed, $x_2 = I_M$ is the rotor

current, $x_3 = V_p$ is the generator voltage, and u is the solar generator current input. The coefficients $a_1; ...; a_7$ are expressed by the following relations that combine the parameters of nonlinear circuit

$a_1 = \frac{K_r}{J}, \quad a_2 = \frac{K_x}{J}, \quad a_3 = \frac{K_x}{L}, \quad a_4 = \frac{R_m}{L}, \quad a_5 = \frac{1}{L}, \quad a_6 = \frac{1}{C}, \quad a_7 = \frac{I_s}{C}.$

The transient state of the nonlinear circuit can be rewritten in state dependent form

$$\begin{bmatrix} \dot{x_1} \\ \dot{x_2} \\ \dot{x_3} \end{bmatrix} = \begin{bmatrix} a_1 & a_2 & 0 \\ -a_3 & -a_4 & a_5 \\ 0 & -a_6 & -a_7 \frac{e^{ax_3}}{x_3} \end{bmatrix} \begin{bmatrix} x_1 \\ x_2 \\ x_3 \end{bmatrix} + \begin{bmatrix} 0 \\ 0 \\ 1 \end{bmatrix} u. \tag{5.2.19}$$

The various parameters of the electrical circuit are given in Table 5.4, with the initial conditions

$$\mathbf{x_0} = [15, 0, 0]'. \tag{5.2.20}$$

Table 5.4: Parameter of The Electrical Circuit Containing Solar Generator and DC Motor

Parameters	Values
R_m	12 [Ω]
k_x	0.5 [Vs]
k_r	0.1 [Vs^2]
J	0.001 [kg-m2]
C	0.5 [mF]
L	0.1 [H]
I_s	0.00128 [A]
a	0.45 [V^{-1}]

Let the desired motor speed be

$$z(t) = \begin{cases} 8 \;\; rad/sec \quad \text{for} \quad t < 2, \\ \\ 2 \;\; rad/sec \quad \text{for} \quad 2 < t < 6, \end{cases} \tag{5.2.21}$$

and the selected weighted matrices be

$$\mathbf{Q} = diag(1000, 20, 20), \quad \mathbf{R} = 4, \quad \mathbf{F} = diag(1, 1, 1). \tag{5.2.22}$$

The covariances of the noises have been taken as

$$\mathbf{Q_w} = diag(1, 1, 1), \qquad \mathbf{R_v} = 1. \tag{5.2.23}$$

The simulations are performed for final time of 6 seconds and the resulting output trajectories is shown in Fig. 5.10, where the dash-dot line denotes *the desired* motor speed, the dashed line denotes *the actual* (without noise) speed, and the solid line denotes *the estimated* (with noise) speed. The optimal control is shown in Fig. 5.11, where the solid line denotes *the estimated* optimal control and the doted line denotes *the actual* optimal control signal.

Comparing the trajectories in Fig. 5.10, it's clear that the proposed method gives very good results as the estimated optimal motor speed is making a good tracking to the desired speed, and the estimated speed is very close to the actual speed with very small error as seen in Fig. 5.12. From these results, it can be seen that the developed technique is able to solve the finite-horizon nonlinear tracking stochastic problem.

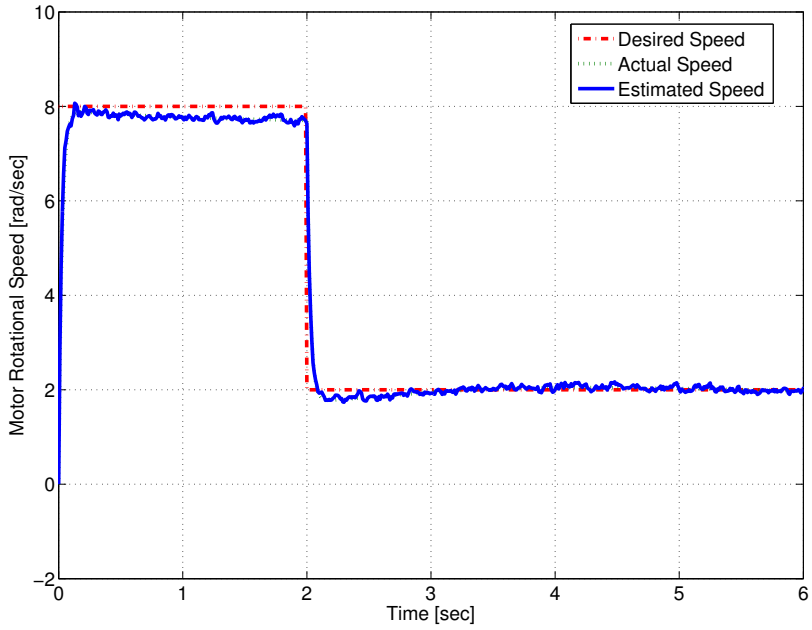

Figure 5.10: DC Motor Optimal Rotational Speed

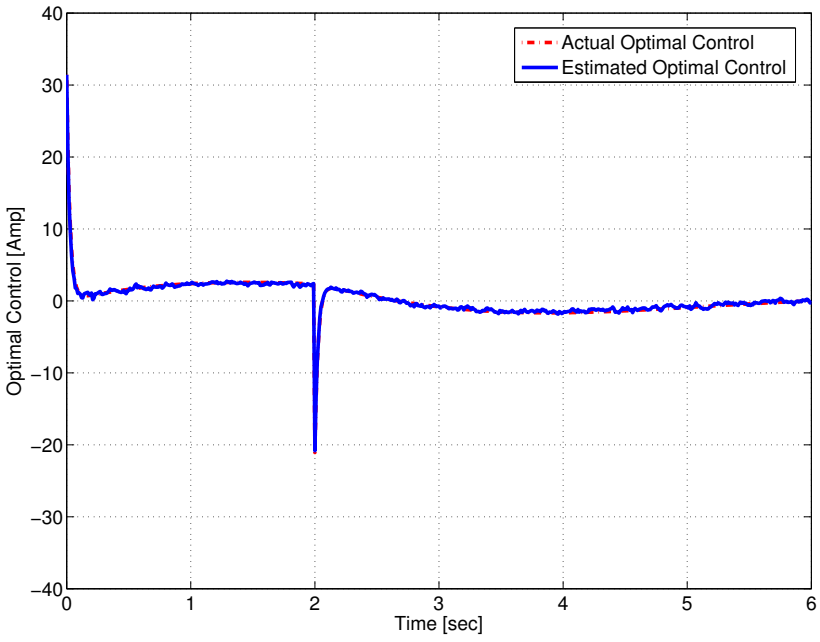

Figure 5.11: Solar Generator Optimal Control

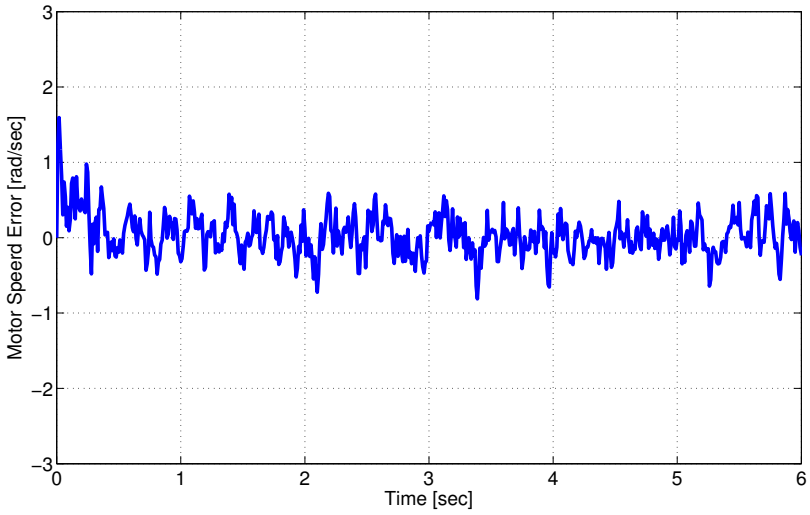

Figure 5.12: DC Motor Optimal Rotational Speed Error

5.3 Conclusions

This chapter discuses a novel efficient online technique used for finite-horizon nonlinear regulator and tracking problems with incomplete state information. This technique based on integrating the Kalman filter algorithm and the finite-horizon differential SDRE technique. Kalman filter estimates the states which are corrupted with noise. In this technique, the optimal control problem of the nonlinear system is solved by using finite-horizon differential SDRE algorithm, which makes this technique effective for a wide range of operating points.

Chapter 6

Nonlinear, Optimal Tracking For Missile Gimbaled Seeker

The frequent minor wars of the last four decades have brought to the forefront guided missiles as weapons against all types of military targets. Before discussing the various ways in which missiles may be guided and the methods of implementation of such guidance systems, it is worth recalling why guided missiles have become so much importance in recent years. Any weapon should have as high a single shot kill probability as possible [66]. There are three main reasons why unguided weapons may fail in this respect: the random dispersion at launch, deflection of flight path, and the target movement. One way of increasing the single shot kill probability is to use a large warhead with a large lethal area, but this will usually mean a larger missile. The other method that is adopted is to use a closed loop system to minimize the miss-distance and thus, improve the single shot kill probability. This can be accomplished by monitoring continuously the flight parameters of the missile and target,

then employing this information to control the missile in space [47].

The majority of homing guided missiles uses gimbaled seekers. The dynamical equations describing seeker gimbal system are highly nonlinear. Accurate nonlinear control of the motion of the gimbaled seeker through the seeker DC motors is required.

6.1 Introduction and Background

Strategic military dependence on missile technology has been growing rapidly since its first use at the beginning of the twentieth century. The critical requirement regarding missile usage is to lead the missile robustly and accurately from its launch point to its designated end point or target. The missile target could be a certain point in its required orbit in space, or a moving hostile object either flying in the sky or rolling on terrain. To achieve this requirement, three operations to be completed, the Guidance, Navigation and Control (GNC) operations [148]. The GNC is illustrated in Fig.6.1 and is simply described by dividing it into two main loops [123]. The guidance loop has the ability to detect the current target parameters through the guidance sensors and to calculate the error between the desired and actual trajectory. This error is delivered to the guidance computer to generate the guidance commands according to the guidance method used [39]. The guidance command is then delivered to the autopilot, which computes the proper inputs to the actuators to move the missile fins and wings. Missile motion is described as a set of angular rotations and accelerations that are sensed by inertial sensors as a feedback in the autopilot loop to verify the desired maneuver of the missile [70].

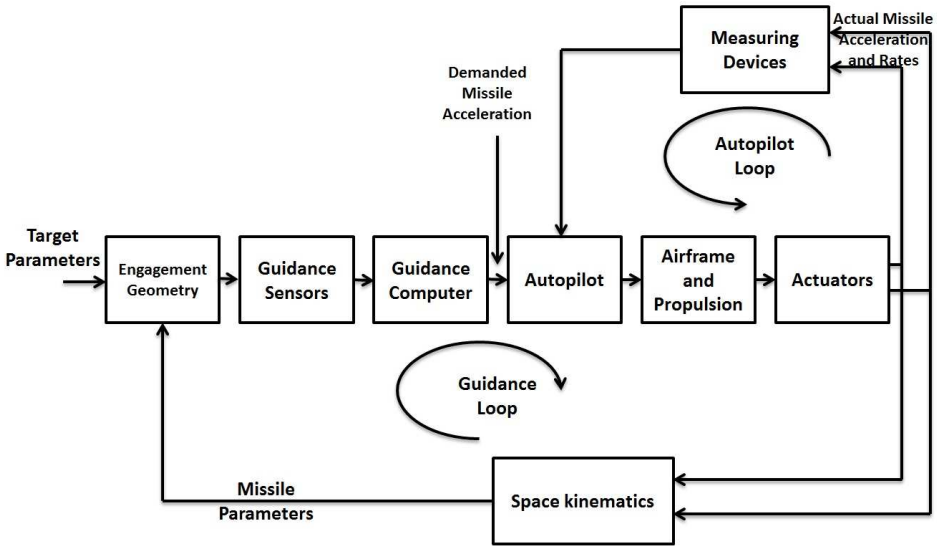

Figure 6.1: Guidance, Navigation, and Control (GNC) Operations

Radio Frequency (RF), Infra Red (IR) and optical sensors are examples of different types of guidance sensors that can be used to detect target parameters. Guidance systems can be categorized into four main categories as shown in Fig.6.2. These categories are command, beam rider, autonomous, and homing guidance [47]. A fifth possible category is a combination between two or more of the previous guidance methods such as some types of cruise missiles that switch from autonomous guidance to homing guidance in the terminal phase for more accurate hits. The difference between command guidance and homing guidance is the location of the guidance computer, which can be on the launching station or on missile board, respectively. Beam rider guidance can be classified under the command guidance category, but it requires a direct Line of Site (LOS) between the beam generator source and the target.

Both command and homing guidance methods can use RF, IR, or optical sensors and are mostly used for maneuvering targets. An autonomous guidance system is

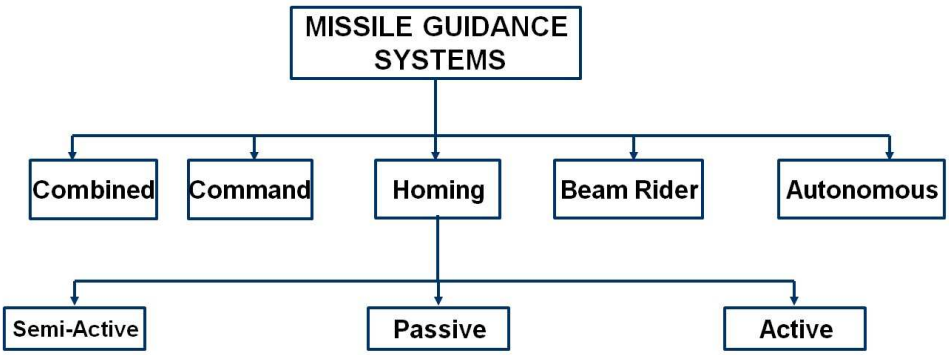

Figure 6.2: Missile Guidance Systems Classification

usually used when predefined way points are desired or a certain target with known position has to be reached. Different types of sensors can be used for precise navigation such as inertial sensors and Digital Scene Matching Area Correlation (DSMAC) radar.

In order to orient the missile toward intended target points, it is vital to acquire the correct information about the states of the targets during the flight of the vehicles. One of the most widely-used ways to achieve this task is the utilization of seekers which act as the guidance sensors mentioned earlier [8]. Physically, the measurement capability of seekers is restricted due to some physical, optical, and electronic limitations such as limited field-of-view (FOV), atmospheric transmittance, and noise effects. Regarding these characteristics, basically two types of seekers are employed in the relevant applications: strap-down or body-fixed seekers and gimbaled seekers. The strap-down seekers are directly mounted on the vehicle body under consideration. Therefore, their measurements become relative to the body fixed reference frame of the missile. For overcoming the FOV limitations of the strap-down seekers, the gimbaled seekers are preferred in some of the implementations. In this scheme, the seeker

is mounted on a platform supported by two orthogonal gimbals usually powered by DC motors, and stabilized by means of rate gyro feedbacks. This way, the FOV range of the seeker is increased considerably. Also, the line of sight (LOS) angle and the LOS angular rate can be measured directly independently of the missile motion. A comparison of gimbaled and strap-down seeker models according to some significant criteria is given in Table 6.1 [137].

The following target intercept rules are possible within homing guidance strategies [123]:

- **Pure Pursuit**

  In the pursuit trajectory, the interceptor missile flies directly toward the target at all times. Thus, the heading of the missile is maintained essentially along the LOS between the missile and the target by the guidance system. The most favorable application of the pursuit course guidance law is against slow-moving aircraft, or head on toward an incoming aircraft.

- **Deviated Pursuit**

  The interceptor missile tracks the target and produces guidance commands. This guidance law is similar to pure pursuit, except that the missile heading leads the LOS by a fixed angle. When the fixed lead angle is zero, deviated pursuit becomes pure pursuit.

- **Lead Pursuit**

  A lead pursuit course is flown by an interceptor (i.e., a missile) directing its velocity vector at an angle from the target so that projectiles launched from

Table 6.1: Comparison of Gimbaled and Strap-Down Seeker Models

	Gimbaled Seeker	**Strap-Down Seeker**
Mounting	Mounted on two-gimbal platform and powered by DC motors	Rigidly mounted on the missiles body
FOV	Up to $\pm 90^o$	About $\pm 3^o$
Angle and Rate Measurements	LOS angle and LOS angular rate error angles with respect to the ground	LOS angle and LOS angular rate error angles between the missile center line and the LOS

any point on the course will impact on the target if it is within the range of the weapon.

- **Proportional Navigation**

  Proportional Navigation (PN) is the most widely known and used guidance law for short- to medium-range homing missiles, because of its inherent simplicity and ease of implementation. Simply stated, classical proportional navigation guidance is based on recognition of the fact that if two bodies are closing on each other, they will eventually intercept if the line of sight (LOS) between the two does not rotate relative to the inertial space. More specifically, the PN guidance law seeks to null the LOS rate against non-maneuvering targets by making the interceptor missile heading proportional to the LOS rate. For instance, in flying a proportional navigation course, the missile attempts to null out any line-of-sight rate that may be developing. The proportionality factor consists of the navigation constant, closing velocity multiplier, and a geometric gain factor that accounts for the fact that the orientation of the missile velocity

is not necessarily along the instantaneous LOS. The navigation constant (N) is based on the missiles acceleration requirements and will vary depending on target maneuvers and other system-induced tracking-error sources. In order to minimize the missile acceleration requirement, the values of N between 3 and 5 are usually used to obtain an acceptable miss distance intercept. Note that for most applications, the effective navigation ratio is restricted to integer values.

The majority of homing guided missiles, uses gimbaled seekers (an example of gimbaled seekers is shown in Fig.6.3 [123]). This allows the sensor to be pointed at the target when the missile is not pointed at the target. This is important for two main reasons. One is that before and during launch, the missile cannot always be pointed at the target. Rather, the missile points its seeker at the target using information from its launching station. After this, the seeker remains locked on the target, even if the launching platform moves. When the missile is launched, it may not be able to control the direction it points until the rocket motor drives the missile to high enough speed for fins to control its direction of travel. Until then, the gimbaled seeker needs to be able to track the target independently.

Even while it is under positive control and on its way to intercept the target, it probably will not be pointing directly at it; unless the target is moving directly toward or away from the launching platform, the shortest path to intercept the target will not be the path taken while pointing straight at it, since it is moving laterally with respect to the missile's view. Old missiles would simply point towards the target and chase it, and this was inefficient. Modern missiles are smarter and use the gimbaled

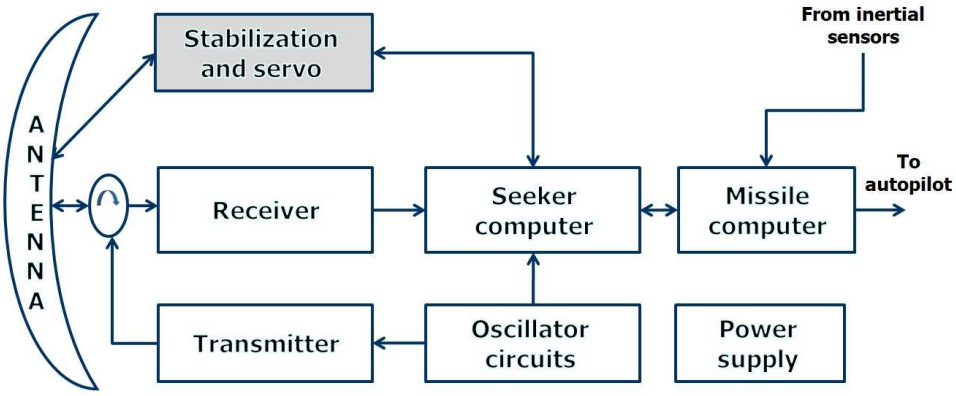

Figure 6.3: Active Radar Gimbaled Seeker Basic Blocks

seeker head combined with what is known as proportional guidance in order to avoid oscillation and to fly an efficient intercept path.

The control technique used for the gimbal system on a tactical missile must provide fast and precise tracking of relative error signals created by the missile's signal processing unit. Poor performance during engagement will result in large miss distances which may lead to low probability of mission success. The equations describing the gimbal system under consideration are highly nonlinear. In order to accurately calculate the missile-target LOS angle and its rate, accurate nonlinear control of the motion of the gimbaled seeker through the attached DC motors is required. The linear control techniques become inadequate and it becomes necessary to use nonlinear control techniques. The era of rapid technological change has motivated the development of nonlinear control theory for application to challenging, complex dynamical real-world problems [18].

The new technique of finite-horizon nonlinear tracking via SDRE is an appropriate solution for the missile tracking problem [74]. Although the SDRE has a great impact in the missile guidance area [28, 113, 134], but none of these works have addressed

the problem of finite-horizon optimal control of nonlinear systems.

6.2 Description of Missile System

The missile examined in this dissertation research is a semi active homing guided missile [81]. The semi-active homing guidance system is based on the principle of utilizing the electromagnetic wave reflection. A ground radar illuminates the target, the missile seeker is designed to home on the reflected energy from the target during its flight. Using this reflected system energy from the target the missile formulates its own correction signals. The missile is steered in space following the proportional navigation guidance method. An on-board guidance kit is utilized to generate the guidance commands. The missile is aerodynamically controlled with an acceleration control autopilot to steer the missile while skid-to-turn (STT) control policy is utilized. The STT steering policy requires two identical lateral (pitch and yaw) autopilots to control the missile attitude while a roll autopilot performs attitude stabilization in the maneuver plane. A roll position controller is utilized to keep an adequate roll damping [41].

The missile flies in the air under the effect of thrust, weight, and aerodynamic forces. The action of these forces has a certain effect on the shape of the missile trajectory. The aerodynamic force is usually distributed to the axes of the velocity coordinate system, which relate to the direction of the missile motion. The components of this force are resolved along the missile body axes as $F_{xa}, F_{ya}, andF_{za}$. These forces create aerodynamic moments owing to the fact that they do not pass

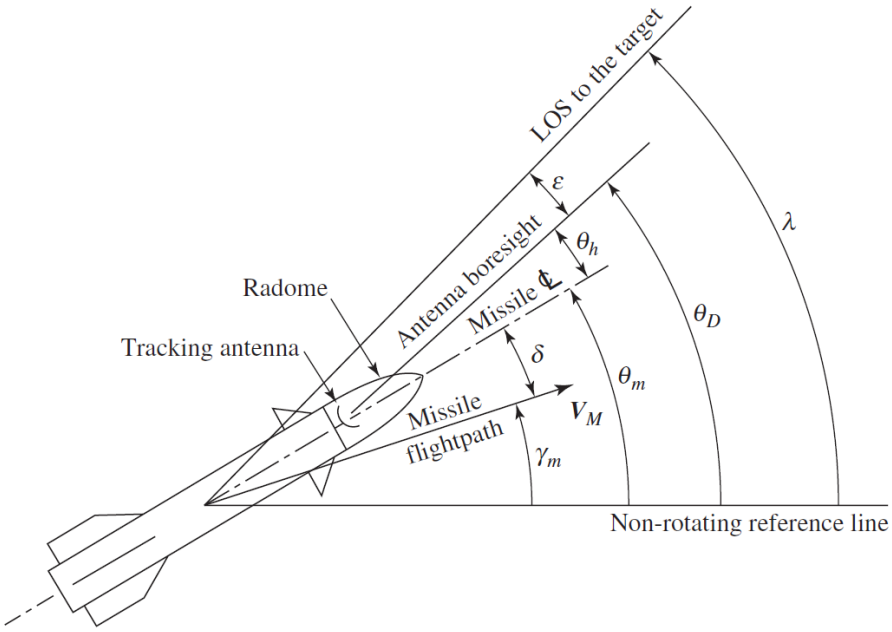

Figure 6.4: Missile Seeker Angular Geometry [123]

through the missile center of gravity. The aerodynamic moment components around the missile body axes are M_{xa}, M_{ya}, and M_{za}. The missile seeker is a narrow band, continuous wave (CW) receiver that operates as a lock on-before-launch, semi-active homing system. The system has limited recede capability and cannot lock on targets incoming at less than a certain threshold (minimum incoming speed). The missile flight and homing head angles are shown in Fig. 6.4.

The goal of gimbaled seeker controller is to control the seeker antenna DC motor to minimize the angle ϵ between the LOS and the antenna axis, as minimum as possible. Then, the missile aerodynamic and/or thrust forces will try to guide the missile body to control the angle between the seeker antenna and the missile body axis, θ_h.

6.3 Simulation Results

For numerical simulation and analysis, the developed nonlinear optimal tracking technique is implemented for a DC motor attached to a realistic gimbaled seeker system. A computer code written under MATLAB©environment is employed to solve a missile simulation model [81]. The code is devoted to evaluate the structure of the 6-Degree of Freedom (6 DOF) model in conjunction with the calculation of the desired seeker angles via numerical implementation [17]. Proportional navigation is the guidance method used in these simulations. In this guidance method, the guidance commands are generated in proportion to the LOS angular rate [132].

Extensive simulation has been carried out for both deterministic case and stochastic case. Three engagement scenarios, in the pitch plane only for better illustrations, including fixed target, non-maneuvering target, and maneuvering target are considered in the form of case studies.

The dynamic equations for the gimbaled seeker DC motor are:

$$V(t) = L\frac{di(t)}{dt} + Ri(t) + k_b\frac{d\theta(t)}{dt}, \tag{6.3.1}$$

$$ml^2\frac{d^2\theta(t)}{dt^2} = -mglsin(\theta(t)) - k_m i(t). \tag{6.3.2}$$

The nonlinear equations of the system can be written in the form:

$$\omega(t) = \frac{d\theta(t)}{dt}, \tag{6.3.3}$$

$$V(t) = L\frac{di(t)}{dt} + Ri(t) + k_w\omega(t), \tag{6.3.4}$$

$$k_i i(t) = J\frac{d\omega(t)}{dt} + B\omega(t) + Csgn(\omega), \tag{6.3.5}$$

where R is the armature resistance, L is the armature inductance, V is the voltage applied to the motor, i is the current through the motor, e is the back Electro magnetic force (EMF) voltage, J is the moment of inertia of the load, B is the viscous friction coefficient, $\tau = k_i i(t)$ is the torque generated by the motor, θ is the angular position of the motor, ω is the angular velocity of the motor k_w is the back EMF constant, k_i is the torque constant of the motor, C is the motor static friction.

The *signum* function $sgn(\omega)$ is defined as

$$sgn(\omega) = \begin{cases} -1 & \text{for} \quad \omega < 0, \\ 1 & \text{for} \quad \omega > 0, \end{cases} \tag{6.3.6}$$

or it can be written in this form:

$$sgn(\omega) = \frac{|\omega|}{\omega}. \tag{6.3.7}$$

The nonlinear state equations can be written in the form:

$$\begin{aligned} \dot{x_1} &= x_2, && (6.3.8)\\ \dot{x_2} &= \left(\frac{-B}{J} - \frac{-C}{J|x_2|}\right) x_2 + \frac{k_i}{J} x_3, && (6.3.9)\\ \dot{x_3} &= -\frac{k_w}{L} x_2 - \frac{R}{L} x_3 + \frac{1}{L} u, && (6.3.10)\\ y &= x_1, && (6.3.11) \end{aligned}$$

where: $\theta = x_1$, $\dot{\theta} = x_2$, $i = x_3$, and $V = u$.

Or alternatively in state dependent form

$$\begin{bmatrix} \dot{x_1} \\ \dot{x_2} \\ \dot{x_3} \end{bmatrix} = \begin{bmatrix} 0 & 1 & 0 \\ 0 & \left(\frac{-B}{J} - \frac{-C}{J|x_2|}\right) & \frac{k_i}{J} \\ 0 & -\frac{k_w}{L} & -\frac{R}{L} \end{bmatrix} \begin{bmatrix} x_1 \\ x_2 \\ x_3 \end{bmatrix} + \begin{bmatrix} 0 \\ 0 \\ \frac{1}{L} \end{bmatrix} u. \qquad (6.3.12)$$

where: $\theta = x_1$, $\dot{\theta} = x_2$, $i = x_3$, $V = u$,

The weight matrices are chosen to be

$$\mathbf{Q} = diag(3000, 0, 0), \quad \mathbf{R} = 30, \quad \mathbf{F} = diag(1, 1, 1). \qquad (6.3.13)$$

For *the stochastic case*, the covariances of the noises have been taken as

$$\mathbf{Q_w} = diag(0.2, 0.2, 0.2), \qquad \mathbf{R_v} = 10. \qquad (6.3.14)$$

6.3.1 The Deterministic Environment

6.3.1.1 Case 1: Fixed Target

In this case the desired seeker angle will be $z(t) = 0^o$, i.e *the problem is now a regulator problem.*

The simulations are performed for final time of 8 seconds, and the engagement scenario is shown in Fig. 6.5. The resulting trajectories for the desired and achieved seeker angles are presented in Fig. 6.6, and the optimal error is shown in Fig. 6.7.

In Fig. 6.6, the solid line denotes the *actual* (achieved) angle trajectory of the finite-horizon tracking controller, the dashed line denotes the *desired* seeker angle.

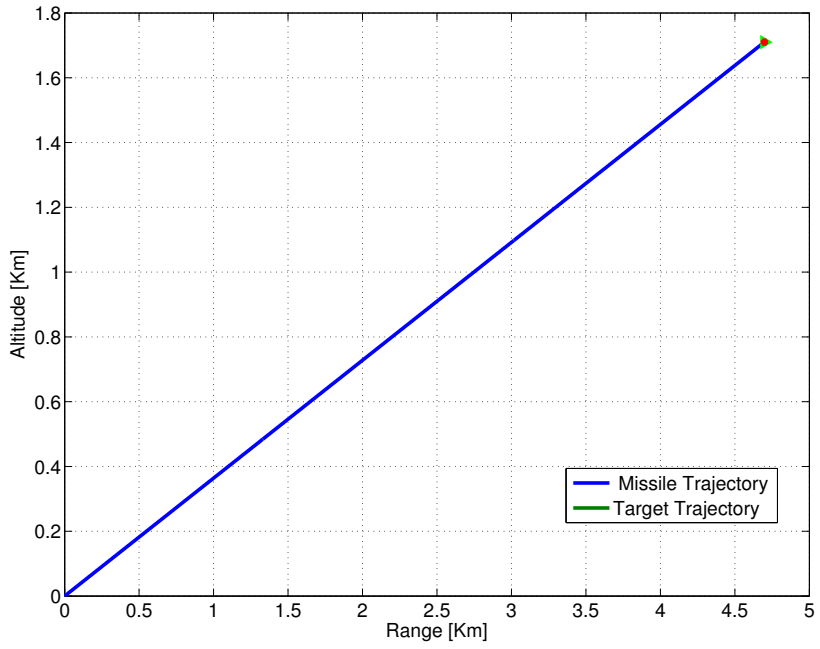

Figure 6.5: Missile-Target Engagement Scenario (Case 1)

As shown in Fig. 6.5, a successful hit is observed. Fig. 6.6 shows that the finite-horizon differential SDRE nonlinear regulating algorithm presenting excellent results

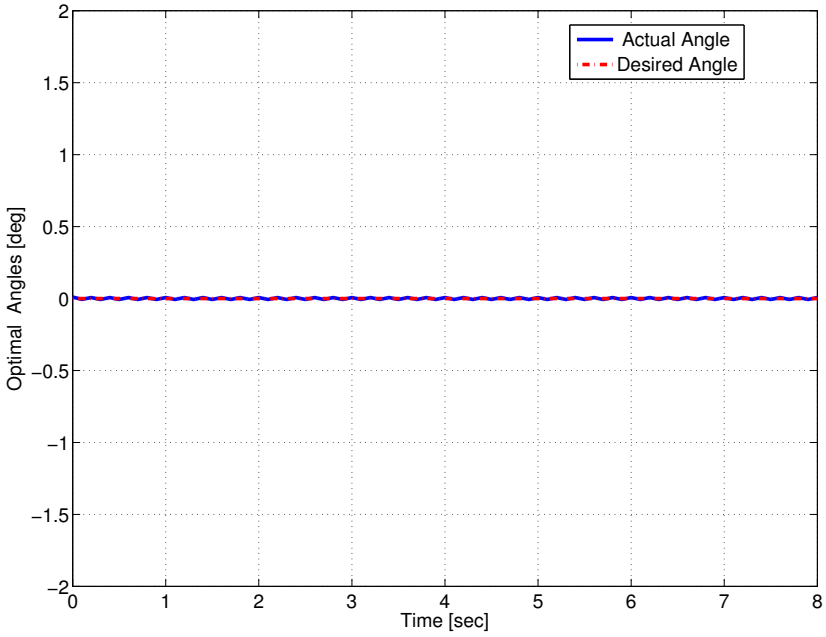

Figure 6.6: Angle Trajectories for Gimbaled System (Case 1)

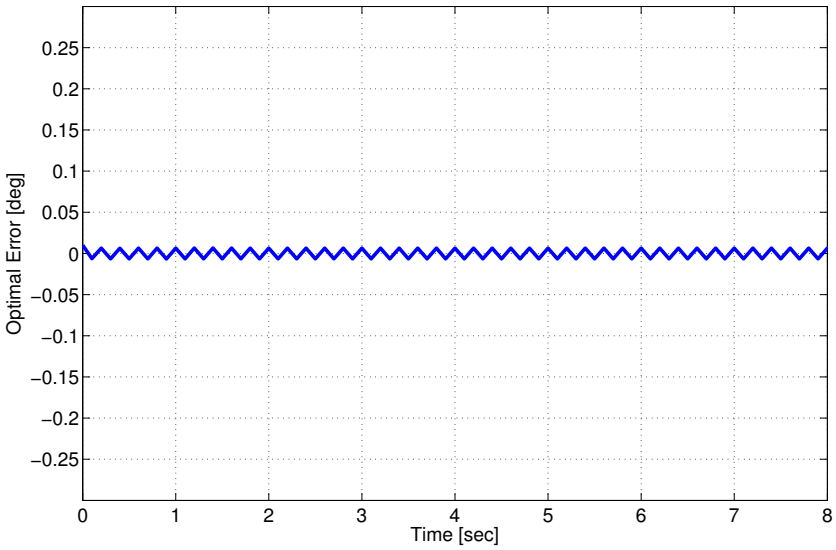

Figure 6.7: Optimal Error for Gimbaled System (Case 1)

and the developed technique is able to solve the differential SDRE finite-horizon nonlinear regulator problem with a zero average optimal error and 0.001^o standard

deviation.

6.3.1.2 Case 2: Non-Maneuvering Target

Consider a non-maneuvering target (with constant velocity). The simulations are performed for final time of 8 seconds, and the engagement scenario is shown in Fig. 6.8. The resulting trajectories for the demanded and achieved seeker angles are illustrated in Fig. 6.9, and the optimal angle error is shown in Fig. 6.10.

In Fig. 6.9, the solid line denotes the *actual* (achieved) angle trajectory of the finite-horizon tracking controller, the dashed line denotes the *desired* seeker angle.

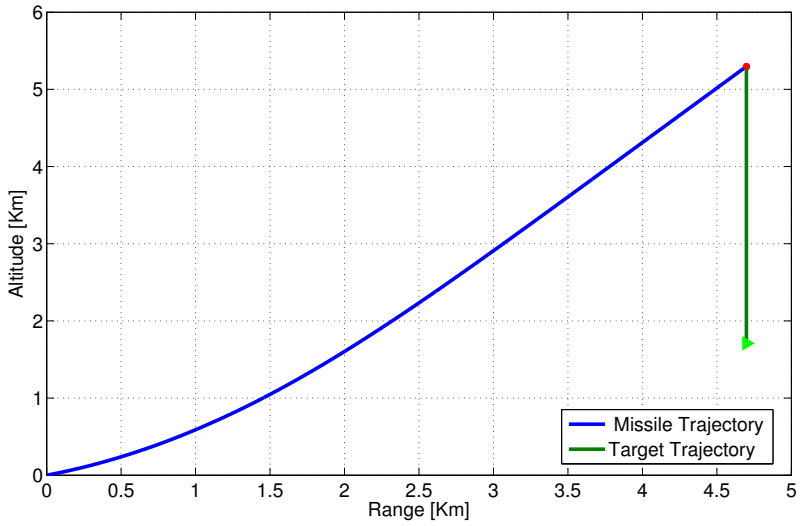

Figure 6.8: Missile-Target Engagement Scenario (Case 2)

Fig. 6.8 show that a successful hit is observed with acceptable miss-distance. Comparing these trajectories in Fig. 6.9, it's clear that the developed finite-horizon differential SDRE nonlinear tracking method is able to solve the finite-horizon nonlinear tracking problem with an reasonable standard deviation error of 0.035^o.

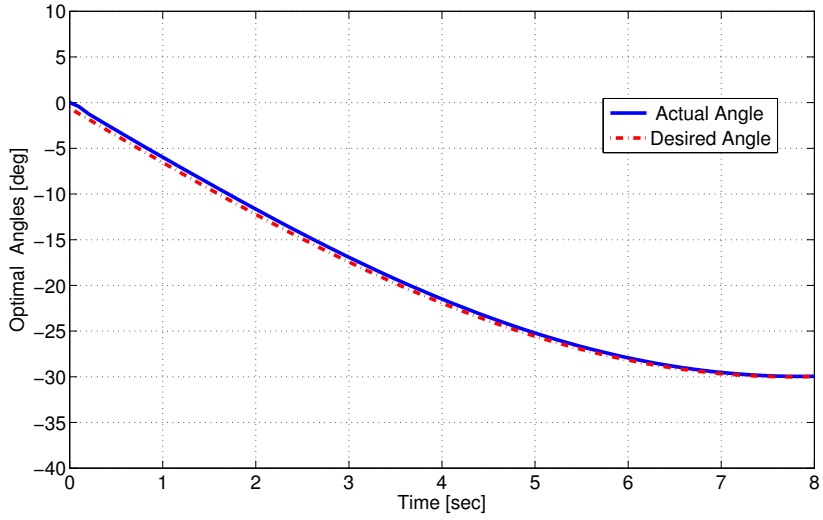

Figure 6.9: Angle Trajectories for Gimbaled System (Case 2)

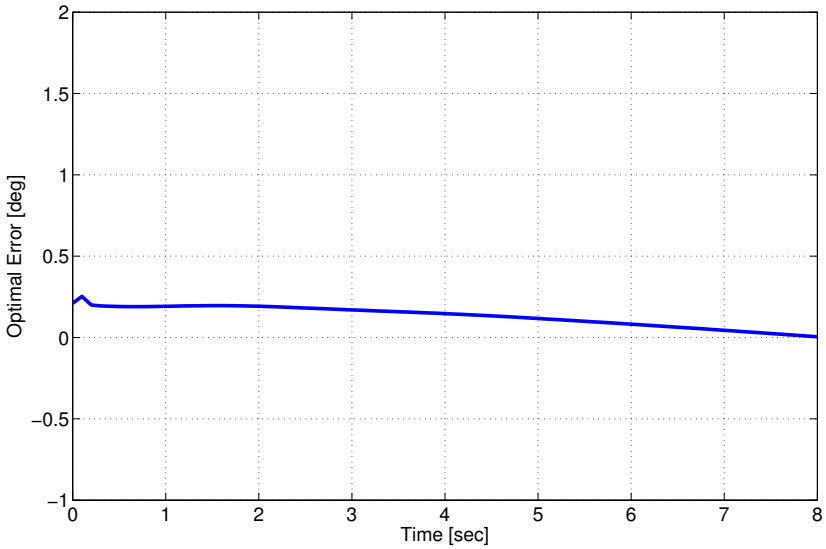

Figure 6.10: Optimal Error for Gimbaled System (Case 2)

6.3.1.3 Case 3: Maneuvering Target

Consider a highly maneuvering target. The simulations are performed for final time of 10 seconds, and the engagement scenario is shown in Fig. 6.11. The resulting trajectories for *the demanded* and *the achieved* seeker angles are illustrated in Fig. 6.12, and the optimal angle error is shown in Fig. 6.13.

In Fig. 6.12, the solid line denotes the *actual* (achieved) angle trajectory of the finite-horizon tracking controller, the dashed line denotes the *desired* seeker angle.

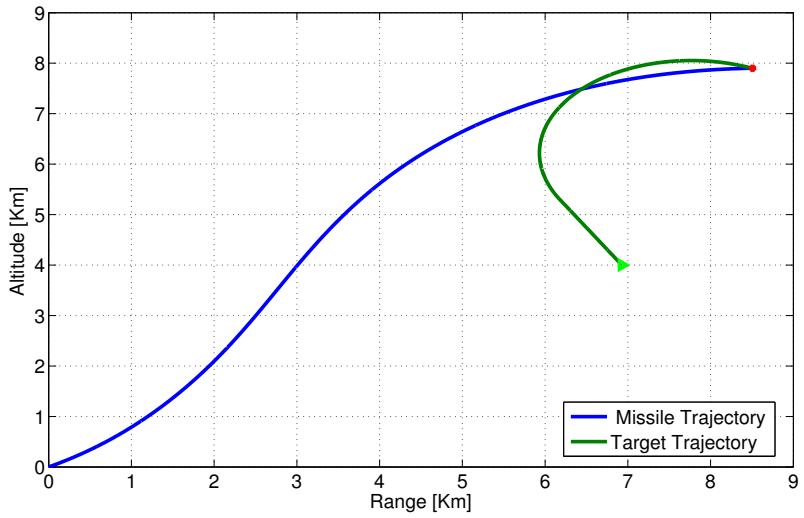

Figure 6.11: Missile-Target Engagement Scenario (Case 3)

Fig. 6.11 show that a successful hit is observed with acceptable miss-distance. Comparing these trajectories in Fig. 6.12, it's clear that the gimbaled seeker performing a very good tracking for the target even when the target tried to make high maneuver. The gimbaled seeker controlled by the developed technique is able to track maneuvering target with standard deviation error of 0.046^o, which is accepted in this high maneuver scenario.

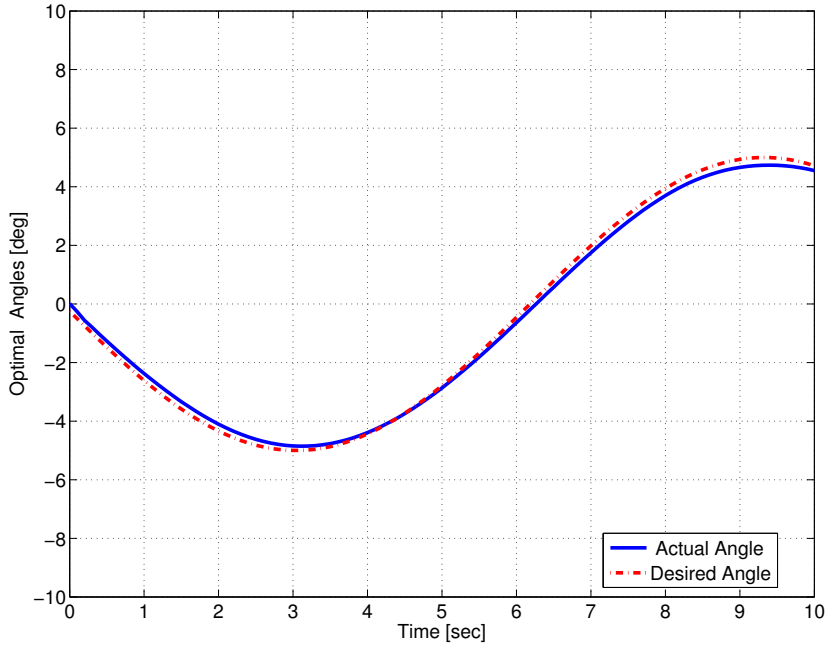

Figure 6.12: Angle Trajectories for Gimbaled System (Case 3)

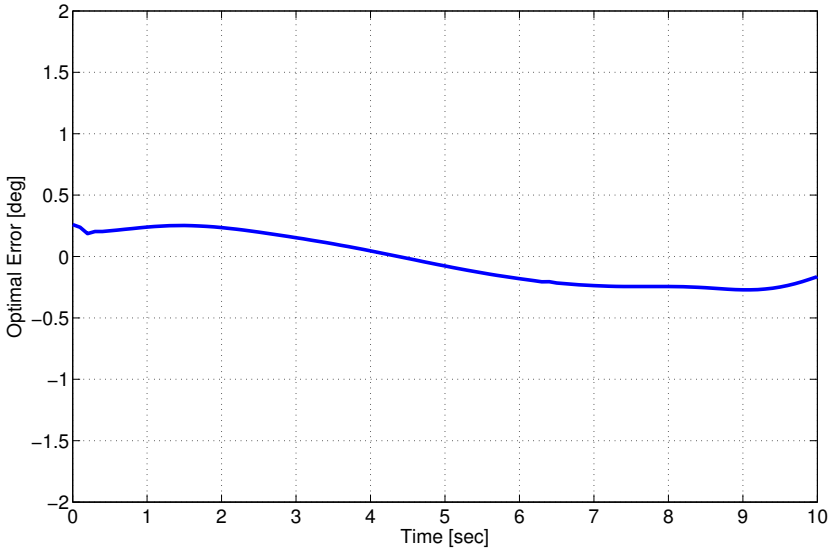

Figure 6.13: Optimal Error for Gimbaled System (Case 3)

6.3.2 The Stochastic Environment

6.3.2.1 Case 1: Fixed Target

In this case the desired seeker angle will be $z(t) = 0^o$, i.e *the problem is now a regulator problem.*

The simulations were performed for final time of 8 seconds, and the engagement scenario is shown in Fig. 6.14. The resulting trajectories for the demanded and achieved seeker angles are presented in Fig. 6.15, and the optimal error is shown in Fig. 6.16.

In Fig. 6.15, the solid line denotes the *estimated* (with noise) angle trajectory of the finite-horizon tracking controller, the dashed line denotes the *desired* seeker angle.

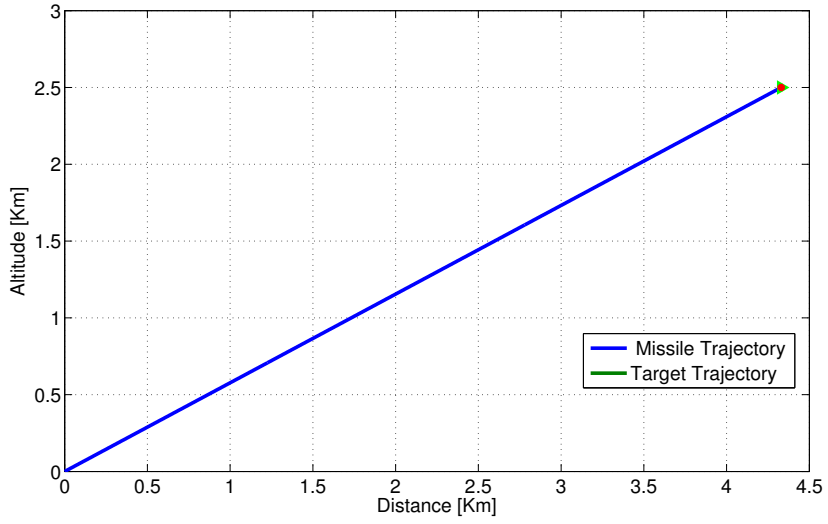

Figure 6.14: Missile-Target Engagement Scenario (Case 1 Stochastic)

As shown in Fig. 6.14, a successful hit is observed. Fig. 6.15 shows that the finite-horizon differential SDRE nonlinear regulating algorithm gives excellent results and the developed technique is able to solve the differential SDRE finite-horizon nonlinear

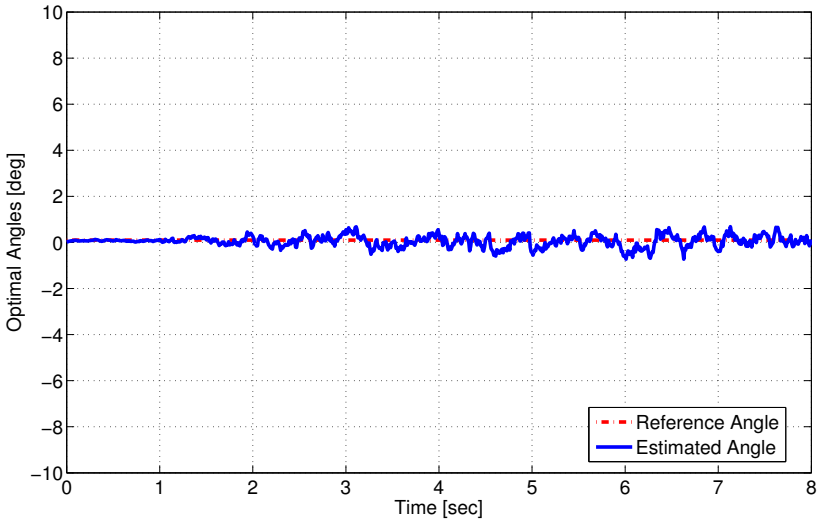

Figure 6.15: Angle Trajectories for Gimbaled System (Case 1 Stochastic)

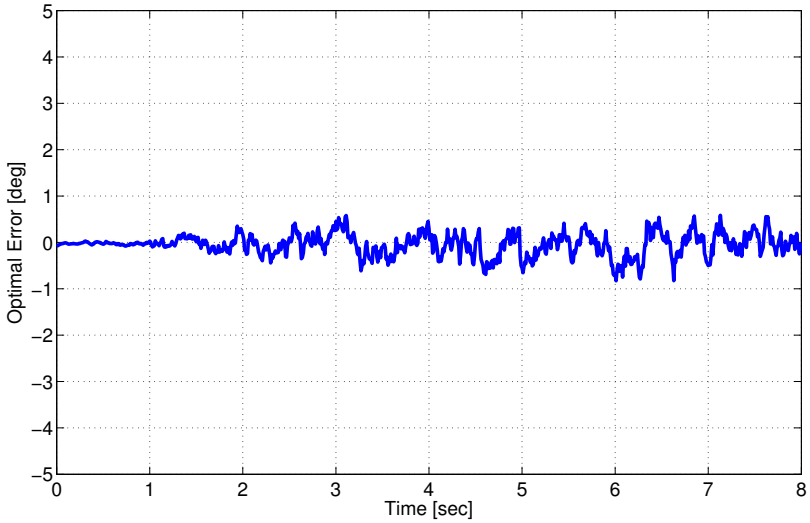

Figure 6.16: Optimal Error for Gimbaled System (Case 1 Stochastic)

regulator problem with a zero average optimal error and 0.003^o standard deviation.

6.3.2.2 Case 2: Non-Maneuvering Target

Consider a non-maneuvering target (with constant velocity). The simulations were performed for a final time of 8 seconds, and the engagement scenario is shown in Fig. 6.17. The resulting trajectories for the demanded and achieved seeker angles are illustrated in Fig. 6.18, and the optimal error is shown in Fig. 6.19.

In Fig. 6.18, the solid line denotes the *estimated* (with noise) angle trajectory of the finite-horizon tracking controller, the dashed line denotes the *desired* seeker angle.

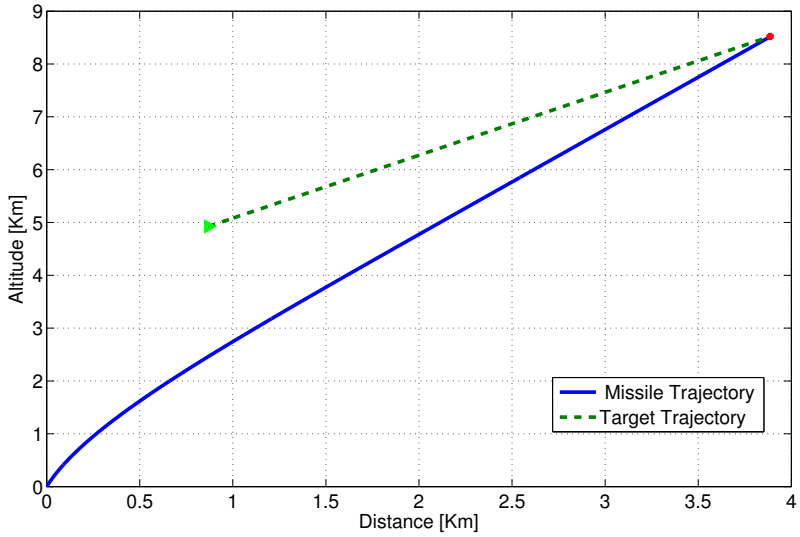

Figure 6.17: Missile-Target Engagement Scenario (Case 2 Stochastic)

Fig. 6.17 show that a successful hit is observed with acceptable miss-distance. Comparing these trajectories in Fig. 6.18, it's clear that the developed finite-horizon differential SDRE nonlinear tracking algorithm is able to solve the finite-horizon nonlinear tracking problem with an reasonable standard deviation error of 0.045^o.

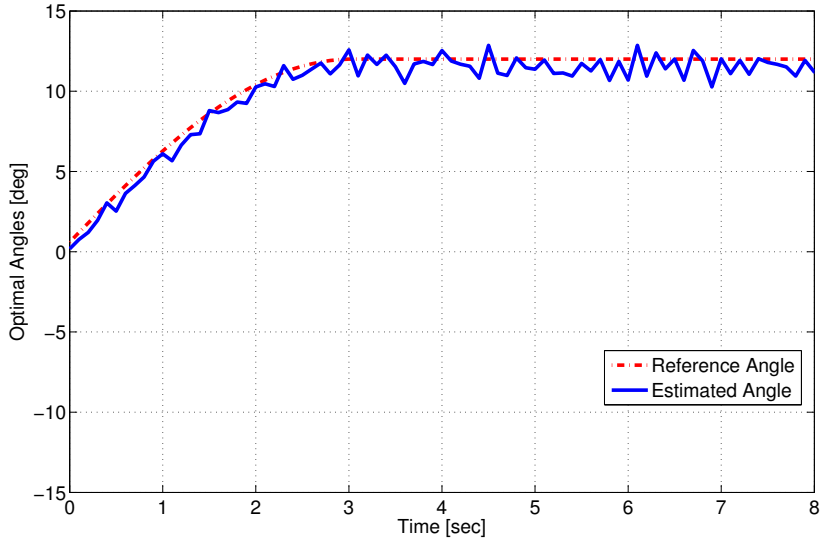

Figure 6.18: Angle Trajectories for Gimbaled System (Case 2 Stochastic)

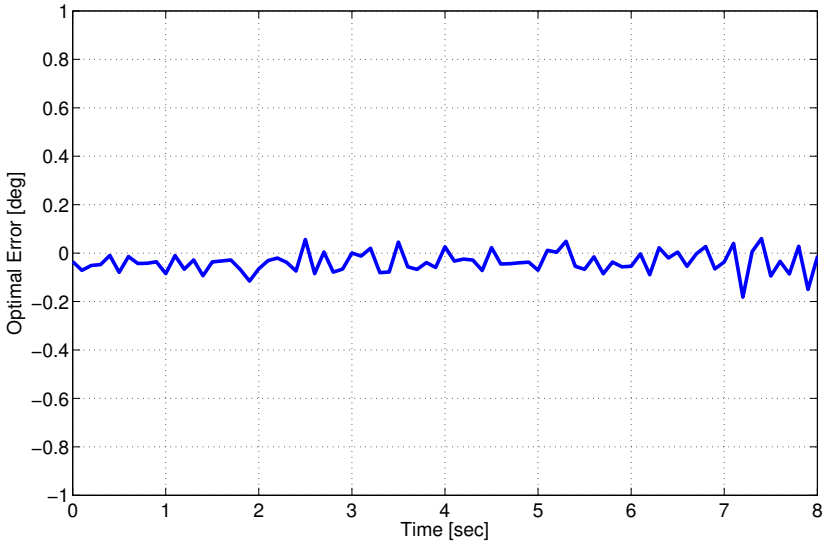

Figure 6.19: Optimal Error for Gimbaled System (Case 2 Stochastic)

6.3.2.3 Case 3: Maneuvering Target

Consider a highly maneuvering target. The simulations were performed for final time of 10 seconds, and the engagement scenario is shown in Fig. 6.20. The resulting trajectories for the demanded and achieved seeker angles are illustrated in Fig. 6.21, and the optimal error is shown in Fig. 6.22.

In Fig. 6.21, the solid line denotes the *estimated* (with noise) angle trajectory of the finite-horizon tracking controller, the dashed line denotes the *desired* seeker angle.

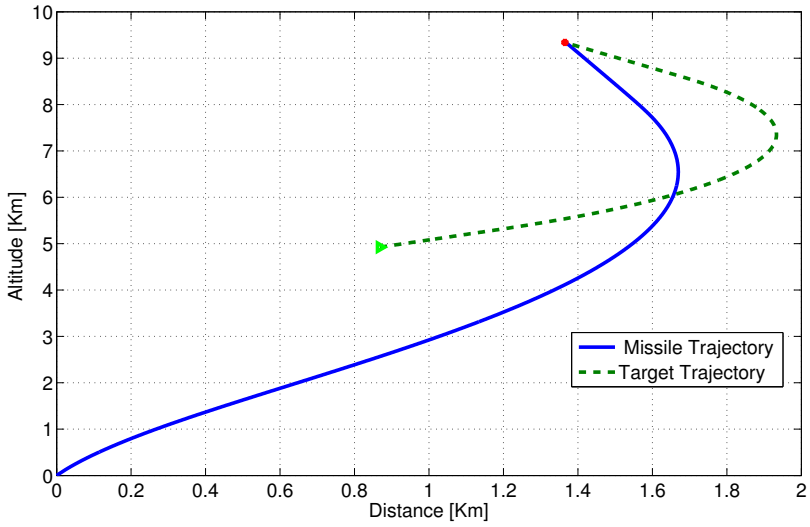

Figure 6.20: Missile-Target Engagement Scenario (Case 3 Stochastic)

Fig. 6.20 show that a successful hit is observed with acceptable miss-distance. Comparing these trajectories in Fig. 6.21, it's clear that the gimbaled seeker performing a very good tracking for the target even when the target tried to make high maneuver. The gimbaled seeker controlled by the developed method is able to track maneuvering target with standard deviation error of 0.054^o, which is accepted with this high maneuver.

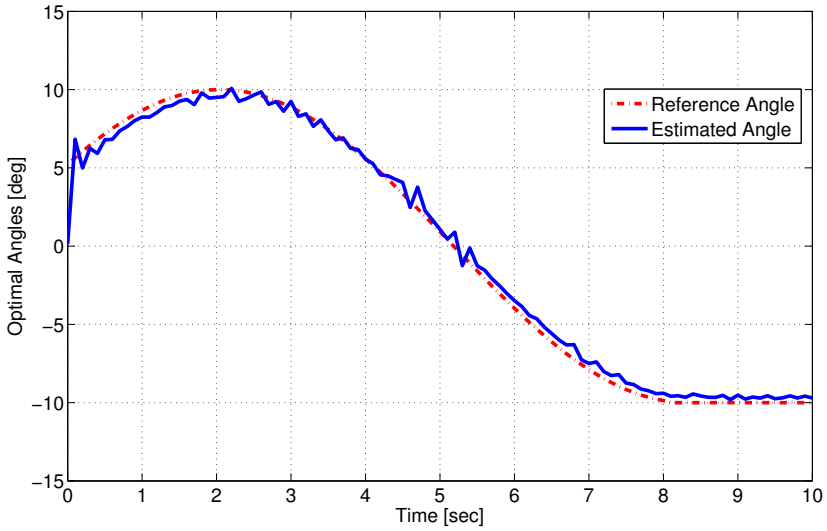

Figure 6.21: Angle Trajectories for Gimbaled System (Case 3 Stochastic)

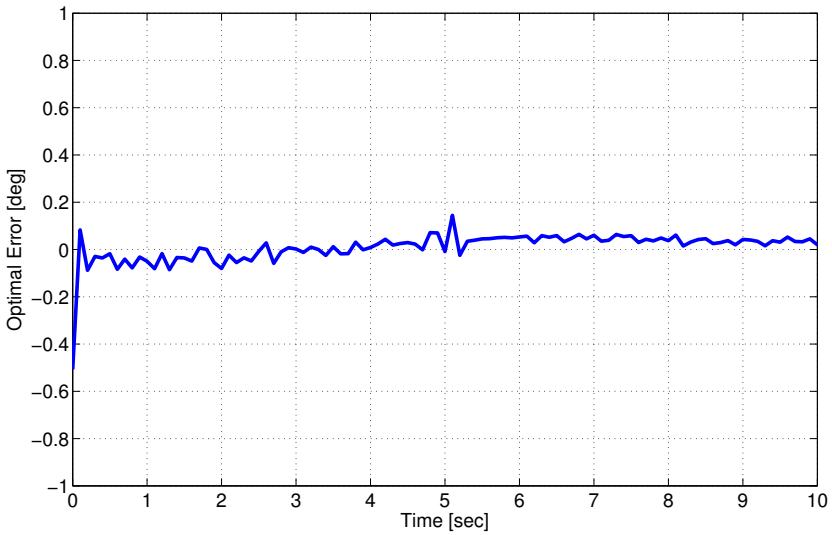

Figure 6.22: Optimal Error for Gimbaled System (Case 3 Stochastic)

6.4 Conclusions

The control technique used for the gimbal system on a tactical missile must provide fast and precise tracking of relative error signals created by the missile's signal processing unit. This chapter presented a finite-horizon nonlinear tracking technique, for both deterministic and stochastic cases, used for the gimbaled system in missile seeker. The proposed technique provides an excellent angle tracking. Simulation results are included to demonstrate the effectiveness of the developed technique. Three engagement scenarios including fixed target, non-maneuvering target, and maneuvering target are considered to demonstrate the effectiveness of the developed technique.

Chapter 7

Finite-Time, Nonlinear Tracking: Experimental/Validation Results

DC motors are widely used in industrial applications. Controlling of DC motor is a great challenge for control engineers. Precise equations describing DC motors are nonlinear. Accurate nonlinear control of the motion of the DC motors is required. Traditional technique to control nonlinear systems is to *linearize* the *nonlinear* system in a small region around the operating point and then design linear controllers. These controllers with constant gains can be expected to perform satisfactorily in the neighborhood of the operating point. However, they may not be capable of dealing with a situation over a large range of operating points. To overcome this drawback, one approach is to use extended linearization design [124]. This approach is to design several linear controllers matching to several operating points that may cover the whole dynamic region of the system. Then these linear controllers are pieced together to obtain a nonlinear controller, which is known as gain scheduling with respect to

constant operating equilibrium points [115]. But the major limitation of gain scheduling is that stability properties of the closed-loop system can be guaranteed only in a vicinity of the equilibrium manifold and under an assumption of a slow variation of signals [102].

In this chapter, we address the problem of finite-horizon position control of a permanent magnet DC motor based on the nonlinear system dynamics. The developed technique for tracking of finite-horizon nonlinear systems is utilized. Hardware in the loop simulation (HILS) system with a DC motor is presented to validate the theoretical analysis.

7.1 Hardware in the Loop Simulation (HILS) Setup

Traditional software-based simulation has the disadvantage of being unable to accurately imitate real operational environment. One way to bridge the gap between simulation and real conditions is the HILS. Real-time HILS replaces some simulation models of a system by one or several real hardware that interacts with the computer models. This increases the realism of the simulation and provides access to some features not accessible in software-only simulation models [91].

The basic principle of HILS is that some subsystems are physically embedded within a real-time simulation model. Real-time means the simulation of each component performed such that input and output signals show the same time dependent values as in real world dynamic operation. In HILS, the embedded system is fooled into thinking that it is operating with real world inputs and outputs, in real-time. A

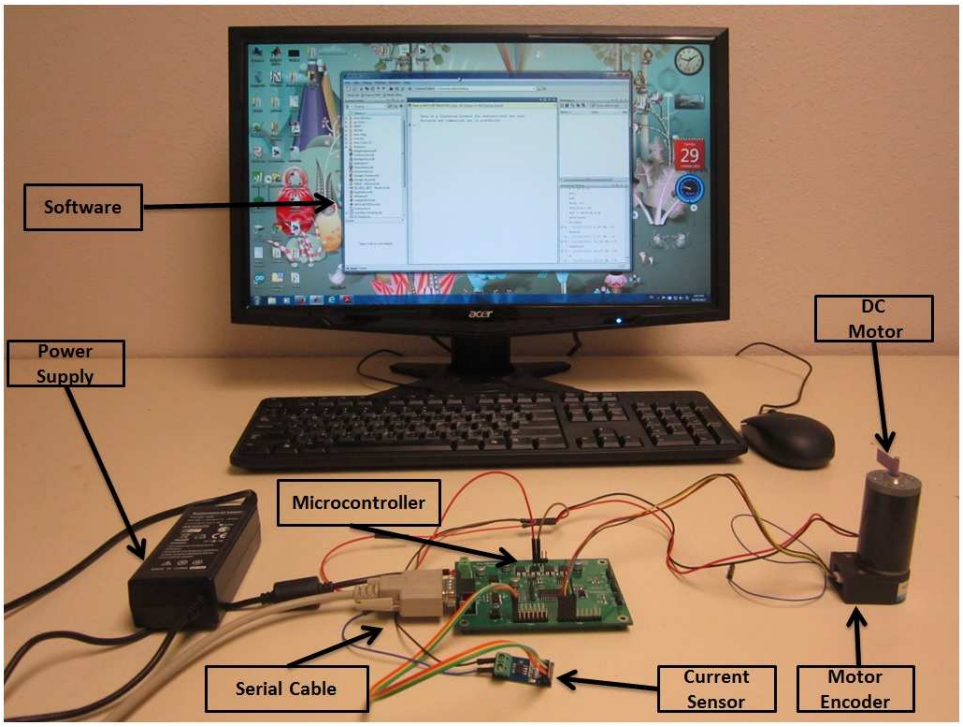

Figure 7.1: Hardware in the Loop (HIL) Experimental Setup

computer software with real-time simulation capabilities and communication abilities is necessary to perform HILS [119].

This section describes the HILS setup and the implementation of the finite-horizon differential SDRE designed in Chapter 4 to control a real DC motor.

The experimental setup shown in Fig. 7.1, consists of a Hilink microcontroller board manufactured by Zeltom Educational and Industrial Control System Company [1], a corresponding SIMULINK©library from MATLAB©and SIMULINK©, DC motor with encoder, and Hall effect current sensor.

7.1.1 The HILINK Platform

The HILINK platform offers a seamless interface between physical plants and Matlab/Simulink for implementation of real-time HILS control systems. It is fully integrated into MATLAB©and SIMULINK©and has a broad range of inputs and outputs. The HILINK platform consists of the real-time control board (hardware) and the associated Matlab interface (software). The real-time control board, which is shown in Fig. 7.2, is based on a dsPIC30F2012 digital signal controller, which is a high performance 16 bit digital signal controller with 12 kB flash program memory and 1 kB SRAM data memory. The HILINK board has 8x12 bit analog inputs, 2x16 bit capture inputs, 2x16 bit encoder inputs, 1x8 bit digital input, 2x12 bit analog outputs, 2x16 bit frequency outputs, 2x16 bit pulse outputs and 1x8 bit digital output. The board also contains 2 H-bridges with 5 A capability to drive external heavy loads. Some inputs and outputs are multiplexed to simplify the hardware. The board is interfaced to the host computer that runs Matlab through a serial port. The software of the HILINK platform is fully integrated into Matlab/Simulink/Real-Time Windows Target and comes with Simulink library blocks associated with each hardware input and output. The platform achieves real-time operation with sampling rates up to 3.8 kHz. The board requires a 6-15 V, at least 0.15 A (without any external load), regulated DC power supply. The recommended power supply for the board is a 12 V well regulated DC power supply with 5 A drive capability.

The functional block diagram of the board is shown in Fig. 7.3, where A0–A7 are the analog inputs, B0–B1 are the analog outputs, C0–C1 are the capture inputs,

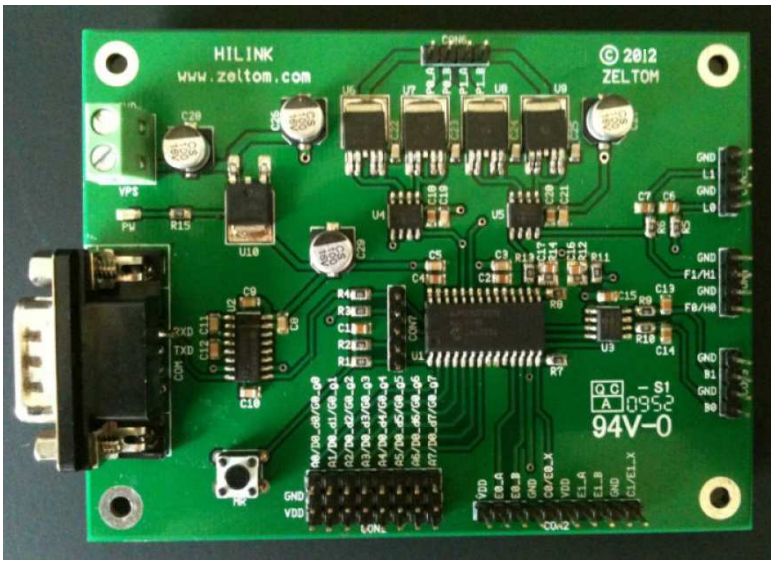

Figure 7.2: HILINK Board

D0-d0–D0-d7 are the digital inputs, E0–E1 are the encoder inputs, F0–F1 are the frequency outputs, G0-g0–G0-g7 are the digital outputs and H0–H1 are the pulse outputs; ADC represents the analog-to-digital converter, DAC represents the digital-to-analog converter, ICM represents the input capture module, OCM represents the output-compare module, DIP represents the digital-input port, DOP represents the digital-output port, QEM represents the quadrature-encoder module and PWM represents the pulse-width modulator, FLs are the low pass filters with outputs L0-L1 and HBs are the H-bridges with outputs P0–P1, and μC is the central microcontroller, UART is the universal-asynchronous-receiver transmitter unit and PC is the host computer.

7.1.2 The DC Motor with Encoder

The DC motor used in this research is a carbon-brush permanent magnet 12v DC motor (see Fig. 7.4). The system model is shown in Fig. 7.5 , where R is the armature

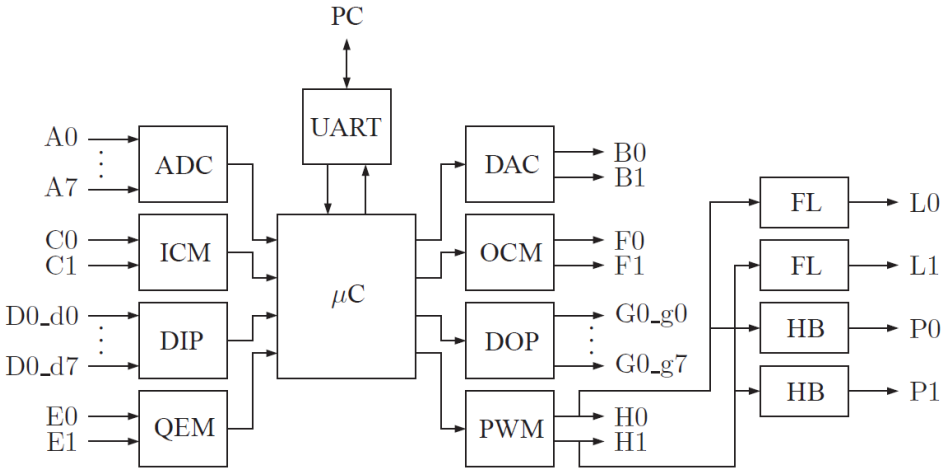

Figure 7.3: HILINK Board Functional Block Diagram

resistance, L is the armature inductance, v is the voltage applied to the motor, i is the current through the motor, e is the back EMF voltage, J is the moment of inertia of the load, B is the viscous friction coefficient, $\tau = k_i i(t)$ is the torque generated by the motor, θ is the angular position of the motor,and ω is the angular velocity of the motor. The encoder is used to measure the motor angular position of the DC motor.

Figure 7.4: Permanent Magnet DC Motor

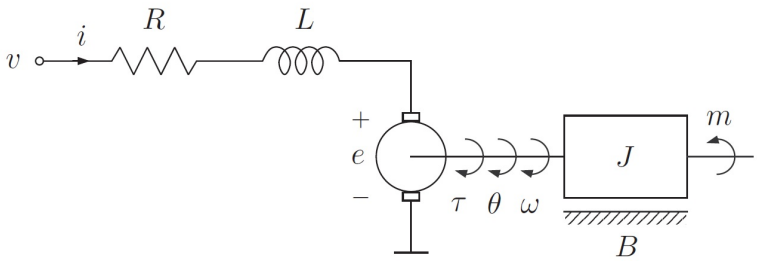

Figure 7.5: Permanent Magnet DC Motor System Model

The dynamic equations for the DC motor are

$$\omega(t) = \frac{d\theta(t)}{dt}, \tag{7.1.1}$$

$$V(t) = L\frac{di(t)}{dt} + Ri(t) + k_w\omega(t), \tag{7.1.2}$$

$$k_i i(t) = J\frac{d\omega(t)}{dt} + B\omega(t) + Csgn(\omega), \tag{7.1.3}$$

where k_w is the back EMF constant, k_i is the torque constant of the motor, and C is the motor static friction, and the signum function $sgn(\omega)$ is defined as

$$sgn(\omega) = \frac{|\omega|}{\omega}. \tag{7.1.4}$$

The nonlinear state equations of the system can be written in the form:

$$\dot{x_1} = x_2, \tag{7.1.5}$$

$$\dot{x_2} = \left(\frac{-B}{J} - \frac{-C}{J|x_2|}\right)x_2 + \frac{k_i}{J}x_3, \tag{7.1.6}$$

$$\dot{x_3} = -\frac{k_w}{L}x_2 - \frac{R}{L}x_3 + \frac{1}{L}u, \tag{7.1.7}$$

$$y = x_1, \tag{7.1.8}$$

where: $\theta = x_1$, $\dot{\theta} = x_2$, $i = x_3$, and $V = u$.

7.1.3 The Hall-Effect Current Sensor

The Hall effect current sensor is used the measure the current through the DC motor. The operating voltage range for this sensor is 4.5 V to 5.5 V, and it has from -5 A to +5 A current range with 0.185 V/A sensitivity.

7.1.4 The Simulink Model

In the Simulink model shown in Fig. 7.6, the reference motor angle is generated in the signal builder block, and H0 block transfers the optimal control voltage from the MATLAB©and SIMULINK©in the host PC to the DC motor via the HILINK card. A0 and E0 are the current sensor and encoder input blocks respectively. The outputs from the current sensor and encoder input blocks should be filtered with a low pass filter to get rid of the high frequency noise resulting from the numerical differentiation. The function of $1/(0.01s + 1)$ is acting as a low pass filter. The reference motor angle generated from the signal builder and the motor actual angle would be shown in the scope in the Simulink model.

7.2 Simulation and Experimental Results

In this section simulation results in Matlab/Simulink are presented and compared with the real-time hardware experimental results via the experimental setup by ZELTOM company. Thus, thereby showing the effectiveness of the proposed method.

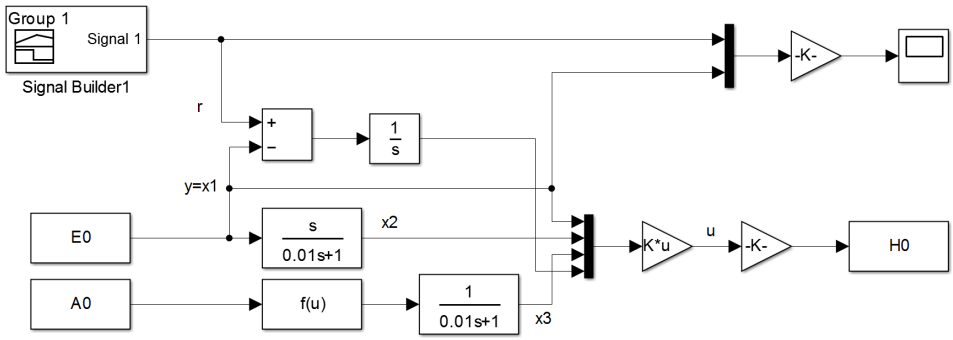

Figure 7.6: HILS Simulink Model

7.2.1 Simulation Results

The nonlinear state equations of the DC motor (7.1.5–7.1.7) can be rewritten in state dependent form

$$\begin{bmatrix} \dot{x_1} \\ \dot{x_2} \\ \dot{x_3} \end{bmatrix} = \begin{bmatrix} 0 & 1 & 0 \\ 0 & \left(\frac{-B}{J} - \frac{-C}{J|x_2|}\right) & \frac{k_i}{J} \\ 0 & -\frac{k_w}{L} & -\frac{R}{L} \end{bmatrix} \begin{bmatrix} x_1 \\ x_2 \\ x_3 \end{bmatrix} + \begin{bmatrix} 0 \\ 0 \\ \frac{1}{L} \end{bmatrix} u. \tag{7.2.1}$$

where: $\theta = x_1$, $\dot{\theta} = x_2$, $i = x_3$, and $V = u$.

Let the reference angle $z(t) = 90^o$,and the selected weighted matrices are

$$\mathbf{Q} = diag(60, 0, 0), \quad \mathbf{R} = 0.7, \quad \mathbf{F} = diag(1, 1, 1). \tag{7.2.2}$$

The simulations are performed for final time of 10 seconds and the resulting angle trajectories are shown in Fig. 7.7, where the dash-dot line denotes the *reference* angle trajectory, and the solid line denotes the *actual* trajectory. The optimal control is shown in Fig. 7.8.

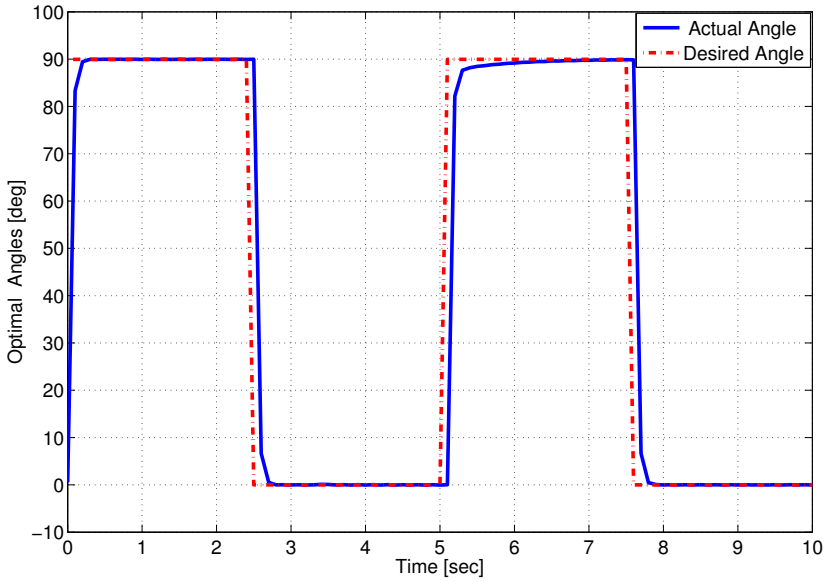

Figure 7.7: Optimal Position Tracking for the Simulated DC Motor

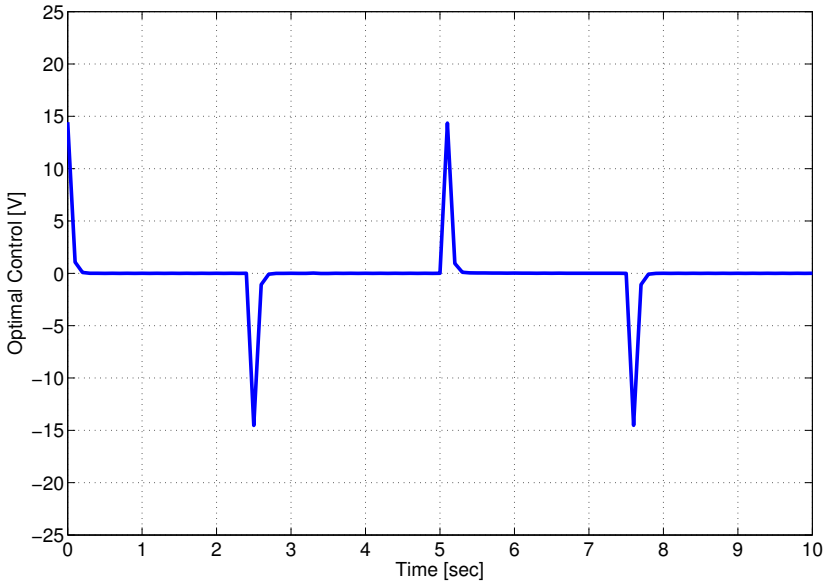

Figure 7.8: Optimal Control Voltage for the Simulated DC Motor

Comparing these trajectories in Fig. 7.7, it's clear that the proposed method gives very good results as the actual optimal angle is making a very good tracking to the reference angle with standard deviation error of 0.02^o.

7.2.2 Experimental Results

Once the algorithms have been developed and tested in software, the next step is to compare the results between software simulation and real world applications. Here, the method of HILS is applied by using the experimental setup introduced in Section 7.1.

A schematic diagram of the experimental setup is given in Fig. 7.9. The experiment is performed for final time of 10 seconds and the resulting angle trajectories is shown in Fig. 7.10, where the dash-dot line denotes the *reference* angle trajectory, and the solid line denotes the *actual* trajectory. Comparing these trajectories in Fig. 7.10, it's clear that the propose algorithm gives very good results as the actual optimal angle is making a very good tracking to the reference angle with standard deviation error of 0.025^o.

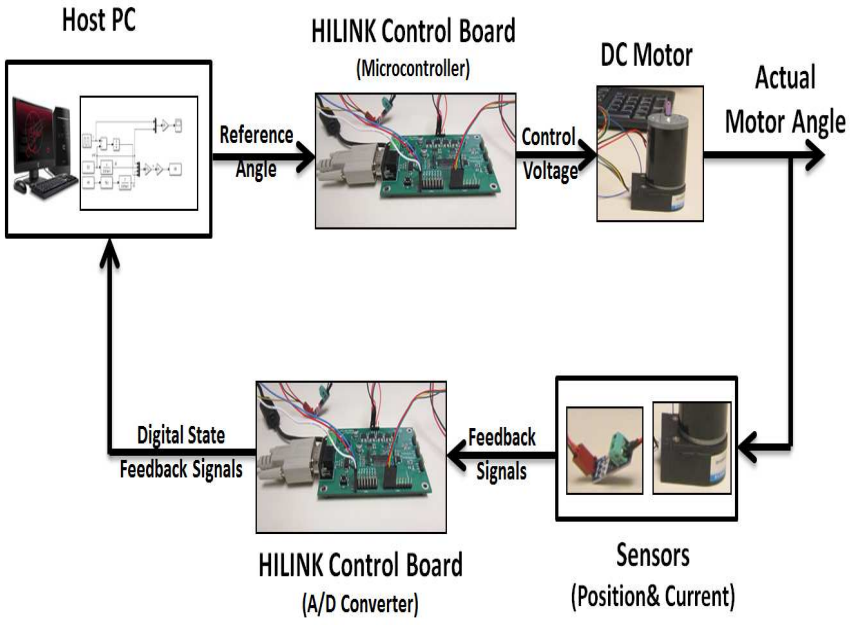

Figure 7.9: Schematic Diagram for Hardware in the Loop Simulation

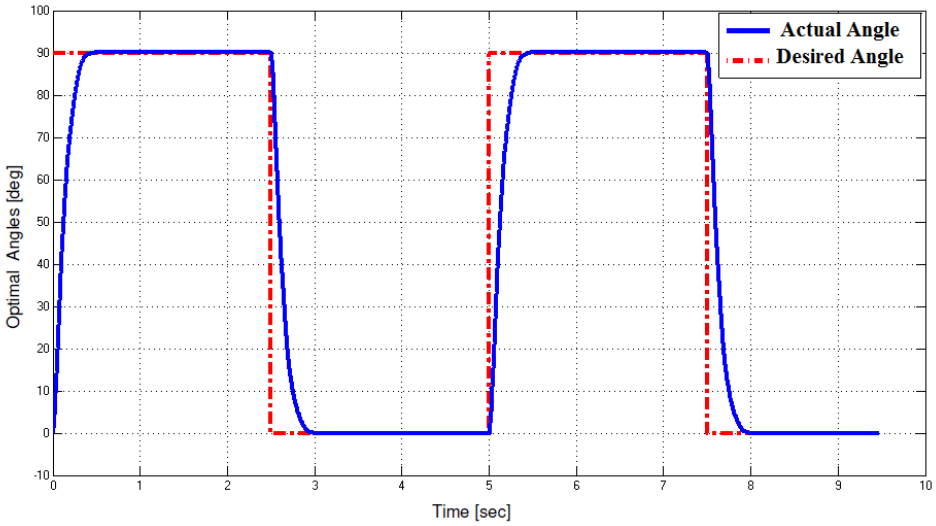

Figure 7.10: Optimal Angle Tracking for the HILS System

For further demonstration, the performance of the DC motor with the finite-horizon differential SDRE controller to track a multi step and multi frequency reference is shown in Fig 7.11 and Fig 7.12 respectively. It shows that the controller gives almost the same performance regardless of the value of the step reference.

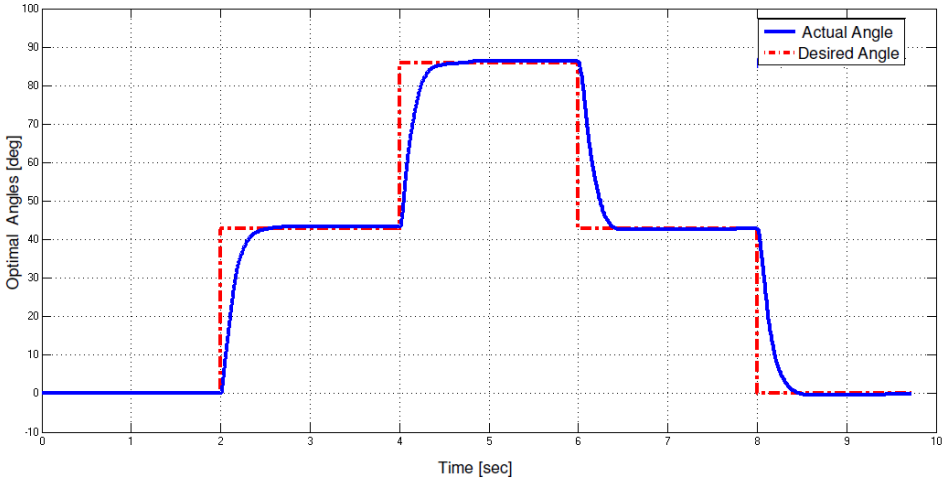

Figure 7.11: Multi-Step DC Motor Position Reference Tracking

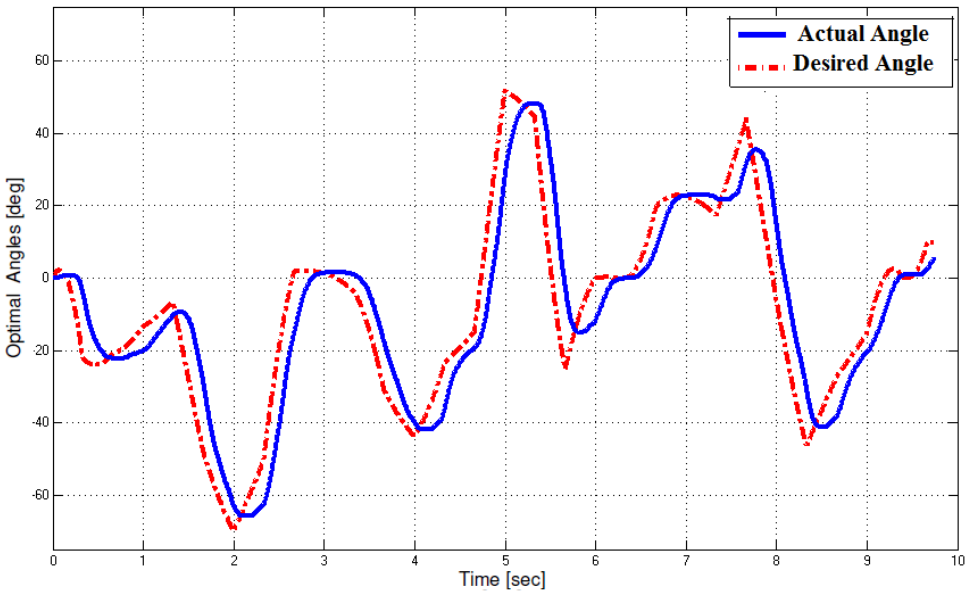

Figure 7.12: Multi-Frequency DC Motor Position Reference Tracking

7.3 Conclusions

The problem of finite-horizon position control of a permanent magnet DC motor based on the nonlinear system dynamics is addressed in this chapter. The developed technique for finite-horizon tracking of nonlinear systems via differential SDRE is utilized. HILS system based on a microcontroller board and a real DC motor is used to validate the theoretical analysis. The consistency of the experimental results with the simulation results demonstrates the effectiveness of the developed technique.

Chapter 8

Conclusions and Future Investigations

In this dissertation, a detailed investigation of advanced regulation and tracking strategies for linear and nonlinear optimal control systems and its application has been presented. The main conclusions derived from this dissertation are discussed in this chapter. Recommendations for future research are also addressed.

8.1 Conclusions

The State Dependent Riccati Equation (SDRE) provide an effective algorithm for optimal control design for nonlinear dynamical systems. The SDRE algorithm captures the nonlinearities of the system, transforming the original nonlinear system to a linear-like structure with State Dependent Coefficient (SDC) matrices, and minimizing a non-quadratic performance index with a quadratic-like structure. The main

advantage of SDRE is the ability to make tradeoffs between control effort and state errors by tuning the SDC.

This research presented an efficient online technique used for *infinite-horizon* nonlinear stochastic regulator and tracking problems. The idea of the proposed technique is the integration of the Kalman filter algorithm and the infinite-horizon algebraic SDRE technique. Unlike the ordinary methods which deal with the linearized system, this technique estimates the unmeasured states of the nonlinear system directly.

Next, this research discussed an online technique for *finite-horizon* regulation and tracking of nonlinear systems. The proposed technique is based on change of variables that converts the nonlinear differential Riccati equation (DRE) (to be solved backward in time using final condition) to a linear differential Lyapunov equation (to be solved forward in time using change in variables).

Then, a finite-horizon differential SDRE nonlinear filtering technique was presented for online implementation. The Kalman filter is used to estimate the states after converting the DRE to a linear Lyapunov equation. Solving the nonlinear optimal control problem with the differential SDRE algorithm, makes this technique effective for a wide range of operating points.

Missile guidance and control is one of the applications that need fast and precise tracking of relative error signals created by the missile's signal processing unit. The proposed finite-horizon nonlinear tracking technique was used for angle tracking of the gimbaled system in missile seeker. Three engagement scenarios, based on real data, including fixed target, non-maneuvering target, and high maneuvering target were considered to demonstrate the effectiveness of the developed technique.

The Hardware In The Loop Simulation (HILS) is used to bridge the gap between software simulation and real world applications. The HILS is applied by using HILS setup based on a microcontroller board manufactured by Zeltom Educational and Industrial Control System Company and a real DC motor. HILS system is presented to validate the theoretical analysis and the simulation results.

8.2 Future Investigations

Some of the recommendations for further research are given below:

1. Development of finite-horizon optimal regulation and tracking for nonlinear, *discrete-time*, stochastic systems with uncertainty and disturbance.

2. Development of finite-horizon optimal regulation and tracking for continuous-time nonlinear systems (both deterministic & stochastic) using singular perturbation and time-scale methods.

3. Development of finite-horizon optimal regulation and tracking for nonlinear, *discrete-time* nonlinear systems (both deterministic & stochastic) using singular perturbation and time-scale methods.

4. Real-time implementation and validation of the above proposed research problems based on real-world situations.

References

[1] Zeltom. educational and industrial control systems.

[2] Tankut Acarman. Nonlinear optimal integrated vehicle control using individual braking torque and steering angle with on-line control allocation by using state-dependent Riccati equation technique. *Vehicle System Dynamics*, 47(2):155–177, 2009.

[3] J. Amirazodi, E. E Yaz, A. Azemi, and Y. I. Yaz. Nonlinear observer performance in chaotic synchronization with application to secure communication. *IEEE International Conference on Control Applications, Glasgow, Scotland, U. K., IEEE Publ.*, pages 76–81, 2002.

[4] B. D. O. Anderson and J. B. Moore. *Optimal Control: Linear Quadratic Methods*. New Jersey: Prentice Hall, 1990.

[5] Brian DO Anderson and John B Moore. *Optimal control: linear quadratic methods*, volume 1. Prentice Hall Englewood Cliffs, NJ, 1990.

[6] M. Athans and P. Falb. *Optimal Control: An Introduction to the Theory and its Applications*. Dover Publications, 2007.

[7] R. Azor, I. Y. Bar-Itzhack, J. K. Deutschmann, and R. R. Harman. Angular-rate estimation using delayed quaternion measurements. *Journal of Guidance, Control, and Dynamics*, 24(3):436–443, 2001.

[8] Teodor Balaz, Radek Doskocil, and Martin Macko. Feeding an information determine optic atmosphere turbulence into the simulation model of a seeker of homing missiles. *Proceedings of 6th WSEAS International Conference on System Science and Simulation in Engineering, Venice, Italy*, pages 21–23, November 2007.

[9] H. T. Banks, H.D. Kwon, J. A. Toivanen, and H. T. Tran. A state-dependent Riccati equation-based estimator approach for hiv feedback control. *Optimal Control Applications and Methods*, 27:93–121, 2006.

[10] S. P. Banks and K. J. Mhana. Optimal control and stabilization for nonlinear systems. *IMA Journal of Mathematical Control and Information*, 9(2):179–196, 1992.

[11] M Barlaud, B De Fornel, M Gauvrit, and JP Requier. Commande optimale d'un système générateur photovoltaïque-convertisseur statique-récepteur. *Revue de physique appliquée*, 19(10):905–915, 1984.

[12] A. Barraud. A new numerical solution of xdot=a1*x+x*a2+d, x(0)=c. *IEEE Transaction on Automatic Control*, 22(6):976–977, Dec. 1977.

[13] S. Belikov, J. Kamali, and B. Friedland. A state-dependent Riccati equation filter for a rapid thermal processing system. *36th IEEE Conference on Decision and Control, San Diego, CA, IEEE Publ.*, pages 2547–2548, 1997.

[14] S. Belikov, J. Kamali, and B. Friedland. Analytical solution for a separate state and parameter SDRE observer for a csi-fed induction motor. *IEEE International Conference on Control Applications, Trieste, Italy, IEEE Publ.*, pages 1286–1291, 1998.

[15] N. Bhoir and S. N. Singh. Control of unsteady aeroelastic system via state-dependent Riccati equation method. *Journal of Guidance, Control, and Dynamics*, 28(1):78–84, 2005.

[16] A. Bogdanov and E. Wan. State-dependent Riccati equation control for small autonomous helicopter. *Journal of Guidance, Control, and Dynamics*, 30(1):47–60, 2007.

[17] A. Calise, S. Lee, and M. Sharma. Direct adaptive reconfigurable control of a tailless fighter aircraft. *AIAA Guidance, Navigation, and Control Conference*, pages 88–97, 1998.

[18] T. Çimen. Recent advances in nonlinear optimal feedback control design. *Proceedings of the 9th WSEAS International Conference on Applied Mathematics, Istanbul, Turkey*, pages 460–465, May 2006.

[19] T. Çimen. State-dependent Riccati equation (SDRE) control: a survey. *Proc. of the 17th IFAC World Congress*, pages 3761–3775, 2008.

[20] T. Çimen. Development and validation of a mathematical model for control of constrained nonlinear oil tanker motion. *Mathematical and Computer Modeling of Dynamical Systems*, 15(1):1749, 2009.

[21] T. Çimen. Systematic and effective design of nonlinear feedback controllers via the state-dependent Riccati equation (SDRE) method. *Annual Reviews in Control*, 34:32–51, 2010.

[22] T. Çimen. A generic approach to missile autopilot design using state-dependent nonlinear control. *8th IFAC World Congress, Milan, Curran Associates, Inc., Red Hook, NY*, 1:9587–9600, 2011.

[23] T. Çimen. Survey of state-dependent Riccati equation in nonlinear optimal feedback control synthesis. *AIAA Journal of Guidance, Control, and Dynamics*, 35(4):1025–1047, 2012.

[24] T. Çimen and S.P. Banks. Nonlinear optimal tracking control with application to super-tankers for autopilot design. *Automatica*, 40:1845–1863, 2004.

[25] Insu Chang, Sang-Young Park, and Kyu-Hong Choi. Decentralized coordinated attitude control for satellite formation flying via the state-dependent Riccati equation technique. *International Journal of Non-Linear Mechanics*, 44(8):891–904, 2009.

[26] Cheng-Hung Chen. *Hybrid Control Strategies for Smart Prosthetic Hand*. PhD thesis, Idaho State University, 2009.

[27] T. Cheng, F. L. Lewis, and M. Abu-Khalaf. A neural network solution for fixed-final time optimal control of nonlinear systems. *Automatica*, 43:482–490, 2007.

[28] Tayfun Çimen. A generic approach to missile autopilot design using state-dependent nonlinear control. In *18th IFAC World Congress*, pages 9587–9600, 2011.

[29] J. R. Cloutier. State-dependent Riccati equation techniques: An overview. *Proc. American Control Conference*, 2:932–936, 1997.

[30] J. R. Cloutier and D. T. Stansbery. All-aspect acceleration-limited homing guidance. *AIAA Paper 1999-4063, Red Hook, NY*, August 1999.

[31] J. R. Cloutier and D. T. Stansbery. Control of a continuously stirred tank reactor using an asymmetric solution of the state-dependent Riccati equation. *IEEE Conference on Control Applications, Kohala Coast, HI, IEEE Publ.*, pages 893–898, 1999.

[32] J. R. Cloutier and D. T. Stansbery. Nonlinear, hybrid bank-to-turn/skid-to-turn autopilot design. *Proceedings of the AIAA Guidance, Navigation, and Control Conference*, 2001.

[33] J. R. Cloutier and D. T. Stansbery. Dynamic conversion of flight path angle commands to body attitude commands. *American Control Conference, Anchorage, AK, IEEE Publ.*, pages 221–225, August 2002.

[34] J. R. Cloutier and P. H. Zipfel. Hypersonic guidance via the state-dependent Riccati equation control method. *IEEE Conference on Control Applications, Kohala Coast, HI, IEEE Publ.*, pages 219–224, 1999.

[35] A. G. Cree and C. J. Damaren. Causal approximate inversion for control of structurally flexible manipulators using nonlinear inner-outer factorization. *journal of Robotic System*, 18(7):391–399, 2001.

[36] S Di Gennaro. Output attitude tracking for flexible spacecraft. *Automatica*, 38(10):1719–1726, 2002.

[37] Travis Dierks and Sarangapani Jagannathan. Optimal control of affine nonlinear continuous-time systems using an online Hamilton-Jacobi-Isaacs formulation. In *49th IEEE Conference on Decision and Control (CDC)*, pages 3048–3053. IEEE, 2010.

[38] J. Doyle, Y. Huang, J. Primbs, R. Freeman, R. Murray, A. Packard, and M. Krstic. Nonlinear control: Comparisons and case studies. *In Notes from the Nonlinear Control Workshop conducted at the American Control Conference, Albuquerque, New Mexico*, 1998.

[39] Y.Z. Elhalwagy and M. Tarbouchi. Three-dimensional missile guidance laws design using fuzzy schemes. *Proceedings of the International Conference on Electronics, Control ,and Signal Processing (WSEAS), Singapore*, pages 9–12, December 2002.

[40] E. B. Erdem and A. G. Alleyne. Experimental real-time SDRE control of an underactuated robot. *40th IEEE Conference on Decision and Control, Orlando, FL, IEEE Publ.*, pages 2986–2991, 2001.

[41] Bernard Etkin and Lloyd Duff Reid. *Dynamics of Flight: Stability and Control*. Wiley New York, 1982.

[42] C. M. Ewing. *An Analysis of a New Nonlinear Estimation Techniques: The State-Dependent Riccati Equation Method*. PhD thesis, University. of Florida, Gainesville, FL, 1999.

[43] B. Friedland. Feedback control of systems with parasitic effects. *American Control Conference, Albuquerque, NM, IEEE Publ.*, pages 937–941, 1997.

[44] Z. Gajic and M. Qureshi. The Lyapunov matrix equation in system stability and control. *New York: Dover Publications*, 2008.

[45] Chen Gao and Hugh HT Liu. Nonlinear multi-objective receding horizon design utilizing state-dependent formulation. *Proceedings of the Institution of Mechanical Engineers, Part I: Journal of Systems and Control Engineering*, 227(1):39–50, 2013.

[46] Gonzalo Garcia and Shahriar Keshmiri. Adaptive and resilient flight control system for a small unmanned aerial system. *International Journal of Aerospace Engineering*, 2013(Article ID 289357), 2013.

[47] P. Garnell. *Guided Weapon Control Systems*. Elsevier, 1980.

[48] Seyed Mostafa Ghadami, Roya Amjadifard, and Hamid Khaloozadeh. Designing SDRE-based controller for a class of nonlinear singularly perturbed systems. *International Journal of Robotics and Automation*, 4:1–18, 2013.

[49] Hamed Ghane and Mohammad Bagher Menhaj. Eigenstructure-based analysis for non-linear autonomous systems. *IMA Journal of Mathematical Control and Information*, page dnt026, 2013.

[50] MT Grabbe and DM Dawson. An application of optimal control theory to the trajectory tracking of rigid robot manipulators. *Optimal Control: Applications and Methods*, 15(4):237–249, 1994.

[51] K. D. Hammett, C. D. Hall, and D. B. Ridgely. Controllability issues in nonlinear state-dependent Riccati equation control. *Journal of Guidance, Control, and Dynamics*, 21(5):767–773, 1998.

[52] D. Han and S. N. Balakrishnan. State-constrained agile missile control with adaptive-critic-based neural networks. *IEEE Trans. Control Systems Technology*, 10(4):481–489, 2002.

[53] Nathan Harl and SN Balakrishnan. Impact time and angle guidance with sliding mode control. *Control Systems Technology, IEEE Transactions on*, 20(6):1436–1449, 2012.

[54] R. R. Harman and I. Y. Bar-Itzhack. Pseudolinear and state-dependent Riccati equation filters for angular rate estimation. *Journal of Guidance, Control, and Dynamics*, 22(5):723–725, 1999.

[55] A. Heydari and S. N. Balakrishnan. Finite-horizon input constrained nonlinear optimal control using single network adaptive critics. *American Control Conference*, pages 3047–3052, 2011.

[56] A. Heydari and S. N. Balakrishnan. Path planning using a novel finite-horizon suboptimal controller. *Journal of Guidance, Control, and Dynamics*, pages 1–5, 2013.

[57] S Kemal Ider. Force and motion trajectory tracking control of flexible-joint robots. *Mechanism and machine theory*, 35(3):363–378, 2000.

[58] J. Imae, H. Sagami, T. Kobayashi, and Guisheng Zhai. Nonlinear control design method based on state-dependent Riccati equation (SDRE) via quasi-newton method. In *43rd IEEE Conference on Decision and Control, CDC 2004*, volume 3, pages 2740–2741 Vol.3, Dec 2004.

[59] M. Innocenti, F. Baralli, F. Salotti, and A. Caiti. Manipulator path control using SDRE. *American Control Conference, Chicago, IL, IEEE Publ.*, pages 3348–3352, 2000.

[60] M. Itik, M. U. Salamci, and S. P. Banks. SDRE optimal control of drug administration in cancer treatment. *Turkish Journal of Electrical Engineering and Computer Sciences*, 18(5):715–729, 2010.

[61] P. Jantapremjit and P. A. Wilson. Control and guidance approach using an autonomous underwater vehicle. *Transactions of the Royal Institution of Naval*

Architects Part A: International Journal of Maritime Engineering, 150(A2):1–11, 2008.

[62] A. Jayaram and M. Tadi. Synchronization of chaotic systems based on SDRE method. *Chaos, Solitons & Fractals*, 28(3):707 – 715, 2006.

[63] Bayu Jayawardhana and George Weiss. Tracking and disturbance rejection for fully actuated mechanical systems. *Automatica*, 44(11):2863–2868, 2008.

[64] Reza N Jazar. *Theory of Applied Robotics: Kinematics, Dynamics, and Control*. Springer, 2007.

[65] Z. Jiang and R. Ordonez. Trajectory generation on approach and landing for rlvs using motion primitives and neighboring optimal control. *American Control Conference*, pages 1091–1096, 2007.

[66] Eaves J.L. Principles of modern radar. *Guidance, Navigation, and Control Conference, Van Nostrand Reinhold company Inc.*, pages 937–941, 1987.

[67] E. N. Johnson, D. P. Schrage, and G. Vachtsevanos. Software enabled control experiments with university-operated unmanned aircraft. *AIAA Paper 2005-6956*, September 2005.

[68] A Jordan, M Benmouna, A Bensenane, and A Borucki. Optimal linearization of non-linear state equations. *Automatique-productique informatique industrielle*, 21(3):263–271, 1987.

[69] AJ Jordan. Linearization of non-linear state equation. *Bulletin of The Polish Academy of Sciences Technical Science*, 54(1), 2006.

[70] A. M. Kamel. *Context Aware High Dynamics GNSS-INS for Interference Mitigation Geomatics Engineering.* PhD thesis, University of Calgary, Calgary, 2011.

[71] G. Kepler, H. Banks, H. Tran, and S. Beeler. Reduced order modeling and control of thin film growth in an HPCVD reactor. *SIAM Journal on Applied Mathematics*, 62(4):1251–1280, 2002.

[72] A. Khamis, Zydek D., Borowik G., and Subbaram Naidu D. Control system design based on modern embedded systems. In *Computer Aided Systems Theory.* Springer Berlin Heidelberg, 2013.

[73] A. Khamis, Zydek D., Borowik G., and Subbaram Naidu D. Control system design based on modern embedded systems. *14th International Workshop on Computer Aided Systems Theory - EUROCAST 2013*, pages 346–347, 2013. Las Palmas de Gran Canaria, Spain.

[74] A. Khamis and D.S. Naidu. Nonlinear optimal tracking using finite-horizon state dependent Riccati equation (SDRE). *Proceedings of the 4th International Conference on Circuits, Systems, Control, Signals (WSEAS)*, pages 37–42, August 2013. Valencia, Spain.

[75] A. Khamis and D.S. Naidu. Experimental validation for real time control of DC motor using novel finite-horizon optimal technique. *IEEE-CYBER 2014, Hong Kong, China*, June 2014. Accepted.

[76] A. Khamis and D.S. Naidu. Nonlinear optimal stochastic regulator using finite-horizon state dependent Riccati equation. *IEEE-CYBER 2014, Hong Kong, China*, June 2014. Accepted.

[77] A. Khamis and D.S. Naidu. Nonlinear optimal tracking for missile gimbaled seeker using finite-horizon state dependent Riccati equation. *IEEE-CYBER 2014, Hong Kong, China*, June 2014. Accepted.

[78] A. Khamis and D.S. Naidu. Nonlinear optimal tracking with incomplete state information using finite-horizon state dependent Riccati equation (SDRE). *Proceedings of the American Control Conference (ACC2014), Portland, Oregon*, June 2014. Accepted.

[79] A. Khamis, D.S. Naidu, and D. Zydek. Nonlinear optimal control with incomplete state information using state dependent Riccati equation (SDRE). *23rd International Conference On Systems Engineering (ICSEng 2014), Las Vegas, NV, USA*, 2014. Accepted.

[80] A. Khamis, D.S. Naidu, and D. Zydek. Nonlinear position control of DC motor using finite-horizon state dependent Riccati equation (SDRE). *23rd International Conference On Systems Engineering (ICSEng 2014), Las Vegas, NV, USA*, 2014. Accepted.

[81] Ahmed Khamis. *Design and Realization of Hardware In Loop Simulation for a Homing Guided Missile*. PhD thesis, Military Technical Collage, Cairo, 2007.

[82] I. S. Kim, J. Chandrasekar, A. Ridley, and D. S. Bernstein. Data assimilation using the global ionosphere-thermosphere model. *Computational Science: ICCS 2006*, 3993, 2006.

[83] D. E. Kirk. *Optimal Control Theory*. Dover Publications, 2004.

[84] Tomoaki Kobayashi, Michiyuki Magono, Joe Imae, Kazutaka Yoshimizu, and Guisheng Zhai. Real-time optimization for nonlinear systems using algorithmic control. *Preprints of IFAC'05*, 2005.

[85] A. Kuzucu and A. Roch. Suboptimal adaptive feedback control of nonlinear systems. *Proceedings of an International Symposium Bochum*, 24:131–140, 1980.

[86] M. W. Lam, Q. M.and Oppenheimer. Investigation of adaptive SDRE control reconfiguration subject to control surface failures. *AIAA Paper*, April 2010.

[87] Q. Lam, P. Krishnamurthy, and F. Khorrami. Enhancing flight control system performance using SDRE based controller as an augmentation layer. *AIAA Paper 2009-6171*, August 2009.

[88] W. Langson and A. Alleyne. Multi variable bilinear vehicle control using steering and individual wheel torques. *American Control Conference, Albuquerque, NM, IEEE Publ.*, pages 1136–1140, 1997.

[89] J. Liang. *Optimal Magnetic Attitude Control of Small Spacecraft*. PhD thesis, Utah State University, Logan, 2005.

[90] Yew-Wen Liang, Jun-Yu Chen, and Li-Gang Lin. A guidance law design using the combination of ismc and SDRE schemes. In *International Conference on System Science and Engineering (ICSSE)*, pages 63–67. IEEE, 2013.

[91] Bin Lu, Antonello Monti, and Roger A Dougal. Real-time hardware-in-the-loop testing during design of power electronics controls. In *Industrial Electronics Society, 2003. IECON'03. The 29th Annual Conference of the IEEE*, volume 2, pages 1840–1845. IEEE, 2003.

[92] Mauro Massari and Mattia Zamaro. Application of SDRE technique to orbital and attitude control of spacecraft formation flying. *Acta Astronautica*, 2013.

[93] Markus Mauder. Robust tracking control of nonholonomic dynamic systems with application to the bi-steerable mobile robot. *Automatica*, 44(10):2588–2592, 2008.

[94] C. P. Mracek. SDRE autopilot for dual controlled missiles. *7th IFAC Symposium on Automatic Control in Aerospace*, 2007.

[95] C. P. Mracek and J. R. Cloutier. Missile longitudinal autopilot design using the state-dependent Riccati equation method. *1st International Conference on Nonlinear Problems in Aviation and Aerospace*, pages 387–396, 1996.

[96] C. P. Mracek and J. R. Cloutier. Full envelope missile longitudinal autopilot design using the state-dependent Riccati equation method. *AIAA Paper 1997-3767*, August 1997.

[97] Sandeep S Mulgund and Robert F Stengel. Optimal nonlinear estimation for aircraft flight control in wind shear. *Automatica*, 32(1):3–13, 1996.

[98] D. S. Naidu. *Optimal Control Systems*. CRC Press, 2003.

[99] D. S. Naidu. *Deterministic and Stochastic Optimal Control Systems*. under preparation, 2014.

[100] Mugdha S. Naik and Sahjendra N. Singh. State-dependent Riccati equation-based robust dive plane control of UAV with control constraints. *Ocean Engineering*, 34(1112):1711 – 1723, 2007.

[101] J. Nazarzadeh, M. Razzaghi, and K. Nikravesh. Solution of the matrix Riccati equation for the linear quadratic control problems. *Mathematical and Computer Modelling*, 27(7):51–55, 1998.

[102] Andrei-Sorin Neamtu and Adrian-Mihail Stoica. A bumpless transfer method for automatic flight control switching. *UPB Scientific Bulletin, Series D*, 74, 2012.

[103] A. Nemra and N. Aouf. Robust ins/gps sensor fusion for UAV localization using SDRE nonlinear filtering. *Sensors Journal, IEEE*, 10(4):789–798, 2010.

[104] T. Nguyen and Z. Gajic. Solving the matrix differential Riccati equation: a Lyapunov equation approach. *IEEE Trans. Automatic Control*, 55(1):191–194, 2010.

[105] A. Papachristodoulou. Robust stabilization of nonlinear time delay systems using convex optimization. *44th IEEE Conference on Decision and Control, and the European Control Conference, Seville, Spain, IEEE Publ.*, pages 5788–5793, 2005.

[106] V. Pappano and B. Friedland. Speed sensorless observer for an induction machine with separate bias estimation. *American Control Conference, Philadelphia, PA, IEEE Publ.*, pages 3788–3790, 1998.

[107] D. K. Parrish and D. B. Ridgely. Attitude control of a satellite using the SDRE method. *American Control Conference, Albuquerque, NM, IEEE Publ.*, pages 942–946, 1997.

[108] Nilanjan Patra, Kaushik Halder, Avijit Routh, Abhro Mukherjee, and Satyabrata Das. Kalman filter based optimal control approach for attitude control of a missile. In *Computer Communication and Informatics (ICCCI), 2013 International Conference on*, pages 1–4. IEEE, 2013.

[109] J. Pittner and M. A. Simaan. *Tandem Cold Metal Rolling Mill Control Using Practical Advanced Methods*. SpringerVerlag, 2011.

[110] Anna Prach and Ozan Tekinalp. Development of a state dependent Ricatti equation based tracking flight controller for an unmanned aircraft. 2013.

[111] Yang Qian, Liu Weiguo, and Huang Yongping. Real time simulation study on backstepping sliding mode control of permanent magnet synchronous motor. In *2011 International Conference on Electrical Machines and Systems (ICEMS)*, pages 1–5, Aug 2011.

[112] A. Ratnoo and D. Ghose. State-dependent Riccati-equation-based guidance law for impact-angle-constrained trajectories. *Journal of Guidance, Control, and Dynamics*, 32(1):320–326, August 2009.

[113] Ashwini Ratnoo and Debasish Ghose. State-dependent Riccati-equation-based guidance law for impact-angle-constrained trajectories. *Journal of Guidance, Control, and Dynamics*, 32(1):320–326, 2009.

[114] G. G. Rigatos and S. G. Tzafestas. Extended Kalman filtering for fuzzy modeling and multi-sensor fusion. *Mathematical and Computer Modeling of Dynamical Systems: Methods, Tools and Applications in Engineering and Related Sciences*, 13(3):251–266, 2007.

[115] Wilson J Rugh and Jeff S Shamma. Research on gain scheduling. *Automatica*, 36(10):1401–1425, 2000.

[116] Rajnish Sharma and Ashish Tewari. Optimal nonlinear tracking of spacecraft attitude maneuvers. *IEEE Transactions on Control Systems Technology*, 12(5):677–682, 2004.

[117] A. M. Shawky, A. W. Ordys, L. Petropoulakis, and M. J. Grimble. Position control of flexible manipulator using non-linear h1 with state-dependent Ric-

cati equation. *Proceedings of the Institution of Mechanical Engineers. Part 1, Journal of Systems and Control Engineering*, 221(3):475–486, 2007.

[118] Alaa Shawky, Dawid Zydek, Yehia Z Elhalwagy, and Andrzej Ordys. Modeling and nonlinear control of aflexible-linkmanipulator. *Applied Mathematical Modelling*, 2013.

[119] Michael Short and Michael J Pont. Hardware in the loop simulation of embedded automotive control system. In *Intelligent Transportation Systems, 2005. Proceedings. 2005 IEEE*, pages 426–431. IEEE, 2005.

[120] D. Simon. *Optimal State Estimation: Kalman, H-infinity, and Nonlinear Approaches*. John Wiley & Sons, 2006.

[121] D. Simon. Using nonlinear Kalman filtering to estimation signals. *Embedded Systems Design*, 19(7):38–53, Dec. 2006.

[122] Sahjendra N. Singh and Woosoon Yim. State feedback control of an aeroelastic system with structural nonlinearity. *Aerospace Science and Technology*, 7(1):23 – 31, 2003.

[123] G. M. Siouris. *Missile Guidance and Control Systems*. Springer, 2004.

[124] Hebertt Sira Ramirez. Design of pi controllers for DC-to-DC power supplies via extended linearization. *International Journal of Control*, 51(3):601–620, 1990.

[125] J. G. Snijders, J. W. van der Woude, and J. Westhuis. Nonlinear observer design for dynamic positioning. *Dynamic Positioning Conference*, 2005.

[126] D. T. Stansbery and J. R. Cloutier. Position and attitude control of a spacecraft using the state-dependent Riccati equation technique. *American Control Conference, Chicago, IL, IEEE Publ.*, pages 1867–1871, 2000.

[127] Brian L Stevens and Frank L Lewis. Aircraft Control and Simulation. 2003.

[128] Arimoto Suguru. *Control theory of multi-fingered hands: a modelling and analytical-mechanics approach for dexterity and intelligence*. Springer, 2008.

[129] M. Tadi. State-dependent Riccati equation for control of aeroelastic flutter. *Journal of Guidance, Control, and Dynamics*, 26(6):914–917, 2003.

[130] M. Tadi. Nonlinear feedback control of slewing beams. *Computer Methods in Applied Mechanics and Engineering*, 195(13):133–147, 2006.

[131] C. S. Tan, R. Sutton, and J. Chudley. An integrated collision avoidance system for autonomous underwater vehicles. *International Journal of Control*, 80(7):1027–1049, 2007.

[132] Yuri Ulybyshev. Terminal guidance law based on proportional navigation. *Journal of Guidance, Control, and Dynamics*, 28(4):821–824, 2005.

[133] S. S. Vaddi, P. K. Menon, and E. J. Ohlmeyer. Numerical state-dependent Riccati equation approach for missile integrated guidance control. *Journal of Guidance, Control, and Dynamics*, 32(2):699–703, August 2009.

[134] Sai Vaddi, Padmanabhan K Menon, and Ernest J Ohlmeyer. Numerical state-dependent Riccati equation approach for missile integrated guidance control. *Journal of guidance, control, and dynamics*, 32(2):699–703, 2009.

[135] Kyriakos G Vamvoudakis and Frank L Lewis. Online actor–critic algorithm to solve the continuous-time infinite horizon optimal control problem. *Automatica*, 46(5):878–888, 2010.

[136] L. Vandenberghe, V. Balakrishnan, R. Wallin, A. Hansson, and T. Roh. *Positive Polynomials in Control*, volume 312, chapter Interior-point methods for semidefinite programming problems derived from the KYP lemma, pages 195–238. D. Henrion and A. Garulli, Eds. Berlin, Germany: Springer Verlag, 2005.

[137] P. L. Vergez and J. R. McClendon. Optimal control and estimation for strap-down seeker guidance of tactical missiles. *Department of the US Air Force Air Force Armament Laboratory (AFSC)*, 1982.

[138] J. Villagra, B. D'Andrea-Novel, H. Mounier, and M. Pengov. Flatness-based vehicle steering control strategy with SDRE feedback gains tuned via a sensitivity approach. *Control Systems Technology, IEEE Transactions on*, 15(3):554–565, 2007.

[139] Ivan Vitanov and Nabil Aouf. Fault detection and isolation in inertial navigation systems with SDRE non-linear filter. 2013.

[140] H. Voos. Nonlinear state-dependent Riccati equation control of a quadrotor UAV. *IEEE International Conference on Control Applications*, pages 2547–2552, 2006.

[141] Draguna Vrabie, Kyriakos Vamvoudakis, and Frank Lewis. Adaptive optimal controllers based on generalized policy iteration in a continuous-time framework. In *Control and Automation, 2009. MED'09. 17th Mediterranean Conference on*, pages 1402–1409. IEEE, 2009.

[142] D. Wang, D. Liu, and Q. Wei. Finite-horizon neuro-optimal tracking control for a class of discrete-time nonlinear systems using adaptive dynamic programming approach. *Neurocomputing*, 78:14–22, 2012.

[143] Ding Wang, Derong Liu, and Qinglai Wei. Finite-horizon neuro-optimal tracking control for a class of discrete-time nonlinear systems using adaptive dynamic programming approach. *Neurocomputing*, 78(1):14–22, 2012.

[144] Haiming Wang, Qingze Zou, and Hongbing Xu. Inversion-based optimal output tracking–transition switching with preview for nonminimum-phase linear systems. *Automatica*, 48(7):1364–1371, 2012.

[145] Xianghua Wang and Jinzhi Wang. Partial integrated missile guidance and control with finite time convergence. *Journal of Guidance, Control, and Dynamics*, pages 1–11, 2013.

[146] Kouki Watanabe, Masami Iwase, Shoshiro Hatakeyama, and Takehiko Maruyama. Control strategy for a snake-like robot based on constraint force and verification by experiment. *Advanced Robotics*, 23(7-8):907–937, 2009.

[147] K. A. Wise and J. L. Sedwick. Nonlinear control of agile missiles using state dependent Riccati equations. *American Control Conference, Albuquerque, NM, IEEE Publ.*, pages 379–380, August 1997.

[148] Craig A Woolsey. Review of marine control systems: Guidance, navigation, and control of ships, rigs and underwater vehicles. *Journal of Guidance, Control, and Dynamics*, 28(3):574–575, 2005.